AN ABSTRACT OF THE THESIS OF

Scott M. Schlechter for the degree of Master of Science in Civil Engineering presented on January 8, 2001. Title: Centrifuge Modeling of the Seismic Performance of Pile Supported Wharves on Sloping Rockfill.

Abstract approved:

Redacted for privacy

Stephen E. Dickenson

Recent earthquakes have highlighted many seismic hazard concerns for western U.S. ports. Port waterfront structures are commonly constructed utilizing pile-supported wharves in combination with rock dike structures retaining a hydraulically placed backfill. The damage is largely associated with the poor seismic behavior of the weak soils that are often prevalent in the marine environment (e.g. liquefiable sands, sensitive cohesive soils). In response to past damage, many ports are instigating soil improvement strategies to mitigate potential ground failures and the resulting damage to wharf structures during earthquakes.

Port authorities are currently adopting seismic performance criteria based on specific damage levels that require engineering evaluation of seismically-induced deformations/strains and residual stresses/loads in soils and structural elements. The current standard-of-practice for the design and remediation of port structures typically utilizes traditional limit-equilibrium methods that are not well suited for estimating permanent deformations of embankment or foundation elements. Although more appropriate performance-based design methods are currently being developed, the

lack of well-documented field case histories has hindered the development of robust guidelines for practical use. In supplementing the limit-equilibrium methods of design routinely used in engineering practice with performance-based procedures, there is a need for a better understanding of the dynamic soil-structure interaction of these complex embankment-pile-wharf structures. This investigation has focused on the physical modeling of wharf structures founded on sloping rock fill in carefully controlled tests utilizing a large-scale geotechnical centrifuge. A centrifuge is utilized for its ability to correctly represent in-situ soil stresses and structural loads at a model scale. The Center for Geotechnical Modeling at the University of California, Davis has a shake table that is placed between the centrifuge platform and model container and is capable of applying the dynamic shaking to the model while the centrifuge is spinning at the desired centrifugal acceleration.

This thesis focuses on the fabrication, instrumentation, testing, and data reduction for two model tests of an on-going suite of tests being conducted by Graduate Research Assistants in the Geotechnical Engineering program at OSU, under the guidance of Professor Stephen Dickenson. The geometry of the centrifuge models was based on typical pile-supported wharf geometries for large western U.S ports, specifically the Port of Oakland and the Port of Long Beach, California. The generalized profile consists of a multi-lift rock dike backfilled with sands and a pile-supported wharf structure installed through the rock dike. The model also included a soft layer of clay between dense sand layers at depth to analyze soil and pile behavior at weak/stiff soil interfaces.

Several earthquake tests were conducted on each model using recorded acceleration time histories as input excitation. The input earthquake motions were recorded during the 1994 Northridge and the 1989 Loma Prieta earthquakes. The performance of both models was monitored using 89 instruments (accelerometers,

pore pressure transducers, linear potentiometers and strain gauges) placed throughout the model. The results presented herein include the observed performance of the piles, the influence of soil improvement on the behavior of foundation piles, and the overall dynamic behavior of the model. The results of this research effort will be used in subsequent investigations regarding the applicability of current limit-equilibrium design procedures and the validation of sophisticated numerical soil-structure interaction models for use in the development of performance-based design methods for port waterfront structures.

© Copyright by Scott M. Schlechter
January 8, 2001

All Rights Reserved

CENTRIFUGE MODELING OF THE SEISMIC PERFORMANCE OF PILE SUPPORTED WHARVES ON SLOPING ROCKFILL

by

Scott M. Schlechter

A THESIS

submitted to

OREGON STATE UNIVERSITY

in partial fulfillment of
the requirements for the
degree of

MASTER OF SCIENCE

Presented January 8, 2001
Commencement June 2001

Master of Science thesis of Scott M. Schlechter presented on January 8, 2001.

APPROVED:

Redacted for privacy

Major Professor, representing Civil Engineering

Redacted for privacy

Head or Chair of Department of Civil, Construction, and Environmental Engineering

Redacted for privacy

Dean of Graduate School

I understand that my thesis will become part of the permanent collection of Oregon State University libraries. My signature below authorizes release of my thesis to any reader upon request.

Redacted for privacy

Scott M. Schlechter, Author

ACKNOWLEDGMENTS

I wish to extend my gratitude to Nason McCullough for his help throughout the duration of this project. Nason did a tremendous job of showing me the ropes of centrifuge modeling and was extremely patient in answering the multitude of questions that surround this type of project. I also would like to thank my major professor, Stephen Dickenson, for his guidance throughout my degree and for making a significant effort to help me complete this thesis even while being overseas.

I need to thank Dan Wilson and Bruce Kutter at the Center for Geotechnical Modeling. In addition to their suggestions for testing, they both sacrificed several late nights and weekends to finish testing models and help accommodate my schedule. I would also like to acknowledge the help from two members of the Oregon State University staff; Manfred Deitrich for the machine work of the structural components and Andy Brickman for the electronics and strain gauge assistance. The suggestions and assistance of Tom Kohnke, Dennis O'Brien, Key Rosebrook, Jon Boland, David Stevens and Amy Smith at the University of California, Davis were also greatly appreciated.

Finally, I need to thank my parents and family for their support throughout my education. I truly appreciate their advice and support regarding the choices I have made that have molded my collegiate activities and experiences.

This research program was funded by the Pacific Earthquake Engineering Research Center (PEER) through grant SA2394JB, with supplementary funding from the National Science Foundation (NSF) under grant CMS-9702744. The author would also like to acknowledge industry contributions from the following organizations:

- Port of Oakland, California
- Port of Long Beach, California
- Hayward Baker, Inc.
- URS Greiner Corporation

TABLE OF CONTENTS

TABLE OF CONTENTS (CONTINUED)

TABLE OF CONTENTS (CONTINUED)

TABLE OF CONTENTS (CONTINUED)

TABLE OF CONTENTS (CONTINUED)

TABLE OF CONTENTS (CONTINUED)

LIST OF FIGURES

LIST OF FIGURES (CONTINUED)

LIST OF FIGURES (CONTINUED)

LIST OF FIGURES (CONTINUED)

LIST OF TABLES

LIST OF APPENDIX TABLES

CENTRIFUGE MODELING OF THE SEISMIC PERFORMANCE OF PILE SUPPORTED WHARVES ON SLOPING ROCKFILL

1 INTRODUCTION

1.1 BACKGROUND

Experience at ports has demonstrated that waterfront structures are highly susceptible to earthquake-induced damage. This seismic vulnerability has been well documented in several recent reports (e.g., Werner, 1998; Martin et. al., 1999; Iai, in press). The poor seismic performance of these waterfront structures is usually attributed to ground failures associated with the weak soils that are often prevalent in the marine environment (e.g., liquefiable sands and sensitive cohesive soils). In the western United States, these port waterfront structures are commonly constructed utilizing pile-supported wharves in combination with rock dike structures retaining a hydraulically placed backfill (Diaz and Warwar, 1986; Egan, et al., 1992; Johnson, et al., 1998). Earthquake-induced damage to these pile supported wharf structures is usually manifested as: (1) ground failures located in the foundation, (2) embankment failure leading to excessive deformations and structural damage, and (3) damage to piles supporting the wharf (e.g. concrete spalling, failure of the wharf deck connection, and shear failures with batter piles).

1.2 SEISMIC PERFORMANCE OF PILE SUPPORTED WHARVES

The recent seismic performance of pile supported wharves will be addressed by reviewing four case histories. A brief description of the earthquake and the modes of damage that occurred will be highlighted. A summary of the seismic performance of pile supported wharves during these earthquakes will be provided in the last subsection.

1.2.1 1964 Alaska Earthquake (M_w=9.2)

With a moment magnitude intensity of 9.2, the 1964 Alaska earthquake became the second largest earthquake ever recorded. The ports of Seward and Valdez were completely destroyed by massive submarine landslides (Werner 1998). The Anchorage dock structures shown below in Figure 1-1 suffered extensive seaward tilting with bowing buckling, and yielding of pile supports. The pile supported piers and docks at Whittier experienced similar damage with buckling, bending, and twisting of steel pile supports.

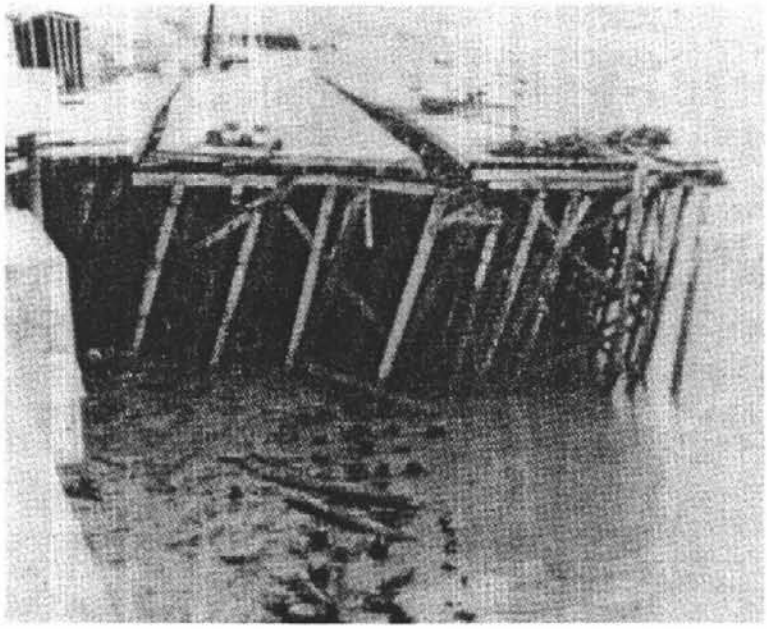

Figure 1-1: Pier Damage at Anchorage Ocean Dock (Werner 1998)

1.2.2 1989 Loma Prieta Earthquake (M_w=6.9)

The most significant damage to pile supported wharf facilities occurred at the 7th Street Marine Terminal at the Port of Oakland. Peak ground acceleration (PGA) values for this ranged from approximately 0.25-0.3-g. A cross section of this terminal

is shown in Figure 1-2. Approximately 95 percent of the battered piles failed at the connection to the wharf deck (Roth et al., 1992). These connections were either separated completely or fractured as shown in Figure 1-3 due to the high inertial loads picked up by the stiff connection provided by a batter pile. The sand behind the dike liquefied causing the deck and piles to move approximately 12–in seaward. The liquefaction of this backfill also caused the front crane rail to settle up to 18-in. This settlement induced noticeable tilting of the crane because the rear rail was pile supported (separately of the wharf). Perimeter dikes settlements at the 7th Street terminal exceeded 3-ft and lateral displacements were about 2-4 ft. The Matson terminal, pictured in Figure 1-4, also suffered significant liquefaction damage where yard settlements reached up to 2-ft (Werner 1998).

In contrast to the damage suffered at other terminals, the wharf structure at the Howard terminal performed well during the Loma Prieta earthquake. This wharf was supported by a vertical pile system and seismically designed to perform as a ductile moment resisting frame. The primary damage at the terminal was confined to subsidence in the paved areas behind the wharf.

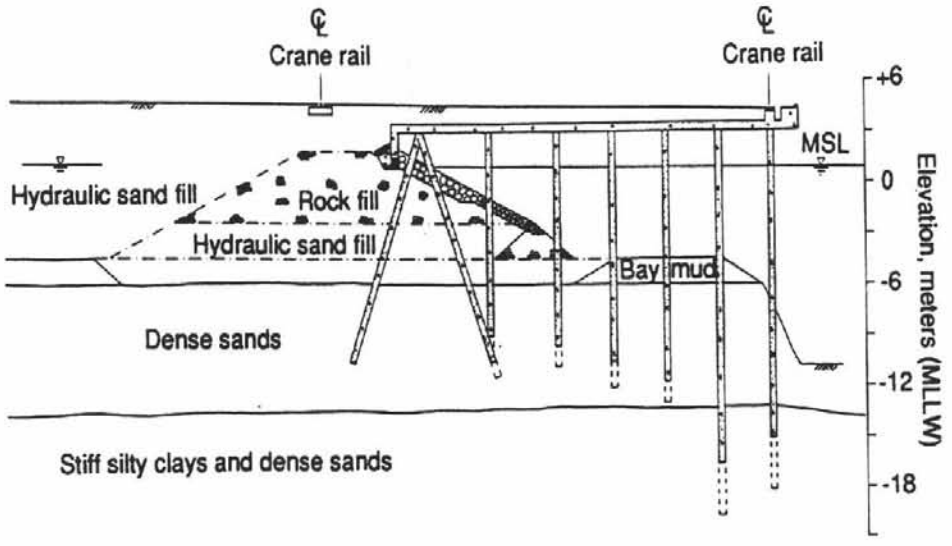

Figure 1-2: 7th Street Terminal at the Port of Oakland (Egan et al., 1992)

Figure 1-3: **Batter pile/wharf deck connection damage, Port of Oakland, 1989 Loma Prieta Earthquake (Werner, 1998)**

Figure 1-4: **Post-liquefaction settlements at Matson Terminal, Port of Oakland, 1989 Loma Prieta Earthquake (Werner 1998)**

1.2.3 1994 Northridge Earthquake (M_w=6.7)

The American Presidents Lines (APL) terminal experienced damage to the wharf structure and subsidence in backfill materials. During this earthquake, peak ground accelerations varied from 0.15-0.2-g. Figure 1-5 shows the layout of the wharf structures at APL terminal B127 and the type of damage that occurred at the batter pile connections to the wharf deck. These observations are consistent with those from the Loma Prieta Earthquake. A hairline crack also developed at the pile cap of the most landward row of piles as the berths moved seaward approximately 0.5-ft (Werner 1998). In addition, Figure 1-6 shows the damage to crane rails due to lateral displacement at an expansion joint. However, similar to the observations during the Loma Prieta earthquake, newer portions of the wharf with vertical pile designs performed well.

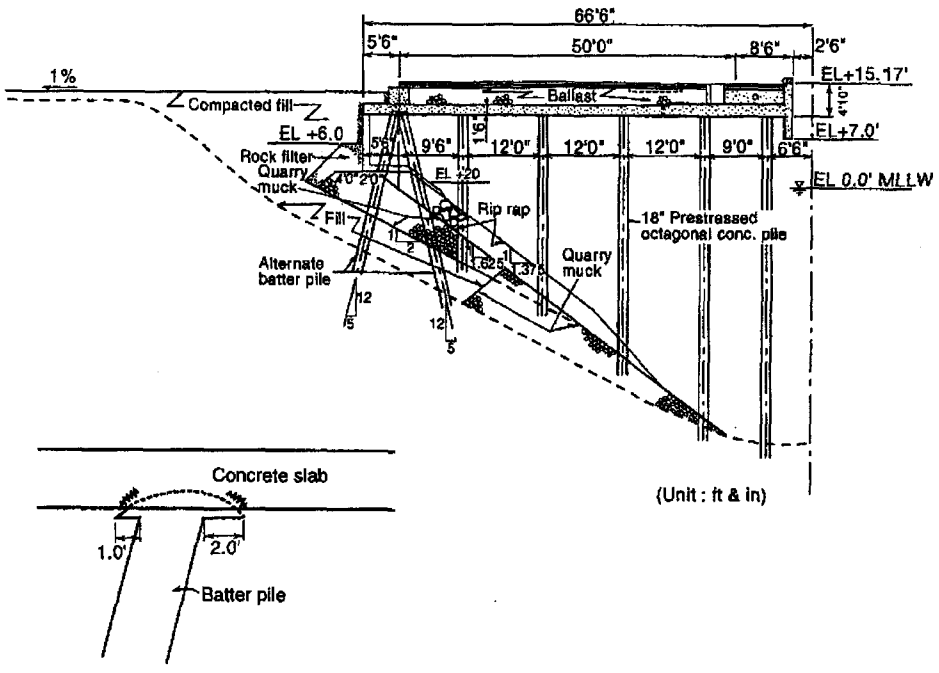

Figure 1-5: Layout of APL terminal B127 and schematic of damage due to pullout- or chipping of concrete off batter pile caps (Iai, in press)

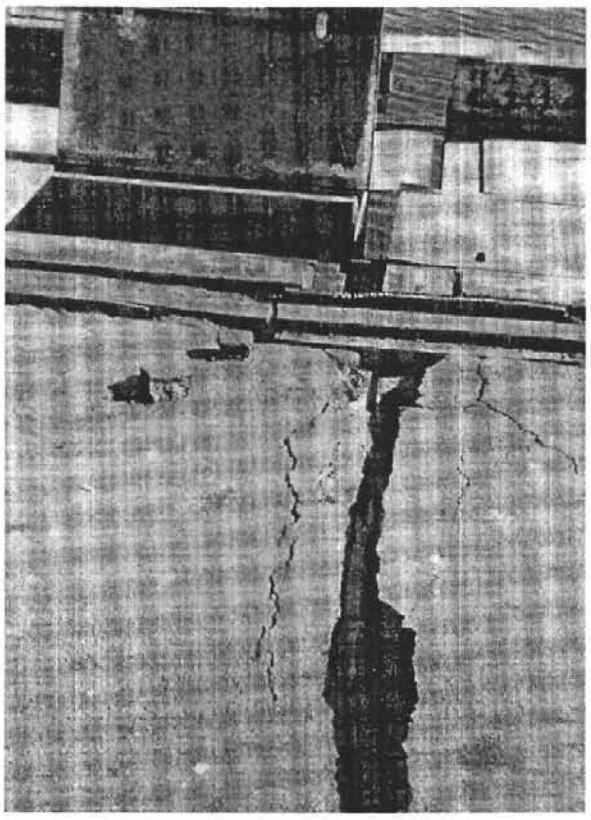

Figure 1-6: Crack in Asphalt Wharf Expansion Joint, Port of Los Angeles, 1994 Northridge Earthquake (Werner 1998)

1.2.4 1995 Kobe Earthquake (M_w=6.8)

The 1995 Kobe Earthquake rendered nearly all container terminals on Port Island and Rokko Island inoperable. PGA values during shaking ranged from 0.2-0.7-g at the Port of Kobe. Caisson quay walls moved up to 25-ft seaward and vertical settlements reached 10-ft in the backfill materials (Werner 1998). However, vertical pile wharf designs also experienced pile damage. For example, Figure 1-7 shows a cross-section of the Takahama wharf with locations of plastic hinge development. These damaged piles were examined by port engineers after the piles were extracted (Figure 1-8). The plastic hinges in the piles developed at a clay/sand interface near the base of the piled foundations and at the pile/wharf deck connection.

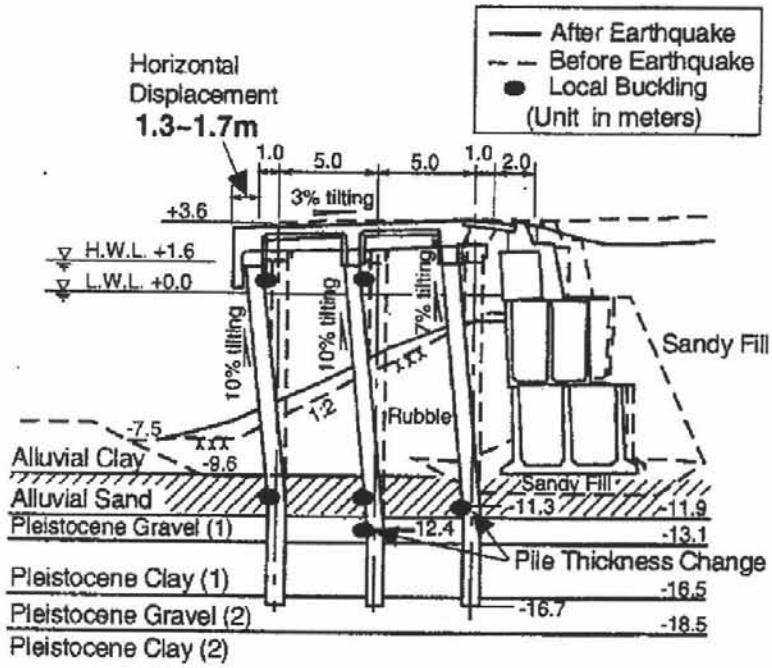

Figure 1-7: **Cross-section of Takahama Wharf with locations of pile buckling shown, 1995 Kobe Earthquake (Iai, 1998)**

Figure 1-8: **Pile damage at depth, Takahama Wharf, 1995 Kobe Earthquake, (Iai, 1998)**

1.2.5 Summary of Wharf Structure Performance

As evidenced by the damage during the 1989 Loma Prieta and 1994 Northridge earthquakes, the performance of batter piles during earthquakes deserves special attention. Due to this damage, Werner (1998) describes the potential trend of the preferred use of vertical pile systems in high seismicity regions. However, batter pile systems still remain the most efficient use of resisting lateral loads due to mooring, berthing, and crane operation (Iai, in press). It should also be noted that several of the newer batter pile designs did perform well during the 1989 Loma Prieta earthquake – the difference being the extent of lateral ground deformation.

The damage to vertical pile designs (e.g. Takahama wharf) has demonstrated that soil-structure interaction involving vertical pile designs warrants further evaluation. This plastic hinge development in vertical pile designs has occurred in three primary locations: 1) pile cap connection, 2) weak/stiff soil interfaces, and 3) about 1 to 3 pile diameters below grade in non-liquefying soils. Although, pile supported wharves have performed better than other types of waterfront retaining structures during earthquakes, it is clear new mitigation techniques are necessary.

1.3 Mitigation of Seismic Hazards to Pile Supported Wharves

For both vertical and batter pile designs, the damage that has occurred has been a result of both the dynamic response of the wharf and the inertial effects of soil acting on the wharf structure. The mitigation of damage to wharf structures therefore requires solutions to both aspects of the problem. The "structural fuse" is one of the solutions that has been proposed to allow the use of batter piles for their inherent stiffness but protect them from extreme forces that accumulate at the pile to deck connection during large earthquakes (Roth et al., 1992). This structural fuse utilizes an elastic plastic connection to the wharf deck that sheds any excess forces exceeding a specified limit. A cross section of this design is shown in Figure 1-9 showing the batter pile connection to the weaker member below the deck.

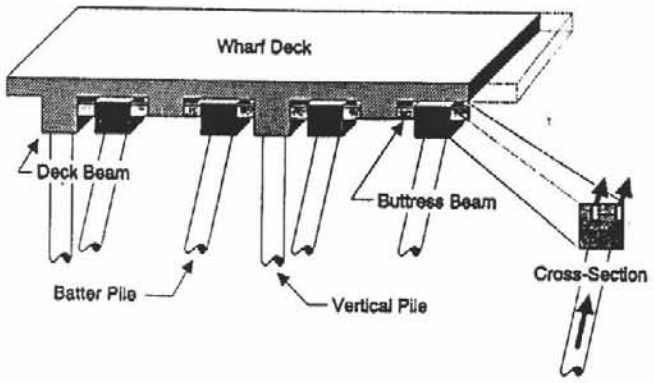

Figure 1-9: Structural fuse scheme implemented at the Port of Long Beach (Roth et al., 1992)

To address the damage due to liquefaction or pile damage at weak/stiff soil interfaces, many ports are instigating soil improvement strategies to limit deformations. Common remediation objectives include densification, increased strength/stiffness, and improved soil drainage. These improvement objectives are accomplished through many methods, including deep dynamic compaction, vibro-compaction, stone columns and cement deep soil mixing (Baez and Martin 1992, Yasuda et al., 1996, Koelling and Dickenson 1998).

Although the use of soil improvement methods is increasing, there are currently very few tools available for designing the extent of ground treatment necessary to limit the earthquake-induced damage of waterfront structures. Those that are available are largely based on limit based design methods (PHRI, 1997). However, it is generally acknowledged that these pseudostatic limit-equilibrium methods are not well suited for estimating the magnitude or pattern of deformations in earth structures. Practice oriented design charts have been developed as screening tools to assess seismic performance, but these performance-based procedures methods are still at an early stage of development (McCullough and Dickenson, 1998; Dickenson and Yang, 1998). The limitations of limit state design are compounded when complex soil-structure interaction (SSI) is considered for embankment-pile-wharf structures.

1.4 DEVELOPMENT OF PERFORMANCE-BASED DESIGN PHILOSOPHY

A new design philosophy for ports has been developed based on the lessons learned from recent earthquakes. This new design philosophy is based of the following observations (Werner, 1998; Iai, in press):

1) Deformations in backfill and foundation soils and the corresponding structural deformation and stress states are key design parameters.
2) Conventional limit equilibrium-based methods are not well suited to evaluating plastic deformations .
3) Some residual deformation of embankments and structural elements may be acceptable.

With this philosophy in mind, many west coast ports have already taken a step in this direction and adopted multi-level performance based seismic designs (Werner, 1998). These design guidelines were set to insure selected performance of waterfront components during the levels of ground shaking that are anticipated to occur during the life of the structure (the *Operating Level Earthquake*), as well as motions that may occur during larger, less frequent earthquakes (the *Contingency Level Earthquake*). In contrast, conventional building code seismic design provides capacity to resist a design seismic force, but does not provide information on the performance of a structure when the design earthquake parameters are exceeded. Werner (1998) and Iai (in press) both provide a more in depth description on the application of performance based design in regards to port facilities.

1.5 MODELING APPLICATIONS

With the need to advance the state of practice to assess the benefits of soil improvement and accurately determine deformations to implement performance based design methods, new design tools are needed to supplement the current limit-state design methods. Over the past two decades, it has been widely recognized that an accurate way of accomplishing this is through the combined use of numerical and

centrifuge modeling. The basis for this combined centrifuge and numerical modeling is perhaps best described in the following passage from Ko (1994).

> *"Numerous analytical procedures, some of which are empirical while others are based on coupled theories of soil/water interaction incorporating elasto-plastic constitutive models, have been proposed to explain and correlate the observed earthquake-induced phenomena. However, due to a lack of quality field data, there remains a considerable gap in our understanding of the phenomena of permanent deformations, especially those occurring during liquefaction, and because of the inherent difficulties in orchestrating full scale seismic events, it has been increasingly obvious that physical modeling in the centrifuge is the best alternative for studying the seismic performance of earth structures. The fact that scale models can be prepared with prescribed soil property profiles and shaken in the simulated gravity environment in a centrifuge with controllable base input motions makes this approach particularly attractive as a means to study the phenomena qualitatively and to obtain quantitative data for calibrating numerical procedures and validating specific prototype designs."*

The use of physical and centrifuge modeling was also highlighted during the 1998 PEER/Industry Workshop on the Seismic Vulnerability of Port Facilities (Martin et. al., 1999). During the session, a number of design projects and case histories were presented that utilized and called for the need for fully coupled analysis accounting for combined wharf/embankment interaction. At the conclusion of this session, the following recommendation was made by Martin (1999): "An integrated research effort which focuses on the numerical and physical modeling of pile supported wharves is highly recommended."

As stated by Martin, these fully coupled analyses are best carried out in two ways. The first involves building, testing, and analyzing an accurately scaled physical model. The second involves using a calibrated numerical model to analyze the structure. The technique used in this research work utilizes large scale centrifuge models to ascertain the behavior of these complicated embankment/pile/wharf structures. However, the purpose of the centrifuge modeling is twofold as it also makes data available for calibrating numerical models. Once the numerical model is

well calibrated, the need for the more expensive centrifuge testing is reduced as different design scenarios can then be carried out in a numerical model much cheaper. This is particularly important as more soil improvement strategies are implemented. The cost/benefit ratio of varying amounts of soil improvement can then by analyzed and implemented in a performance based design scheme.

1.6 Statement of Objectives and Scope of Work

In light of the lack of available case histories of pile supported wharves during earthquakes and the need for validation of numerical models, the Graduate Research Assistants in the Geotechnical Engineering program at OSU, under the guidance of Professor Stephen Dickenson have undertaken a comprehensive study of the seismic performance of pile supported wharves utilizing both centrifuge and numerical modeling. The author's contribution has focused on the centrifuge modeling phase of this research program. To date, five large scale centrifuge test have been carried out as part of this comprehensive investigation. This thesis focuses specifically on the second and third models in this sequence. The following objectives were established for this portion of the research:

1) Design, build, and test centrifuge models of pile supported wharves.
2) Contribute to the database of physical modeling studies for the dynamic performance of pile supported wharves.
3) Provide a preliminary analysis of model behavior.

1.6.1 Design, build, and test centrifuge models of pile supported wharves

The centrifuge models built for this test sequence represent the most complex large scale centrifuge models built to date. In light of the inherent complexity of the models being tested, a primary portion of this report is spent on a thorough explanation of the design and construction of these models. The fabrication issues

surrounding topics such as saturation of multi-layered soil deposits with clay, eccentric soil profiles, and instrument layout are addressed. Based on these experiences, the author provides an explanation of the lessons learned and recommendations for future work

1.6.2 Contribute to the database of physical modeling studies for the dynamic performance of pile supported wharves

To supplement the available case histories, an extensive database of recorded centrifuge data is made available by the presentation of the data within this report. This data is needed by the scientific and academic communities for calibration of both existing and new numerical models. This research program also follows the PEER Research Plan for integrated physical and numerical modeling of pile supported wharves (Martin, 1999). The data within this report and on the accompanying CD-ROM has been reduced and presented in a form that will facilitate future research on the results of this study.

1.6.3 Provide a preliminary analysis of model behavior

An overview of key aspects of model behavior including dynamic soil behavior, embankment deformations, pile performance, and overall soil-structure interaction are presented. In addition, the author has utilized software to analyze model behavior by plotting the data of all recorded instruments in real time simulations. These simulations allow for a clear picture of the overall model behavior to be generated. By combining general observations made from these computer generated simulations with a brief analysis of the data, a summary of the seismic performance of the modeled configuration will be provided.

1.7 THESIS ORGANIZATION

This thesis is organized and presented in the following format. Chapter 2 provides a literature review of recent work related to the modeling and analyses of these wharf configurations. Chapter 3 describes the scaling relationships and an in depth description of the design of the model and component properties. A background of the prototype geometry and properties are also included. Chapter 4 describes the model design and instrument layout for test NJM02. Chapter 5 outlines the chronological construction sequence used to build model NJM02. Complete details of each aspect of the construction sequence are explained where needed. Chapter 6 describes the testing sequence of model NJM02 and how the results of the data are presented. Chapter 7 begins the presentation of the data from the second centrifuge model discussed within. Along with the following two chapters, these chapters are outlined nearly identically to the three chapters that describe model NJM02. However, these subsequent chapters also provide comparisons between test procedures to highlight any changes in the modeling process. Therefore, Chapter 7 describes the model design and instrument layout, Chapter 8 presents the construction sequence, and Chapter 9 outlines the test sequence and presentation of data for model SMS01. The following two chapters then describe the results and provide preliminary analyses of each respective test with Chapter 10 focusing on test NJM02 and Chapter 11 describing test SMS01. Chapter 12 synthesizes the results from the previous two chapters, summarizes the work done for this research, and provides recommendations for future work. An accompanying CDROM contains all data from the results of the two tests described within this report.

2 LITERATURE REVIEW

The wharf/embankment system modeled in this investigation is a pile supported wharf founded in a multi-lift rock dike with clay and backfilled sands as foundation layers. A literature review of modeling this type of structure requires the distinction between the research surrounding (a) piles and pile foundations, and (b) embankments. The lateral and axial performance of piles on the centrifuge has been analyzed by a number of researchers. Meymand (1998) provides an extensive review of both past model pile centrifuge tests. This work includes analysis of piles ranging from the axial capacity of a single pile to the lateral pile capacity of piles installed in flight with a miniature pile driving hammer. The type of work surrounding embankments ranges from saturated soil embankments (Dewoolkar et al., 1999a) to the modeling of large earth dams (Scott, 1983) However, there has been no work done analyzing pile supported structures embedded in sloping embankments subjected to dynamic loading. The relevant work from the areas of modeling piled foundations and embankments will be highlighted within, including the limitations of their work as it applies to analyzing the pile supported wharf structures modeled within this study.

The only centrifuge model study specifically developed for the evaluation of waterfront dikes at ports to design embankment port facilities was carried out by Maruleethan and his co-workers (Maruleetharan et al., 1997). This work combined numerical and centrifuge modeling to analyze and design Pier 400 at the Port of Los Angeles (POLA). The centrifuge modeling focused on a single-lift rock dike overlying a silt and sand base, with sand as a backfill material. The primary objectives of the centrifuge modeling were to evaluate embankment deformations and calibrate a 2-dimensional numerical model. As shown in Figure 2-1, five different variations of this basic configuration were modeled. Centrifuge model tests were conducted at the University of California, Davis and the California Institute of Technology.

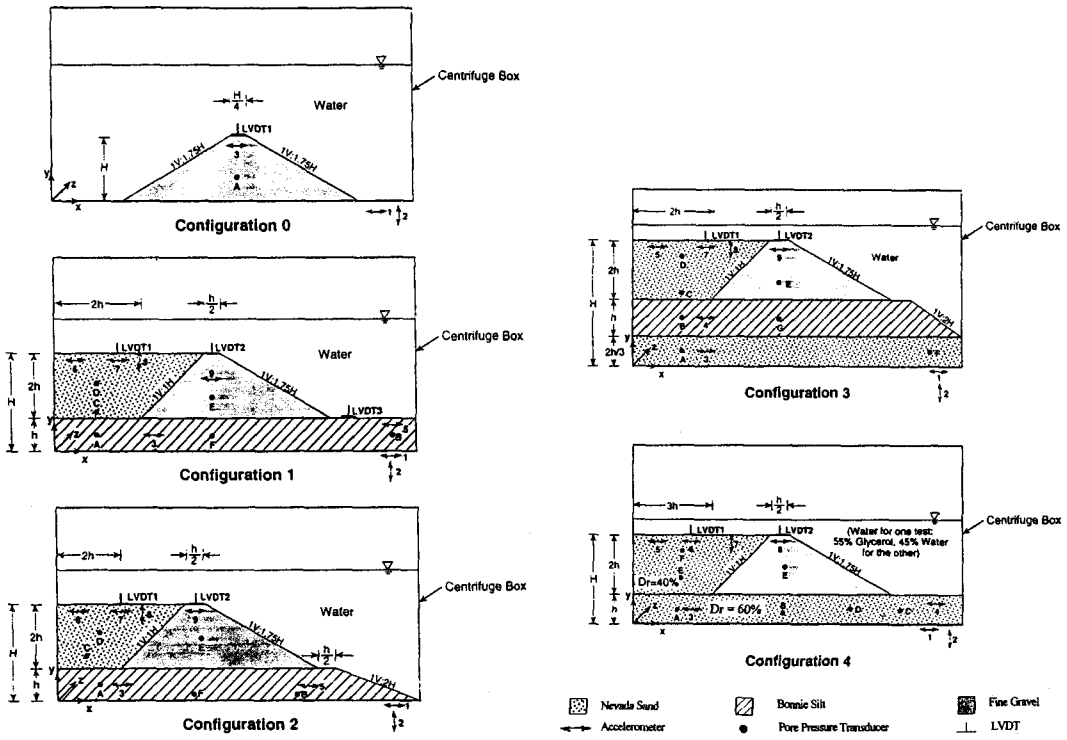

Figure 2-1: Pier 400 centrifuge model configurations (Maruleetharan, 1997)

At the completion of physical modeling, this work was used to validate the numerical code DYSAC2 (Muraleetharan et al., 1988). Using this software, an additional analysis of a conceptual cross section at PIER 400 was carried out which included a five-lift rock dike. The centrifuge and numerical model tests indicated that rock dikes move essentially as a rigid block during shaking. Because of this rigid body movement, simplified Newmark analyses of the dikes were conducted. The modeling results were used to calculate the yield accelerations required for Newmark's method by using the average excess pore pressures predicted by the calibrated numerical model in stability calculations.

Pile elements were not incorporated in any of the models in the Pier 400 study. The stabilizing, or perhaps de-stabilizing effects, of a pile supported wharf inserted through the rock embankment into the foundation soils was not accounted for within the model. The addition of piles clearly introduces another degree of complexity to the

analyses of these embankments. Many of the lateral pile studies or analysis techniques account only for loading due to cyclic static loading of the pile head or wharf deck (Chari and Meyerhoff, 1983, Yenumula et al., 1999). However, extrapolating these results for use during earthquake loading neglects any inertial effects from the embankment and soil material on the pile. The extensive pile damage deep in the soil profile shown in Figure 1-8 clearly shows the importance of accounting for this behavior.

The earth pressure induced on piles due to soil movements has been evaluated for cases involving slope stability. For example, Lee et al., (1991) analyzed the effect of seafloor instability on offshore pile foundations. They successfully used a non-linear boundary element approach to analyze the response of offshore piles in the Mississippi River Delta. Chen and Poulos (1997) and Chen et al. (1997), have also looked at the experimental modeling of piles and pile groups subjected to lateral soil loading. The general configuration modeled is shown in Figure 2-2. When examining group effects, the lateral response was found to be a function of position of the pile in the group, the pile spacing, the number of piles, and the head fixity condition. While these studies accounted for the effect of soil movement on piles, they still disregard the soil structure interaction (SSI) affects encountered with dynamic loading.

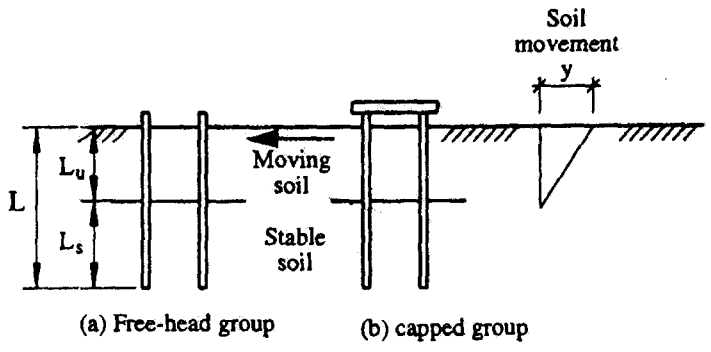

Figure 2-2: Model pile groups subjected to lateral soil movement (Chen et al., 1997)

Over the past few decades, analysis and design procedures have been developed for evaluating pile behavior under earthquake loading to help evaluate the effects of soil structure interaction (Meyersohn, et al., 1992; Finn, et al., 1994; Stewart, et al., 1994; Martin and Lam, 1995; Chen and Poulos, 1997). However, due to a continued lack of understanding of the mechanisms involved in SSI, the application of these procedures is uncertain. Some of the uncertainties that lead to the limitations of these analyses and the state of practice in regards to application to the pile supported wharves in this study include:

- Pile behavior in liquefied soils
- Pile behavior in soft soils
- Pile behavior at weak/stiff soil interfaces
- 2 or 3 dimensional pile effects
- The inertial effects of the pile wharf system on the soil mass.
- The inertial effects of the soil on the piled foundation
- Pile spacing effects

However, a significant amount of research has been carried out in recent years to help address the issues surrounding soil pile interaction. For example, Wilson (1998) carried out a number of large scale centrifuge tests to examine soil-pile superstructure interaction in liquefying sand and soft clay. This work included both single pile and pile group supported structures embedded into two primary geometries. The first included a soft clay overlying a stiff sand and the second incorporated a loose to medium dense sand overlying a stiff sand foundation. Wilson analyzed the dynamic behavior of the piles by treating the pile as a beam or column supported on a Winkler-type foundation, i.e., by a series of independent horizontal or vertical springs (p-y curve approach, p = soil resistance, y = pile deflection) distributed along pile's length. His work provided the first experimentally determined dynamic p-y curves in liquefying sand. Boulanger et al, (1999) and Curras et al., (1999) expanded upon these results by analyzing site response and developing further dynamic p-y analyses. This work provided more experimental support for the use of dynamic p-y analysis in seismic soil pile interaction problems. However, they called for the need for additional

soil-pile structural configurations to further evaluate the reliability of dynamic p-y analysis methods and their extension to pile groups.

Meymand (1998) carried out an additional study focusing on the non-linear seismic soil-pile-superstructure interaction in soft clays. Meymand evaluated pile response under pseudostatic structural loads and the applicability of simplified reduction factors for p-y relationships. He found the static and seismic test data compared very well to the p-y curves recommended by API. The methods for computing dynamic stiffness from elastic theory provided unrealistically high estimates of stiffness. Meymand's research provided good insight to the dynamic behavior of clay, however it did not address the issues surrounding pile behavior at interfaces of clay and stiffer materials that are present at many port facilities.

The other primary aspect that is lacking in previous studies is that most of the work has focused on level ground sites. However, piles in waterfront wharf structures are primarily placed in *sloping* fills. The foundation material is generally rock to some depth overlying native stratified soils or loose backfilled sands. The movement of the rock dikes and hence the induced pile movements are largely caused by liquefaction of the loose backfill materials. Many researchers have analyzed the forces induced in piles due to liquefaction induced lateral spreading (Ohtomo and Hamada, 1994, Liu and Dobry, 1995, and Meyersohn, 1995). However, the forces generated many of the modeled configurations are not necessarily indicative of the pressures piles would feel due to the liquefaction induced movement of more competent, steeper sloping rockfill. For example, some of the work has focused on situations such as the configurations shown in Figure 2-3. The work by Liu and Dobry (1995) and Toboada (1995) included instrumented piles in a sloping, saturated sand with the use of an inclined box. The results of both of these configurations are useful in their own respect but are not directly applicable to the configurations of pile/wharf geometries.

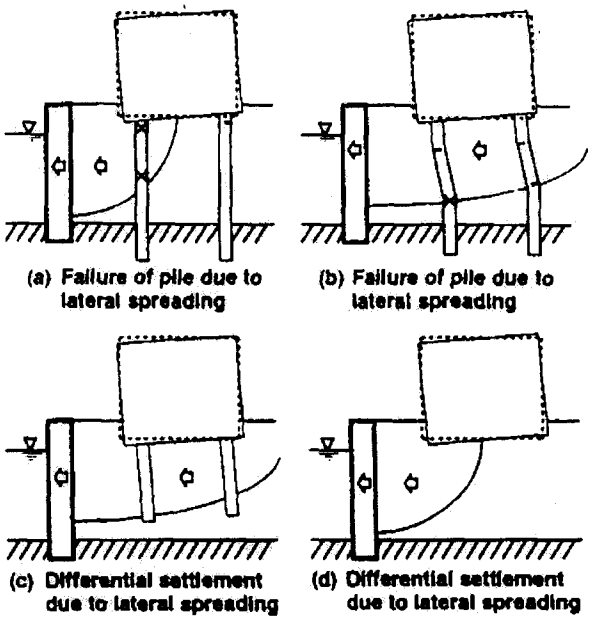

Figure 2-3: Typical pile damage due to lateral spreading damage in 1995 Kobe Earthquake (Tokimatsu et al., 1996)

In summary, the experimental work to date has analyzed the performance of embankments in a variety of configurations. However, none of this research directly applied to waterfront structures has included a wharf structure and very little work has studied the effect of piles on slope behavior, particularly in dynamic applications. A significant amount of research has taken place utilizing the centrifuge to analyze piled foundations. However, none of this work can be directly applied to wharf structures due to the complex geotechnical and structural geometries. Therefore, in light of the lack of any experimental data regarding the seismic performance of pile supported wharves embedded in sloping rockfill and layered soil profiles, a centrifuge modeling study was developed for this research project. With this background, the next chapter describes the model scaling relationships and the design of the models in this research program.

3 SCALING RELATIONSHIPS AND DESIGN OF THE MODELS

Many fields of engineering use scaled models of large structures to study physical phenomena. The use of scaled models allows the advantage of replicating the field behavior of complex systems under controlled conditions. Scale models often create a more economical option than developing a full scale test and also allows the investigation of certain phenomena that cannot be created at will (e.g. earthquake loading). The use of a centrifuge for geotechnical modeling has increased dramatically over the past four decades. The principal advantage of centrifuge testing is that the gravitational stress field in the model can replicate the prototype. Following the schematic in Figure 3-1, the model is placed on the bucket arm. While the model is spinning on the centrifuge, an earthquake motion can be introduced to the model through a shake table at the base of the model. The scaling factor used to design the model is then a function of the angular velocity of the arm and the proportional increased gravitational stresses. The replication of stresses is extremely important in modeling soils because their strength and stress strain behavior is a function of the overburden pressure.

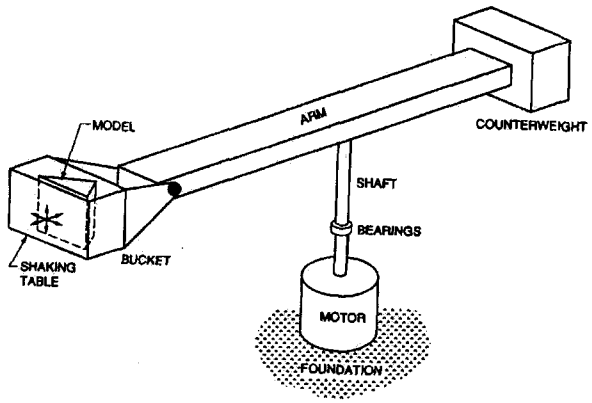

Figure 3-1: Basic schematic of a geotechnical centrifuge (Meymand, 1998)

A second modeling method that is commonly employed for geotechnical applications includes the building and testing of models under normal gravity. The scaling relationships required for this modeling are typically referred to as "geometric" or "1-g" scaling. Dynamic modeling at 1-g is carried out using "shake table" tests where the earthquake motion is applied to the base of a model container. Following appropriate dimensional scaling, the model components can be developed accordingly. However, because the stresses are not accurately modeled with depth in a 1-g model, the strength of the soil has to be modeled. Models developed at 1-g are inherently less expensive and easier to work with than models developed on a centrifuge. Shake tables can also accommodate much larger models than centrifuges because the model height is not directly restricted by the size of the centrifuge bucket.

Iai (1989), Gibson (1996), and Meymand (1998) describe the theory behind varying levels of model similitude and their application to 1-g modeling. Centrifuge scaling is further described by Schofield (1980) and Kutter (1991). The scaling relationships used within this study are described below.

3.1 Model Scaling Relationships

At the time of testing, the maximum centrifugal acceleration possible at the Center for Geotechnical Modeling (section 3.3) was 40-g. The first model in this test series, NJM01, (McCullough et al., 2000) was designed based solely upon the use of centrifugal scaling factors. Due to the size of the prototype model and the maximum centrifugal acceleration available, the pile tips were driven to the bottom of the model container and concerns about boundary effects were raised. Therefore, to ensure boundary effects were not an issue in the next two tests, the prototype geometry was scaled further.

To accomplish the centrifugal and geometric scaling of the prototype, a two stage scaling process was used. First, a primary model scaling from the prototype geometry was done based on a centrifugal acceleration of 40-g. Secondly, a geometric scaling

was employed to reduce the centrifugal scaled model by a factor of 0.7. Therefore, with n as the centrifugal acceleration and λ as the geometric scaling, the following scaling relationships were developed:

$$n = \frac{\text{prototype}}{\text{model}} \cong 40$$

$$\lambda = \frac{\text{prototype}}{\text{model}} \cong \frac{1}{0.7}$$

Centrifuge and geometric scaling factors and values for this test are given in Table 3-1.

Table 3-1: Model scaling factors and values (after Scott, 1991)

Quantity	*Centrifuge Scale Factors*	*Centrifuge Scale Values*	*Geometric Scale Factors*	*Geometric Scale Values*
Acceleration	1/n	0.025	1	1
Velocity	1	1	$\lambda^{1/2}$	1.20
Displacement/Length	n	40	λ	1.43
Time (Dynamic)	n	40	$\lambda^{1/2}$	1.20
Time (Diffusion)	$n^2 \cdot (c_v^*)^{-1}$	$1600 \cdot (c_v^*)^{-1}$	λ if $c_v^* = \lambda$ $\lambda^{0.5}$ if $c_v^* = \lambda^{1.5}$	1.43 if $c_v^* = \lambda$ 1.20 if $c_v^* = \lambda^{1.5}$
Mass Density	1	1	1	1
Mass	n^3	64000	λ^3	2.92
Force	n^2	1600	λ^3	2.92
Stress	1	1	λ	1.43
Pile Stiffness (EI)	n^4	2560000	λ^5	2.92
Moment	n^3	64000	λ^4	4.16

Where $c_v^* = \left(\frac{c_{v\text{-}p}}{c_{v\text{-}m}} \right)$

Based on these scaling relationships, the results of the tests can be evaluated in one or more of the following procedures depending on the primary goal of the investigator:

1) Examine the behavior of the centrifuge model directly in model units. This is considered the most accurate procedure for validating numerical SSI models.
2) Examine the behavior of the model with only the centrifugal scaling relationships applied. This evaluation would lead to an adjusted, smaller prototype.
3) Extrapolate the behavior of the centrifuge model to full field prototype scale by employing both the centrifuge and geometric scaling factors. This analysis procedure yields results that can be used directly for comparing model response to field case histories.

It should be noted that all three of these procedures are appropriate, however the level of confidence is thought to decrease with the application of additional scaling factors. The most direct application of these results is the first procedure listed (i.e., the results of the scale model). Full extension of results in prototype units implies a high confidence in all aspects of the modeling process (Meymand, 1998). Data in this report will be made available for cases 1 and 3 as described above. This provides easy reference for the user in formats for either numerical modeling or comparison of the data to full prototype scales.

3.2 PROTOTYPE GEOMETRY

The models were constructed as a generalization of the pile-supported wharf structures common at numerous ports along the Pacific coast of the United States (e.g., Port of Oakland (POOAK), Port of Los Angeles (POLA), and Port of Long Beach (POLB), California). The prototype wharf geometry consists of 61 cm (24-in) diameter octagonal prestressed concrete piles. The wharf deck is assumed to be a uniform 1.22-m (4-ft) thick deck and pavement section. Figure 3-2 shows a typical section of the 7th Street terminal at the Port of Oakland, which suffered significant damage during the 1989 Loma Prieta earthquake. Figure 3-3 shows a representative

section at the Port of Long Beach. Both figures show rock dikes founded upon and backfilled with loose hydraulically placed fills that are highly susceptible to liquefaction. The 7th Street terminal cross-section also shows the presence of a relatively weak clay layer at depth, which is common at many ports.

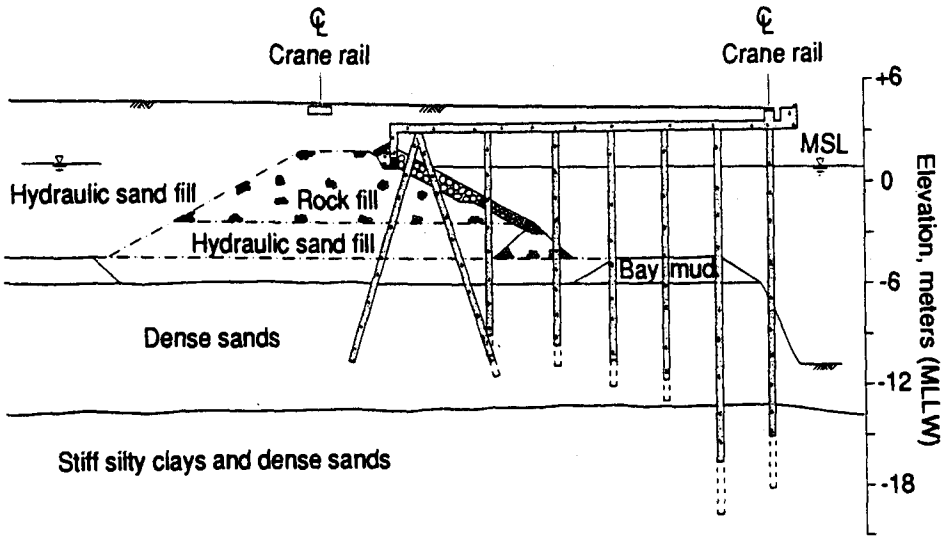

Figure 3-2: 7th Street Terminal at the Port of Oakland (Egan et al., 1992)

The hybrid configuration developed for the model tests incorporates many of these common field conditions into a single model design. The wharf model incorporates only vertical piles due to the ease of model construction and the desire to incorporate batter piles in future models. The generalized soil profile of both models in this study (not including soil improvements) is shown in Figure 3-4 and described herein. A base layer of dense sand was used to provide a stiff embedment material for the piles. A relatively weak layer of clay and another layer of dense sand of approximately equal thickness overlie the thick lower dense sand layer. In the backland (the landside region behind the wharf structure), these layers of sand and clay were overlain by a relatively thick layer of loose sand used to represent the

hydraulic fills that are typical at port facilities. A multi-lift rock dike with 1.5 to 1 (H:V) slopes forms the waterfront face of the soil profile. The backland surface was then finished with a relatively thin layer of dense sand, used to represent the soil above the waterline at ports that is generally compacted due to construction and operational activity. The full design layouts of both models are provided individually in subsequent chapters.

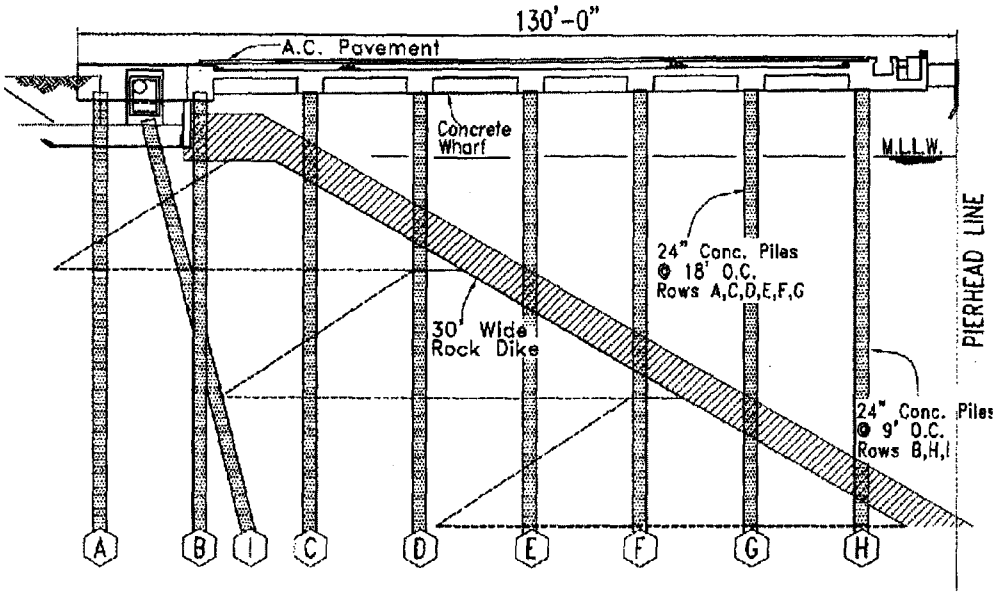

Figure 3-3: Typical section at the Port of Long Beach (Mukhopadhyay, 1989)

The hybrid configuration developed for the model tests incorporates many of these common field conditions into a single model design. The wharf model incorporates only vertical piles due to the ease of model construction and the desire to incorporate batter piles in future models. The generalized soil profile of both models in this study (not including soil improvements) is shown in Figure 3-4 and described herein. A base layer of dense sand was used to provide a stiff embedment material for the piles. A relatively weak layer of clay and another layer of dense sand of approximately equal thickness overlie the thick lower dense sand layer. In the

backland (the landside region behind the wharf structure), these layers of sand and clay were overlain by a relatively thick layer of loose sand used to represent the hydraulic fills that are typical at port facilities. A multi-lift rock dike with 1.5 to 1 (H:V) slopes forms the waterfront face of the soil profile. The backland surface was then finished with a relatively thin layer of dense sand, used to represent the soil above the waterline at ports that is generally compacted due to construction and operational activity. The full design layouts of both models are provided individually in subsequent chapters.

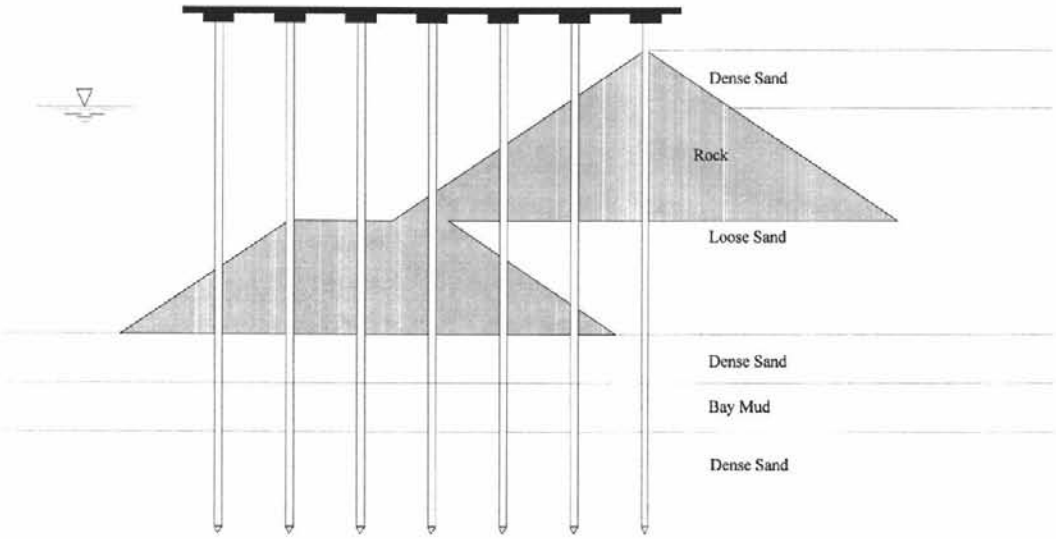

Figure 3-4: Generalized wharf/embankment configuration

In addition to the general geometry of the wharf configuration, all components used within the model were scaled as closely as possible from existing wharfs or those currently under construction at POLB and/or POOAK. The design of the model components is described below.

3.3 DESCRIPTION OF THE CENTRIFUGE

Centrifuge model tests NJM02 and SMS01 were carried out at the Center for Geotechnical Modeling located at the University of California at Davis (UC Davis). The centrifuge has a 9-m radius and is equipped with a large, one-dimensional shake table driven by two pairs of servo-hydraulic actuators acting in parallel, one pair mounted on either side of the model (Kutter et al., 1994). The centrifuge was designed for a maximum model mass of 2500-kg, an available bucket area of 4.0-m^2, and a maximum centrifugal acceleration of 50-g (Wilson, 1998). The shake table is designed to accommodate a 1.7-m long model container and provide input accelerations of up to 15-g. Kutter et al., (1991) provide a thorough introduction to the UC Davis centrifuge facility.

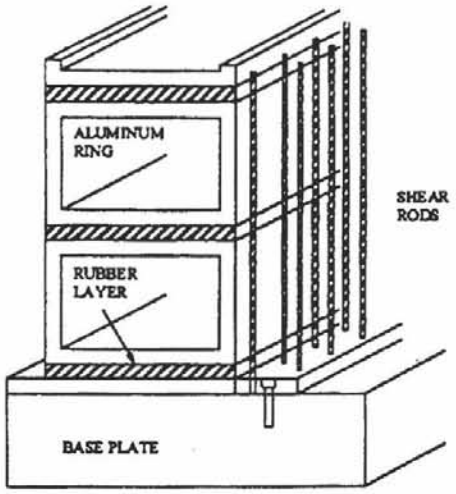

Figure 3-5: Cross-section of the flexible shear beam container, FSB1 (Divis et al., 1996)

The wharf models were constructed in the facility's large flexible shear beam container (FSB1). The flexible shear beam container was designed and built to have a shear modulus with depth that approximates that of a liquefied soil deposit. FSB1 is

approximately 1720-mm long, 685-mm wide, 702-mm deep, and consists of six hollow aluminum rings separated by 12-mm thick layers of 20-durometer neoprene rubber (Figure 3-5). The mass of each of the upper three rings is about one-half the mass of each of the lower three rings. The thickness of neoprene varies, such that the shear stiffness of the box increases with depth (as the shear modulus of the soil increases with depth). Vertical shear rods (all-thread rods) are attached to the bottom of the box to provide complimentary shear stresses (Divis et al., 1996).

3.4 WHARF DESIGN

The wharf deck mass was scaled from a prototype wharf deck at the Port of Oakland. The mass scaling was based on a uniform 1.22-m (4-ft) thick reinforced concrete deck assuming the concrete, aggregate fill, and AC as a single unit weight (150 psf). The prototype wharf deck mass was scaled appropriately and a target dead load per pile was calculated. The distributed area used for this calculation is based on the pile spacing adopted for these models. As shown in Figure 3-6, a model pile spacing of 88.9-mm by 101.6-mm (3.5-in by 4-in) was used which corresponds to a prototype spacing of 5-m by 5.77-m (16.6-ft by 18.9-ft). The wharf deck and pile caps were then sized appropriately relative to each other such that the sum of their masses would match the scaled distributed mass.

Table 3-2: Wharf deck mass scaling

Wharf Deck Properties	*Values in Model Scale*	*Values in Prototype Scale*
Mass of Deck	3.2375 kg	1.65×10^5 kg
Mass of All Pile Caps (21) with connection bolts	883.5 g	6×10^5 kg
Tributary Mass Per Pile	196.2 g	36,620 kg

The pile caps were made from aluminum, 38.1-mm (1.5-in) in diameter and 12.7-mm (0.5-in) thick. Properties of the scaled wharf deck and pile caps are included in Table 3-2. The wharf deck was 6.35-mm (0.25-in) thick aluminum sheeting. The in-plane stiffness of the wharf deck was not directly scaled but can be assumed infinitely stiff in comparison to the rest of the wharf structure.

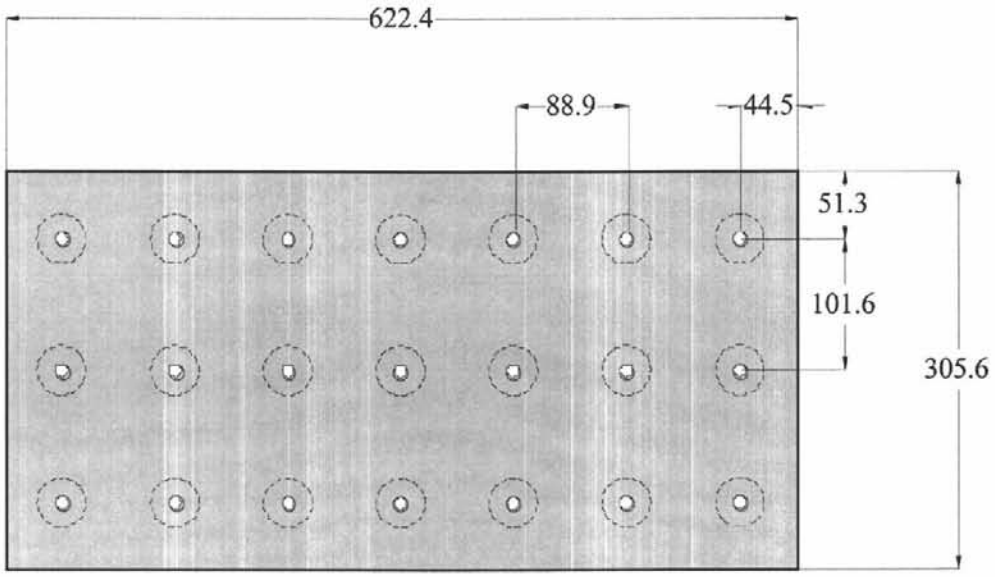

Figure 3-6: Wharf deck dimensions (mm)

3.5 PILE DESIGN

As mentioned previously, the target prototype pile is a 24-inch octagonal prestressed concrete pile. Aluminum (6061-T6) tubing was used to represent the prestressed concrete piles. The aluminum tubing was chosen such that the elastic behavior and the diameter would match the scaled concrete piles. Based on the available tubing sizes, the resulting pile size for both tests had a 9.525-mm (0.375-in) diameter and 0.889-mm (0.035-in) wall thickness, which approximately match the scaled prototype diameter and stiffness assuming an uncracked section. However, the

author was not able to match the bending moment capacity at model scale due to a lack of available material thicknesses and strengths at the model pile size. Therefore, with the stiffness matched, the T-6 aluminum resulted in a model bending moment capacity significantly greater than that of the prototype piles. The larger model moment capacity resulted in an acceptable design because moments in excess of the scaled prototype plastic moment capacity could still be recorded. In addition, this design maintained pile integrity through all shaking events. Properties of the piles are shown below in Table 3-3. Figure 3-7 shows the overall model pile dimensions with the pile tip and cap included.

Table 3-3: Pile properties

	Aluminum Tubing		*Target Prestressed Concrete Piles*
Pile Properties	***Values in Model Scale***	***Values in Prototype Scale***	***Target Values in Prototype Scale***
Diameter (mm)	9.525	546	610
Length (m)	0.625	35.7	Varies
Wall Thickness (mm)	0.889 mm	50.8	NA
Moment of Inertia (I)	227.2 mm^4	2.42 x 10^{-3} m^4	3.78x 10^{-4} m^4
Modulus of Elasticity (E)	70 GPa	70 GPa	30 GPa
Stiffness (EI) Pa-m^4	15.90	1.69 x 10^8	1.15 x 10^8
Plastic Moment (N-m)	28.12	7.5 x 10^6	6.1-9.8 x 10^5

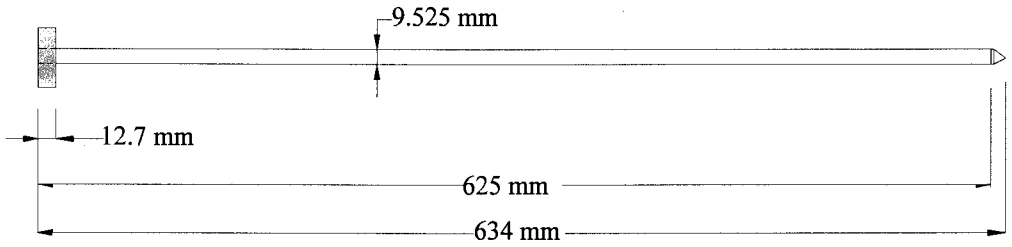

Figure 3-7: Model pile dimensions

The pile cap was designed to attach snugly and tighten over the pile top. The pile cap is then fixed with two additional bolts to the wharf deck during testing. This configuration essentially models a fixed head condition for the piles at the base of the pile cap.

3.6 SOIL SPECIFICATIONS

3.6.1 Sand

Nevada sand was set as the standard for centrifuge modeling at the completion of the VELACS project (Arulmoli, 1994). Therefore, all sandy soil layers were built using Nevada Sand. Details of the sand properties are given in Table 3-4. Maximum and minimum dry unit weights of 16.98-kN/m^3 (108-pcf) and 13.83-kN/m^3 (88-pcf) were used for the calculation of relative densities during model construction.

Table 3-4: Nevada sand properties (Woodward Clyde, 1997)

Soil	No. 120 Nevada Sand, UCD Batch #3
Supplier	Gordon Sand Co., Compton, CA
Classification	Uniform, Fine Sand; SP
Specific Gravity	2.67
Mean Grain Size, D_{50} (mm)	0.15
Coefficient of Uniformity, C_U	1.6
Maximum dry unit weight (kN/m^3)	16.76
Minimum dry unit weight (kN/m^3)	13.98

Scott (1991) proposed that the density of modeled sand in a geometrically scaled model should be placed at a lower relative density than the prototype soil. This reduced model density would yield a more appropriate stress-strain behavior and allow the sand to more closely follow the correct implied prototype stress path and behavior relative to the steady state line. The reduced scale (model) soil will then

exhibit the same volumetric strains, over the same range of scaled shearing stresses, at the reduced stress level as the prototype at the higher stresses. Figure 3-8, shows a sketch of this behavior suggested by Gibson (1996) in work following Scott's earlier study. Using appropriate values suggested by Scott, this adjustment accounted for only a 4 percent change in relative density due to the small geometric scaling factor employed in this study. This change is relatively small and the values of relative densities shown within have *not* been corrected for this change in density.

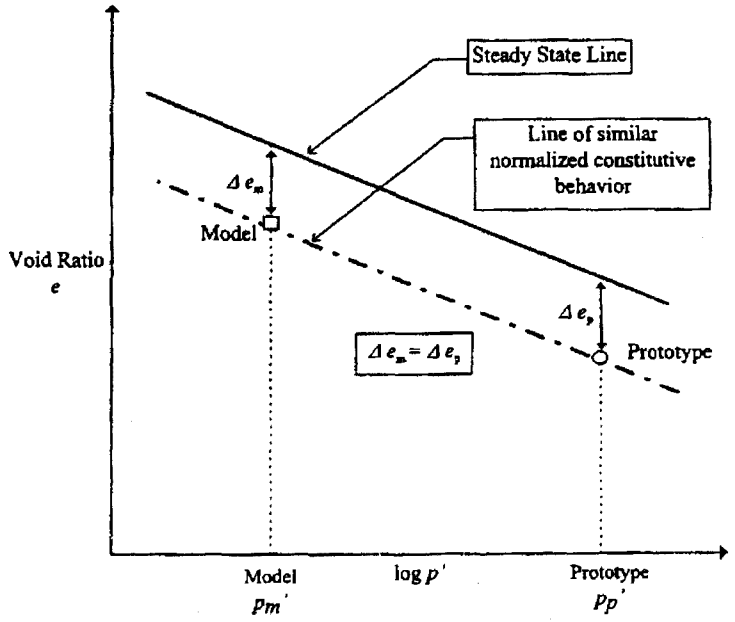

Figure 3-8: Model soil properties based on steady-state line (Gibson, 1996)

3.6.2 Rock

Soil materials are generally not scaled in centrifuge testing to maintain the mechanical properties of the soil and therefore not affect the stress strain behavior of the model. However, due to the relatively large size of rock used for prototype dike construction, size constraints of the model box, and the significantly scaled pile size, a

scaling was needed to properly represent the rock/pile interaction at model scale. The rock used for this test sequence was imported from a quarry on Catalina Island (the same quarry used to supply rock to the POLA and POLB) and then crushed to an appropriate size. The material was then dry sieved and mixed to obtain the gradation shown below in Figure 3-9. It can be seen that the scaled gradation used for SMS01 deviates from a direct scaling at smaller grain sizes. This technique was chosen to remove the fines material and attempt to maintain the relative permeability of the rock/sand interface.

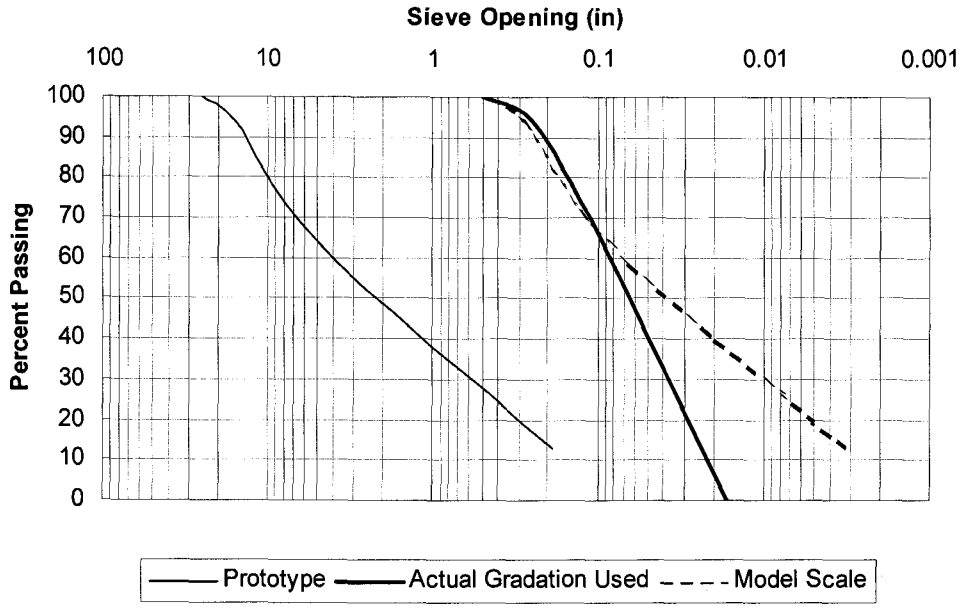

Figure 3-9: Rock gradation

3.6.3 San Francisco Bay Mud

The San Francisco Bay Mud used within the models was obtained from the on-site storage facility at the Center for Geotechnical Modeling. A series of tests at the University of California, Davis were run to analyze the material properties and consolidation characteristics of the clay (Tarin, 1997). From these tests, it was found

that the Plasticity Index (PI) averaged about 40 and the Liquid Limit (LL) was approximately 85. The recompression index, C_r, and the compression index, C_c, were found to be 0.11 and 0.723, respectively. A description of the hydration technique, model fabrication, and clay placement, and consolidation are described in the construction sequence of each model.

3.6.4 Cement Deep Soil Mixing

Cement deep soil mixing (CDSM) was simulated as a soil improvement technique in test SMS01. The soil-cement mix design was based on the material used during the Berth 55/56 expansion project at the Port of Oakland (Subsurface Consultants et al., 1999). In the field, the CDSM soil improvement procedure involves construction of overlapping soil-cement columns to form a series of wall arranged in a grid pattern. This prototype grid is created by injecting a grout using an auger with an approximate 20-percent overlap. The target prototype cement ratio was 200-kg of cement (by dry weight) per cubic meter of in situ undisturbed soil. The prototype wall was created using a 0.91-m (3-ft) diameter auger. A water-cement ratio of 1:1 was used to achieve the target cement ratio and 0.12-m^3 (32-gallons) of slurry per 0.91-m (3-ft) of depth for each auger shaft was used. An example of a test pile and CDSM wall at the Port of Oakland is shown in Figure 3-10.

This field application was modeled as a 22.8-mm wide wall. It should be noted that this scaling did *not* include the geometric scaling factor. The author sought to match the water:cement:soil ratio as accurately as possible following appropriate assumptions for field mixing at the prototype scale. However, the water content of the clay slurry available for mixing was slightly higher than ideal to match the prototype mix given the authors assumptions for field replacement ratios. Therefore, the mix design was modified to best match the prototype design resulting in a slightly higher water content than ideal. The final CDSM mixture used was 3.63-kg (8-lbs) of Type I-II Portland Cement mixed with 22.68-kg (50-lbs) of clay slurry at 133-percent water content. The design grid layout is shown in Figure 3-11.

Figure 3-10: Test pile at Port of Oakland surrounded by CDSM material

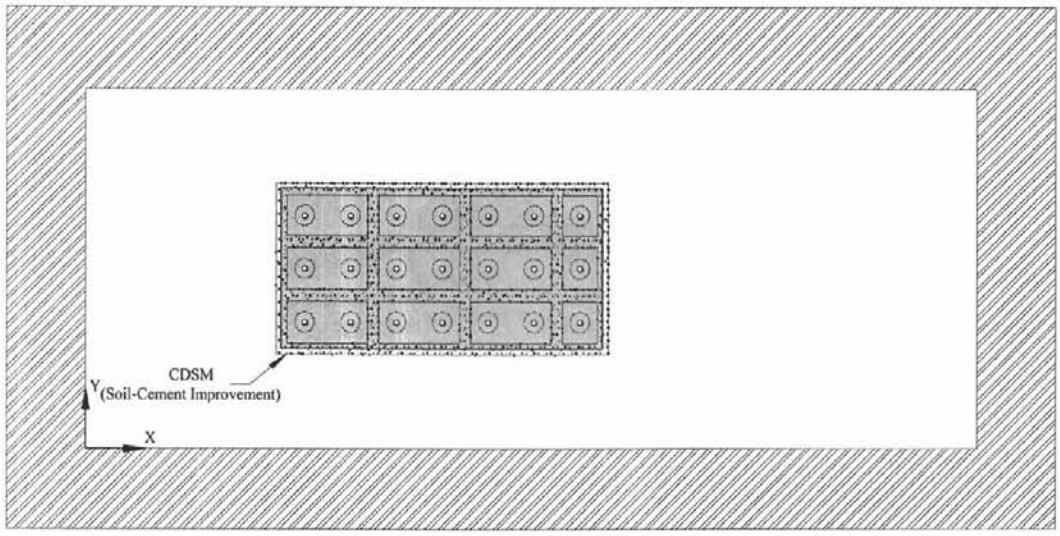

Figure 3-11: CDSM grid layout

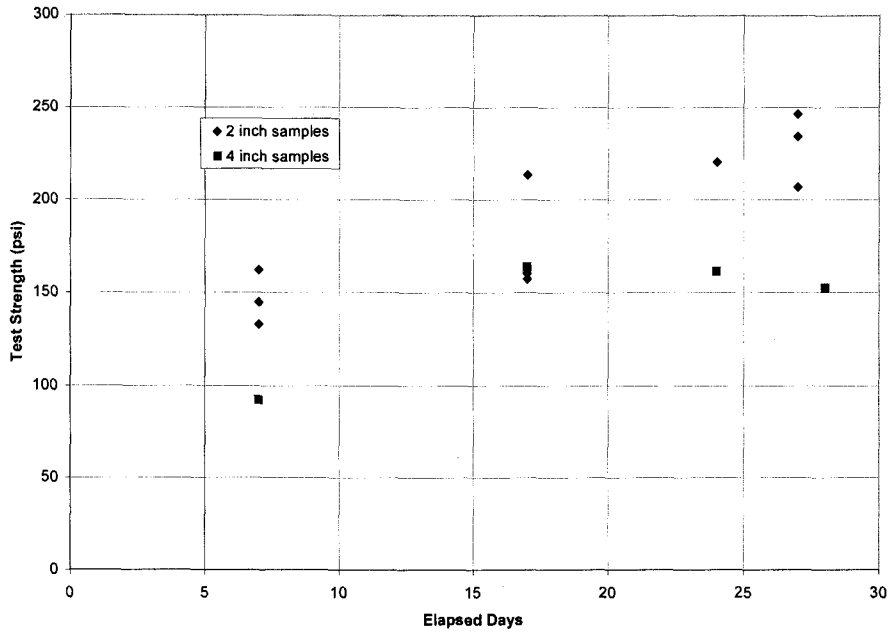

Figure 3-12: Laboratory CDSM test strengths extracted from mixes identical to the material used in test SMS01

Figure 3-12 shows the variation of unconfined compressive strength versus time after mixing. This figure shows two sets of samples were molded from identical batches of the CDSM material that was placed within the model. On the day the CDSM was placed in the model, four 101.6-mm (4-in) diameter samples were made. The following day, an additional twelve 50.8-mm (2-in) diameter samples were cast from a second batch of the CDSM material. All samples were placed in a water bath at room temperature until they were transported to Oregon State University and tested in the geotechnical engineering laboratory. It should be noted that the earthquake test sequence was run on the 7^{th} and 8^{th} days after mixing. The unconfined compressive strengths of the laboratory samples show values varying between 95 and 170 psi at a corresponding length of time from sample creation. The project specifications required a minimum 28-day strength of 105 pounds per square inch (psi) and an average strength of 160 psi for all samples. The lab data from the model mixture show this mix

criteria would have been met at 28 days. At the time of testing, the four data points averaged 135 psi, which is approximately 15% below the desired average strength.

3.7 PORE FLUID

For centrifuge models with applications that involve fluid flow, a key factor that needs to be addressed is the conflict between different time scales. As illustrated in Table 3-1, the scale factor in centrifuge modeling for diffusion time is $\mathbf{n}^2$ (prototype:model). However, the inertial or dynamic time is scaled by a factor of **n**. In applications where the buildup of excess pore pressures due to seismic excitation is expected, this time conflict must be addressed to accurately compare model and prototype behaviors. Dewoolkar et al. (1999 a,b), have shown the importance of accounting for pore fluid viscosity on the behavior of saturated sands, particularly for liquefaction behavior.

Theoretically, this phenomena can be accounted for in two ways. The first option would be to scale the soil particles accordingly so that the permeability of the soil would be reduced and the time scales would match accordingly. The second option is to use a substitute pore fluid that is **n** times more viscous than water thereby reducing the permeability of the soil by the same factor. The first approach is usually avoided because scaling the soil can cause significant differences in the mechanical properties of the soil and affect the stress strain behavior of the model. The second approach of using a substitute pore fluid has most consistently been used by researchers and was utilized during this study.

Due to the added complexity of a clay layer in the middle of the model, it was necessary to saturate SMS01 at two different times with different fluids. The bottom dense sand layer was saturated immediately after placement with only de-ionized water. The remainder of the saturation took place after completion of the model with a more viscous pore fluid. The fluid used was a mixture of de-ionized water, hydoxy-propyl methylcellulose (HPMC), and benzoic acid as a preservative (Stewart and Kutter, 1998). HPMC was not used during initial saturation because of the possible adverse effects of interaction of the HPMC with organic materials in the clay. The

HPMC used in this experiment was supplied by the Dow Chemical Company and marketed under the trade name of Methocel, premium grade F. Stewart and Kutter (1998) have shown that for concentrations of less than 5%, the solutions have a specific gravity within 1% of the value of pure water. Therefore, the specific gravity can readily be assumed to be equal to that of water. Details of the mix design and saturation procedures are provided in section 5.8.

4 NJM02 MODEL AND INSTRUMENTATION LAYOUT

This chapter will describe the soil and structural geometry of centrifuge model NJM02. Locations, descriptions, and comments on the layout of all instrumentation will be provided in each subsection.

4.1 NJM02 MODEL LAYOUT

The design model layout for test NJM02 (Figure 4-1) closely resembles the general configuration shown in Figure 3-4. The base of the model was a relatively deep, dense sand layer used to provide a stiff embedment material for the piles. A relatively weak layer of clay and another layer of dense sand of approximately equal thickness were placed over the base foundation dense sand. In the backland (the landside region behind the wharf structure) these layers of sand and clay were overlain by a relatively thick layer of loose sand used to represent the hydraulic fills that are typical at port facilities. A two-lift rock dike with 1.5 to 1 (H:V) slopes forms the waterfront face of the soil profile. The backland surface profile was then finished with a relatively thin layer of dense sand, used to represent the soil above the waterline at ports that is generally compacted due to construction and operational activity. Table 4-1 provides a description of all elevation layers used to describe model locations along with *design* model and prototype dimensions

The dense sand layers were placed at a relative density (D_r) of approximately 85%. All loose sand layers were placed at approximately 45% D_r. The clay was initially consolidated in a large hydraulic press to match the desired field conditions beneath the dredge line (OCR of 1.5). Overburden pressures increase in the clay layer during centrifuge spinning, bringing the clay to a normally consolidated condition beneath the rock and sand fills. The measured strengths of the clays are presented along with the clay consolidation explanation in the construction sequence in section 5.3.

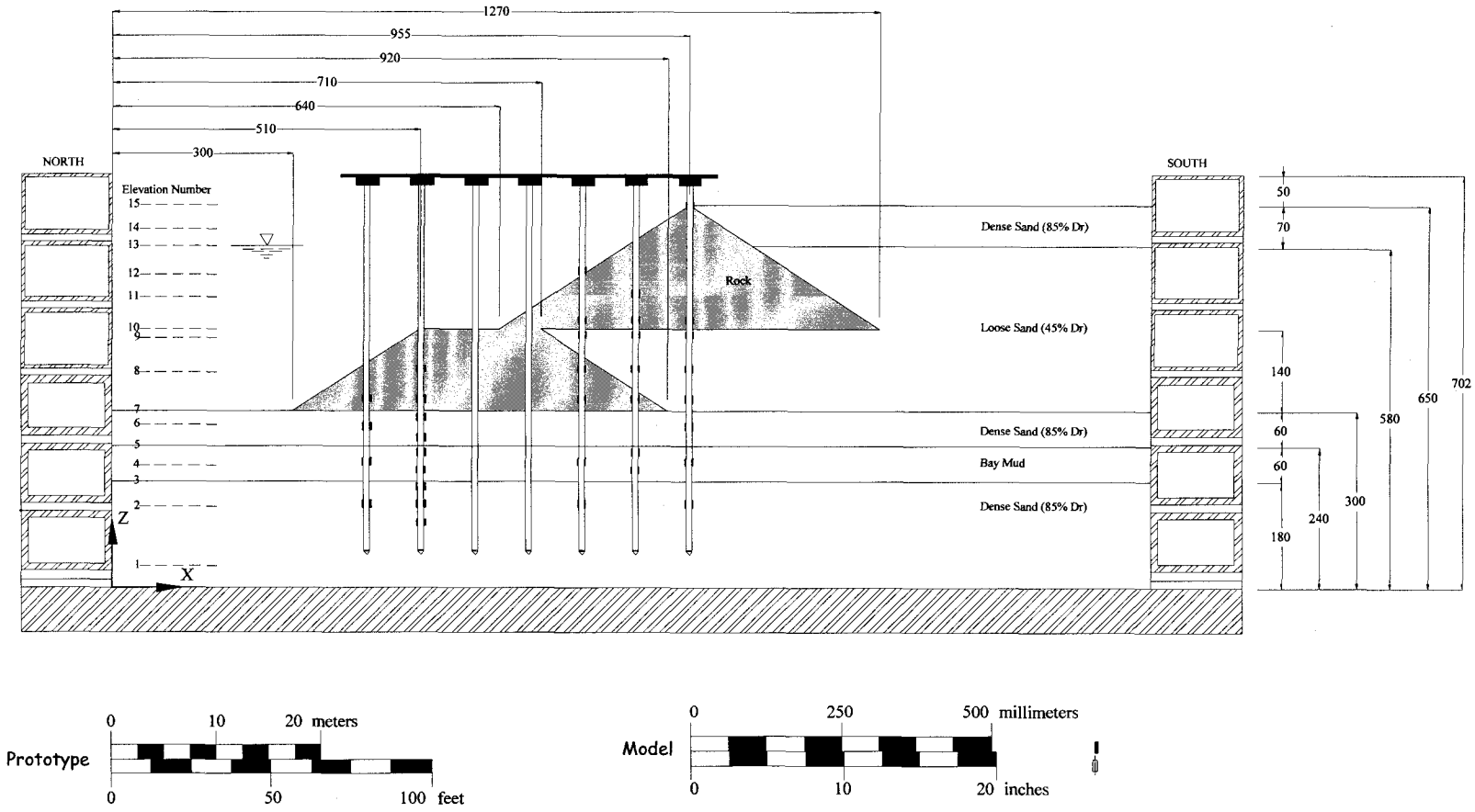

Figure 4-1: NJM02 soil profile and dimensions (mm)

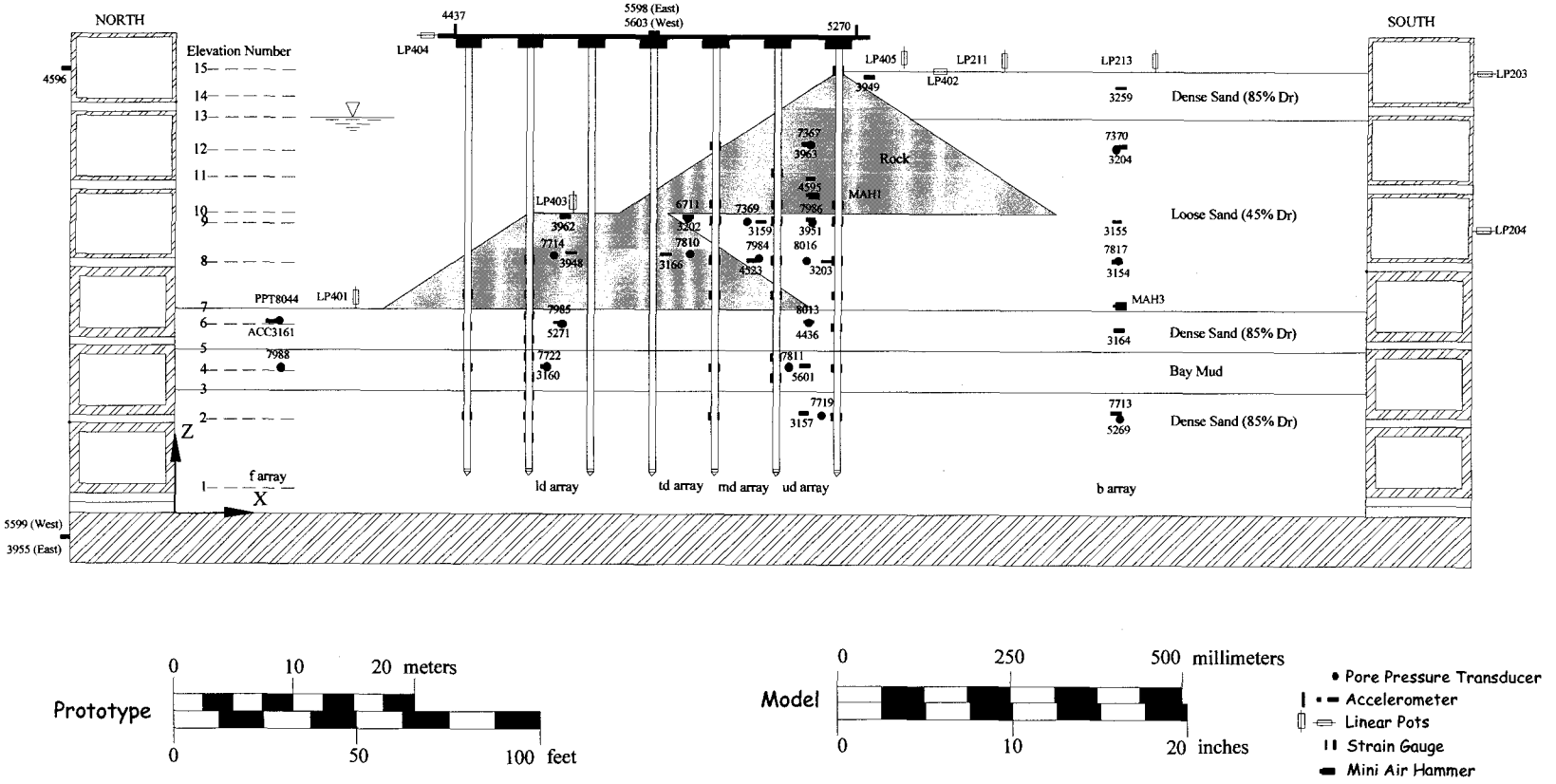

Figure 4-2: NJM02 cross-section with as built instrument locations and elevation labels

Table 4-1: NJM02 design elevation descriptions and dimensions

Elevation	*Description*	*Model Elevation (mm)*	*Prototype Elevation (m)*
0	Base of Model Box – Datum	0	0.0
1	Instrument Layer – Lower Dense Sand	60	3.4
2	Instrument Layer – Lower Dense Sand	140	8.0
3	Interface – Lower Dense Sand and Bay Mud	180	10.3
4	Instrument Layer – Bay Mud	210	12.0
5	Interface – Bay Mud and Middle Dense Sand	240	13.7
6	Instrument Layer – Middle Dense Sand	270	15.4
7	Interface – Top of Middle Dense Sand	300	17.1
8	Instrument Layer – Loose Sand and Rock	380	21.7
9	Instrument Layer– Loose Sand and Rock	430	24.6
10	Interface Layer – Upper and Lower Rock Dikes	440	25.1
11	Instrument Layer – Loose Sand and Rock	490	28.0
12	Instrument Layer – Loose Sand and Rock	540	30.9
13	Interface – Ground Water Table	580	33.1
14	Instrument Layer – Upper Dense Sand	615	35.1
15	Top of Soil Profile	650	37.1

4.2 INSTRUMENTATION

At the time of testing, the centrifuge facility had the ability to record approximately 90 channels of data. The use of these channels was split between four types of instrumentation to capture pertinent data for the chosen configurations. The following four types of instrumentation were used: 1) accelerometers, 2) pore pressure transducers, 3) linear potentiometers, and 4) strain gauges. Accelerometers were placed in the model to capture dynamic soil response. These accelerometers were also installed on the wharf to record structural response and on various rings of the box to monitor the dynamic behavior of the box in respect to the soil. Pore pressure transducers were placed throughout the models to monitor water levels and capture the buildup of excess pore pressure during dynamic events. Because the locations of the transducers were known, these instruments can provide information regarding how close a soil is to liquefaction. Linear pots provide direct readings of soil settlement

and horizontal wharf movement. Strain gauges can be used to provide a detailed moment profile with depth. The readings from these gauges can then be appropriately integrated to estimate pile deflections.

Instrumentation in the model was placed in a series of vertical arrays throughout the model to capture dynamic soil response with depth (Figure 4-2). The instrument array labels for each test are described in Table 4-2. A complete tabulation of all pre- and post-test instrument locations is included in the corresponding data report (Schlechter et al., 2000a).

Table 4-2: Instrument array labels and descriptions

Array Label	*Location*
"b array"	Backland Array
"ud array"	Upper Dike Array
"md array"	Mid-slope of Upper Dike Array
"td array"	Toe of Upper Dike Array
"ld array"	Lower Dike Array
"f array"	Front Array

The origin of coordinates for instrument position was located at the bottom, inside *northwest* corner of the FSB1 container. By convention, direction herein is determined by considering the stationary centrifuge arm to be a compass needle, with the bucket forming the north arrow. As illustrated in all model layouts within this thesis, "x" was positive in the south direction, "y" was positive in the east direction, and "z" was positive in the up direction.

The orientation of the instrumentation was noted to insure that a datum direction is maintained upon data reduction. For example, because of instrument location, the accelerometers on the box were orientated 180 degrees opposite the accelerometers in the model, and the horizontal linear pots measuring the movement on the outside of the box were orientated 180 degrees opposite the linear pot measuring the wharf displacement. The reduced and converted data presented within this report uses the notation that positive values of ground and/or wharf motion indicate positive x, y and

z directions. For example, all the data has been corrected so that a positive acceleration in the data is an acceleration in the positive x direction (i.e., moving from the bay toward the backfill), and a negative horizontal displacement is a displacement in the negative x direction. Pile moments have been converted such that when appropriately integrated to obtain displacements these displacements of the pile are consistent with the sign convention.

4.2.1 Accelerometers

Approximately 30 accelerometers were utilized during the testing model NJM02. The location of all recorded instruments are shown in Figure 4-2. Accelerometers were placed on each of the centrifuge loading arms that applied the earthquake motion to the FSB container in order to measure the input motion. Additionally, accelerometers were placed on the top ring of the box to measure the box behavior. All accelerometers placed in the soil were centered between the middle and eastern set of piles. One accelerometer was also embedded in the south end of the CDSM grid to obtain the response of the grid and it was placed in line with the accelerometers in the sand layers. The accelerometer (ACC) labels used within this thesis are consistent with their permanent UC Davis identification numbers.

4.2.2 Pore Pressure Transducers

Pore pressures within model NJM02 were monitored using 19 pore pressure transducers (PPTs) of which 17 were recorded at a time. As described later, two PPTs in loose sands were recorded in place of two of the instruments in the clay layer during the final three large shaking events. All PPTs placed in the soil during test NJM02 and those placed in the sand for SMS01 were centered between the middle and western set of piles. The PPTs were placed oriented in the y-direction (i.e. perpendicular to ground motion), so that any *sloshing* of the soil column into the head

of the PPT would not be measured. The pore pressure transducers are of type Druck Miniature Series # PDCR 81. The PPT labels used within this thesis are consistent with their permanent UC Davis identification numbers.

4.2.3 Strain Gauges

A total of 34 strain gauge locations were recorded for test NJM02: 6 on pile 1, 7 on pile 2, 7 on pile 3, 9 on pile 6, and 4 on pile 7. The recorded gauges and their relative elevations are shown in Figure 4-3 with the distance from the pile toe to each strain gauge shown in Table 4-3. The strain gauge labels are a combination of their respective pile numbers and elevation. The notation *pile toe* refers to the bottom of the pile without the pile tip (i.e., the end of the aluminum tubing). After the piles have been driven, the distances from pile toe to strain gauge location can be adjusted to model elevations by adding an adjustment factor. This adjustment accounts for the distance from the pile toe to the base of the model box. NJM02 model elevations were obtained by adding 70.65-mm to the distances given in Table 4-3.

Each gauge is composed of a pair of 6.35-mm (0.25-in) perpendicularly stacked gauges. A full bridge was completed at each elevation on the piles by connecting to the complimentary stacked gauge on the opposite side of the pile. The strain gauges were calibrated to measure moments by subjecting the piles to a known moment and measuring the voltage output in a controlled laboratory setting prior to the centrifuge testing. The strain gauges are Micromeasurements type CEA-13-125 WT-350.

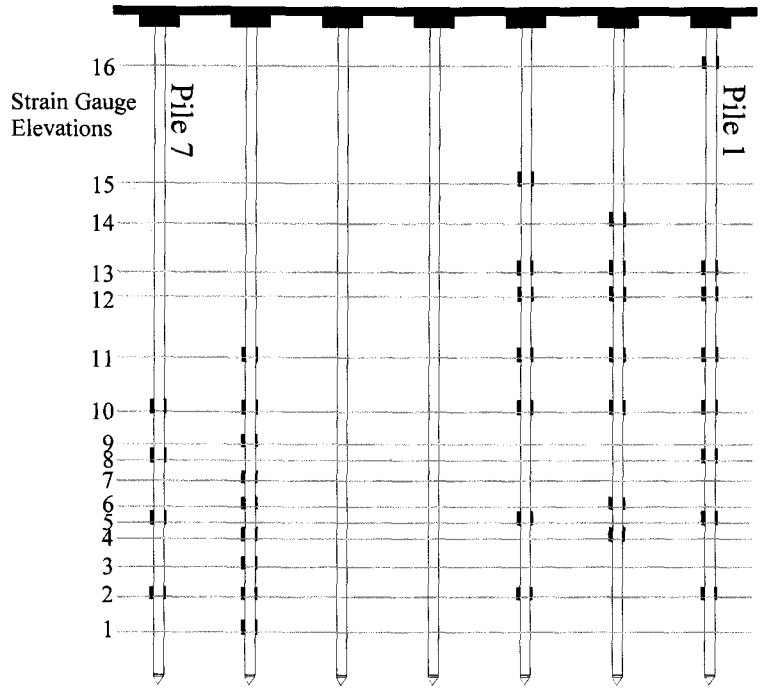

Figure 4-3: NJM02 strain gauge elevations

Table 4-3: Distances from the pile toe to each strain gauge (NJM02)

Instrument	Distance (mm)
SG1-2	76.5
SG1-5	149.75
SG1-8	208.75
SG1-10	256.5
SG1-11	304.25
SG1-12	364.25
SG1-13	389.75
SG1-16	584.25
SG2-4	133.75
SG2-6	165.0
SG2-10	254.15
SG2-11	306.25
SG2-12	364.5
SG2-13	389.7
SG3-2	78.25
SG3-5	150.5
SG3-10	256.5

Instrument	Distance (mm)
SG3-11	307.25
SG3-12	365.25
SG3-13	391
SG3-15	475
SG6-1	45
SG6-2	77.75
SG6-3	107.25
SG6-4	135.0
SG6-6	164.5
SG6-7	189.25
SG6-9	225.0
SG6-10	255.25
SG6-11	305.0
SG7-2	78.0
SG7-5	149.75
SG7-8	209.25
SG7-10	255.75

4.2.4 Linear Potentiometers

Linear potentiometers (linear pots) were used to measure both vertical and horizontal displacements within the models. Two linear pots measured the movement of the top and middle rings of the box, relative to the base of the box. The remaining linear pots were used to measure horizontal and vertical displacements within the model. These linear pots were attached to horizontal cross members mounted across the top ring of the box and therefore all movements are referenced to the top ring of the box. Their locations within the model can be seen in Figure 4-2. Horizontal displacements were measured with two linear pots. One of these horizontal linear pots was placed behind the wharf deck and measured displacements by using a thin aluminum plate that was inserted into the sand. The other linear pot measured the horizontal displacements of the wharf deck by attaching the instrument to a vertical member fastened to the wharf deck. Five linear pots were used to measure vertical displacements: three measured vertical displacements of the soil surface south of the wharf; one measured the vertical displacements of the top of the lower rock dike; and one measured the vertical displacements of the toe of the lower rock dike. Since all of the linear pots are referenced to the top ring of the box, absolute horizontal displacements are the sum of the linear pot within the model and the linear pot measuring the displacement of the top ring of the box. The linear pots used were Duncan Electronics 600 Series. The linear pot labels used within this thesis are consistent with their permanent UC Davis identification numbers.

5 NJM02 CENTRIFUGE MODEL CONSTRUCTION

The relative complexity of this model (including multi-layered soil profiles with clay, approximately 90 instruments, and a complete wharf structure) necessitated a rigorous model construction plan. The general construction sequence of the model is described in the chronological order it was built. A description of general techniques used to build the model will be included as the construction sequence is described. This construction sequence has been broken down into the following stages and is outlined below.

1) Placement of the lower dense sand
2) Initial saturation of the lower dense sand with de-ionized water
3) Placement and consolidation of the clay
4) Placement of the middle dense sand
5) Pile driving and superstructure installation
6) Placement of the lower rock dike
7) Placement of the lower loose sand
8) Placement of the upper rock dike
9) Placement of the upper loose sand
10) Placement of the upper dense sand
11) Saturation of the remainder of the model with HPMC

5.1 SAND PLUVIATION

Model construction involved air pluviation of Nevada Sand layers within the model container. These layers ended up with an undulating surface, which was leveled using a depth-controlled vacuum to ensure a uniform horizontal layer. The model was weighed after the completion of each full layer of soil using the facility's manual crane, lifting frame, and scale. The density of soil placed in each layer could then be estimated and used as a check against the pluviator calibration.

The calibration of the pluviator was performed by examining the relationship between the sand drop height, pluviator flow rate, and the density of the placed sand. The majority of the calibrations were performed using a 971-ml container. The calibrations were then intermittently checked using a much larger container (13,680-

ml) to ensure boundary effects of the smaller container were not affecting the calibration.

Two pluviation methods were utilized to place the sand layers at their appropriate densities. A *large* pluviator (Figure 5-1a) was used to place the dense sand layers and a *small* barrel pluviator (Figure 5-1b) was used to place the loose sand layers. The large pluviator drops sand over the complete width of the model box, while the barrel pluviator drops sand from a nozzle that is approximately 50-mm (2-in) in diameter. Difficulties were initially encountered using the small pluviator due to small debris (predominantly grass seeds) clogging the nozzle's mesh screen. This problem was later avoided by sieving the sand in three stages and frequent cleaning of the nozzle's mesh screen.

The calibration of the *large* pluviator gave dense sand relative densities of approximately 85 percent. Calibrations of the *small* pluviator during placement of the loose sand showed relative densities that varied between 41 and 53 percent, with an average relative density of approximately 45 percent.

a) 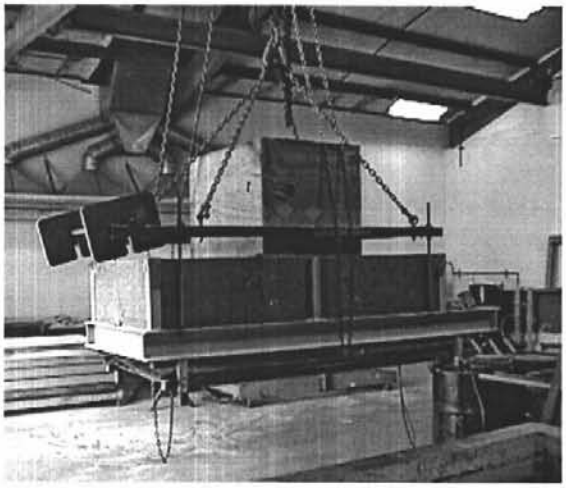 b) 

Figure 5-1: a) *Large* barrel pluviator b) *Small* barrel pluviator

5.2 INIITIAL SATURATION

The saturation procedure consisted of four processes: 1) de-air the available de-ionized water; 2) create a vacuum in the model box; 3) flood the sealed model box with carbon dioxide, and reapply the vacuum; and 4) introduce the fluid into the model box to complete saturation. The vacuums were created using a pneumatic vacuum regulator, with a maximum capacity of approximately 91-kPa (27-inHg). A description of these processes is provided below.

1) De-ionized water was introduced through a spray nozzle into a sealed holding tank (Figure 5-2) under vacuum (91-kPa), essentially creating de-aired, de-ionized water.

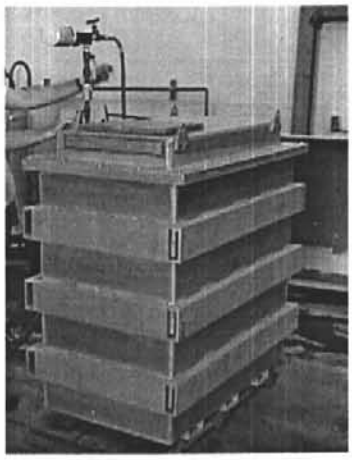

Figure 5-2: Fluid holding tank with pneumatic vacuum regulator

2) The maximum vacuum (91-kPa) was initially applied very quickly to seal a tight-fitting container lid (Figure 5-3) for a few seconds until the vacuum within the model box began to rise. After this initial jump, the vacuum was reduced to 17-kPa (5-inHg) and increased in 8.5-kPa (2.5-inHg) increments until 91-kPa was reached. This process removes approximately 97 percent of the air from the container and soil voids.

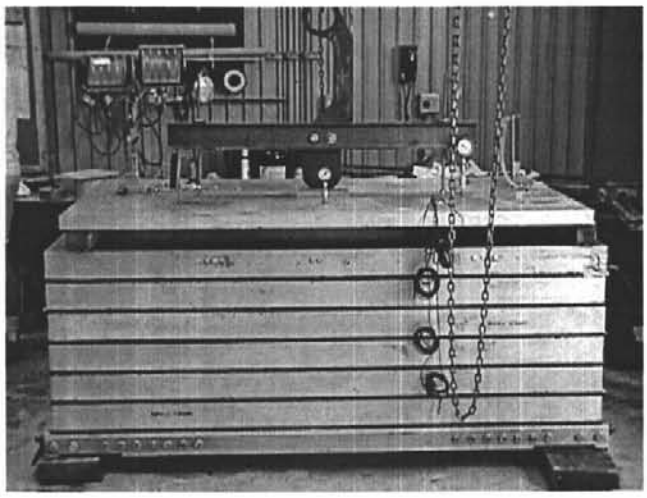

Figure 5-3: Model box and tight-fitting saturation lid

3) After the model box was under full vacuum, the vacuum line was closed, and carbon dioxide was allowed to flood into the model container as the vacuum was slowly released. After the box was fully saturated with carbon dioxide, the vacuum was again increased incrementally to 91-kPa. The carbon dioxide was introduced into the model due to its greater ability to dissolve in water. Applying the vacuum the second time removed approximately 97 percent of the carbon dioxide, with only an insignificant portion of the original air remaining.

4) The de-ionized, de-aired water was then drawn into the model box using hoses and a differential vacuum between the holding tank and the model box of approximately 24-kPa (7-inHg). The fluid dripped into trays at both ends of the model box to which six hoses were attached that ran to specified depths within the box. The saturation process was therefore gravity driven within the model box and saturation was allowed to continue until a film of water was visible at the top of the soil profile. The flow valve into the model was then shut-off and the fluid level was allowed to reach equilibrium. The vacuum was then slowly released, allowing any remaining voids to fill with the de-aired, de-ionized water.

After saturation of the lower dense sand layer, small sand boils were discovered along the wall in the southeast corner of the model during both tests. This suggests an

air leak occurred at one of the ring interfaces below this point. The effect of the sand boils on the saturation process will be described in section 6.5.2.

5.3 CLAY CONSOLIDATION

The clay used in the model was already stockpiled at the centrifuge facility. This clay was originally obtained from San Francisco Bay and is known locally as *Bay Mud*. The clay was thoroughly mixed in a 0.283-m^3 (10-ft^3) ribbon mixer Figure 5-4) until a uniform slurry was obtained. De-ionized water was then added until the water content of the slurry was 137 percent. Calculations were performed to estimate the magnitude of settlement that would occur during consolidation (both on the consolidation press and in the centrifuge). An appropriate layer thickness was then determined such that the final layer thickness (after consolidation) would match the design profile. In order to decrease the time to reach consolidation, the drainage path was shortened by dividing the clay layer into three sub-layers, with each sub-layer separated by a horizontal drainage layer. The horizontal drainage layers consisted of filter paper (Whatman chromatography, Chr1 paper) sandwiching horizontal sand columns laid out in a grid pattern (Figure 5-4). Care was taken to ensure the horizontal sand columns would not interfere with pile placement or significantly affect the overall clay strength.

The filter paper was also placed at the interface between the clay and dense sand layers to prevent mixing of the clay and sand layers. Before any clay was placed, aluminum sheets were attached at the north and south ends of the box to isolate the shear rods from the clay layer. These sheets were set approximately 50-mm (2-in) from the ends of the box. Sand was placed between the aluminum sheets and the box to allow fluid movement between the lower and middle dense sand layers. The clay was consolidated using a consolidation press with two large hydraulic cylinders (Figure 5-6). The corresponding data report (Schlechter et al., 2000 a) provides details

on the consolidation press and the calibration factors that were developed for its use during this test sequence.

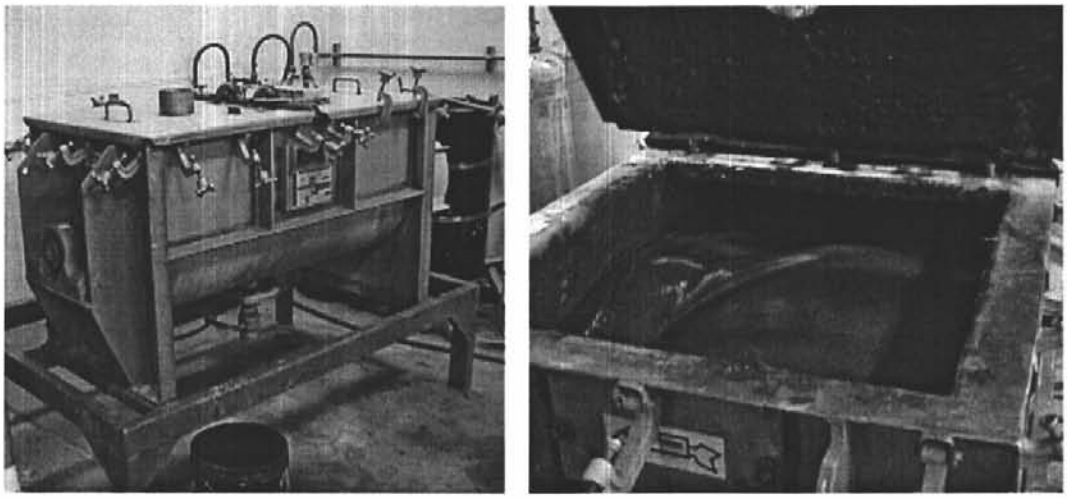

Figure 5-4: Ribbon mixer used to mix the clay

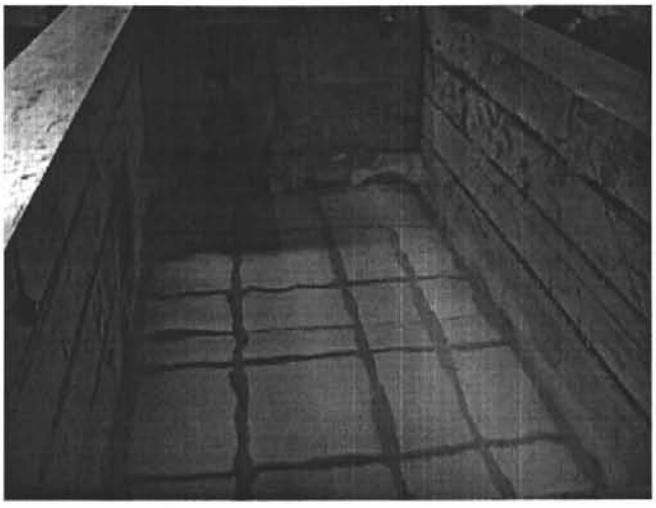

Figure 5-5: Drainage layer between clay sub-layers

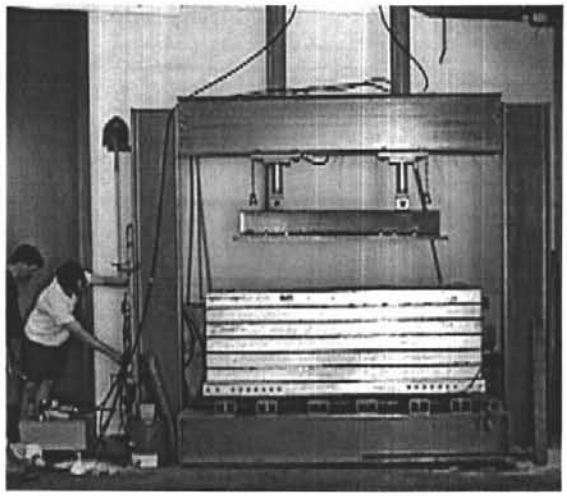

Figure 5-6: Model box on consolidation press

The clay placement followed several steps: 1) filter paper was placed on top of the lower dense sand; 2) a sub-layer of clay was placed on top of the filter paper; 3) the sub-layer was consolidated using the consolidation press; 4) a drainage layer was installed between sub-layers; 5) steps 2 through 4 were repeated for the remaining two sub-layers with the instruments being installed in the middle of the second sub-layer; 6) filter paper was placed on top of the clay layer to prevent the middle dense sand from mixing with the clay.

During the placement of each clay sub-layer, a steel screed was used to level the layer and provide a flat, horizontal surface for the consolidation press to apply the load. A 5-mm thick geocomposite was placed between the filter paper and the consolidation press steel plate to ensure adequate horizontal surface drainage during consolidation. The application of the consolidation pressure was incrementally increased until the desired consolidation pressure was reached. Settlement measurements were recorded using dial gauges. The consolidation press was also continually monitored to make sure that a uniform pressure was being applied. The data was periodically plotted and the next load increment was placed once the time to 90 percent consolidation had been reached for each load.

During NJM02, the clay was initially consolidated in the hydraulic press to obtain an OCR of 1.5 in the front of the model relative to the dredge line. After the consolidation of each clay sub-layer, a Torvane was used to evaluate the undrained shear strength at the top of each sub-layer. However, the pre-test clay strengths were not accurate representations of the clay strength during testing due to the consolidation and strength gain during centrifuge spin-up. Therefore, an effort was made to obtain clay strengths immediately after spin down following the last dynamic centrifuge test of the model. After a detailed surface profile was measured, the model was excavated in the backland along the west side of the box to the clay layer. Clay strengths were obtained with a Torvane in each of the sub-layers (exact depths were not noted). The averaged values are presented in Table 5-1.

Table 5-1: NJM02 post-test clay strengths

Location	*Strength (kPa)*	*Strength (psf)*
1st Clay Layer	28.7	600
2nd Clay Layer	24.9	520
2nd Clay Layer	27.8	580
3rd Clay Layer	28.7	600

Table 5-2: NJM02 clay strength variation with location in the model

x-location	*Strength (kPa)*	*Strength (psf)*
200	14.4	300
400	19.2	400
600	25.9	540
800	33.5	700
1000	30.6	640
1250	33.5	700
1400	28.7	600
1600	19.2	400

During the dissection process two days later (section 5.9), Torvane readings were again taken in the clay layers and are given in Table 5-2. The strengths obtained are

from approximately the top of each of the sub-layers and at the center of the box. It must be emphasized that all clay strengths presented herein are direct readings and conversions from Torvane calibrations. The strengths have therefore *not* been adjusted to account for the geometric scaling factor used to design the model.

5.4 PILE DRIVING AND WHARF PLACEMENT

After the clay, middle dense sand layers, and all corresponding instruments were placed, the pile-supported wharf was installed. Care was taken to align the wharf deck and piles parallel to their respective axes of the box to insure one-dimensional alignment with the primary direction of shaking. A four-piece template was attached at the approximate midpoint of the piles. This template helped insure that the piles were installed vertically so that any residual driving moment would be limited. A handheld rotary vibration device and considerable pressure were applied to the wharf deck to push the pile group through the middle dense sand and clay layers. However, it was found that the vibration from the vibration device and the pressure due to the weight of two researchers was not enough to push the pile group through the lower dense sand layer. Therefore, the wharf deck was removed and the piles were driven individually with a rubber mallet (Figure 5-7). Care was taken to ensure that the individual piles remained vertical. The wharf deck was then reconnected to the piles when all of the piles were slightly above their target elevations. The remainder of the driving was done with simultaneous blows from rubber mallets on opposite sides of the wharf deck until the target elevation was reached. Care was taken to orient individual piles (and their corresponding strain gauges) in the same direction so that the calibration sign could correctly be applied during data reduction.

For both tests, the wharf deck was then removed to make it possible to place the remainder of the soil and rock layers. The tops of the piles were temporarily sealed with tape to prevent sand from filling the piles during subsequent construction. The wharf deck was then reattached prior to testing.

Figure 5-7: Driving the piles through the template with a rubber mallet (NJM02)

5.5 PLACEMENT OF THE ROCKFILL AND REMAINING SANDS

Placement of the rock was calibrated so that a uniform rock placement could occur between the piles, and achieve a density representative of the field conditions. The rock was dropped from approximately 30-cm (1-ft) and tamped in 5-cm (2-in) layers. Box weights were measured before and after known volumes of rock were placed, and the dry density of the rock averaged 15.72-kN/m^3 (100-pcf). The lower rock dike was placed first, followed by the loose and improved sand in the backland up to elevation 9. The upper rock dike was then placed, followed by the rest of the loose and improved sands.

5.6 INDICATOR LAYERS

In addition to the electronic instrumentation, a variety of techniques were used to determine both vertical and horizontal displacements. Nevada sand was mixed with India ink to produce black sand that was placed in a thin layer at each instrument and

interface layer (Figure 5-8). The black sand was also inserted into thin wall brass tubes that were pushed vertically into the model (Figure 5-8). The brass tubes were 3.2-mm in (1/8-in) diameter and inserted at 100-mm intervals in the x direction. The brass tubes were then removed (with the help of an electric vibrating engraver), leaving vertical black sand columns within the model. The location of the black sand layers and columns were noted during construction and their locations were measured during the post-test dissection of the model. General deformation patterns could then be discerned through a comparison of the pre- and post-test locations.

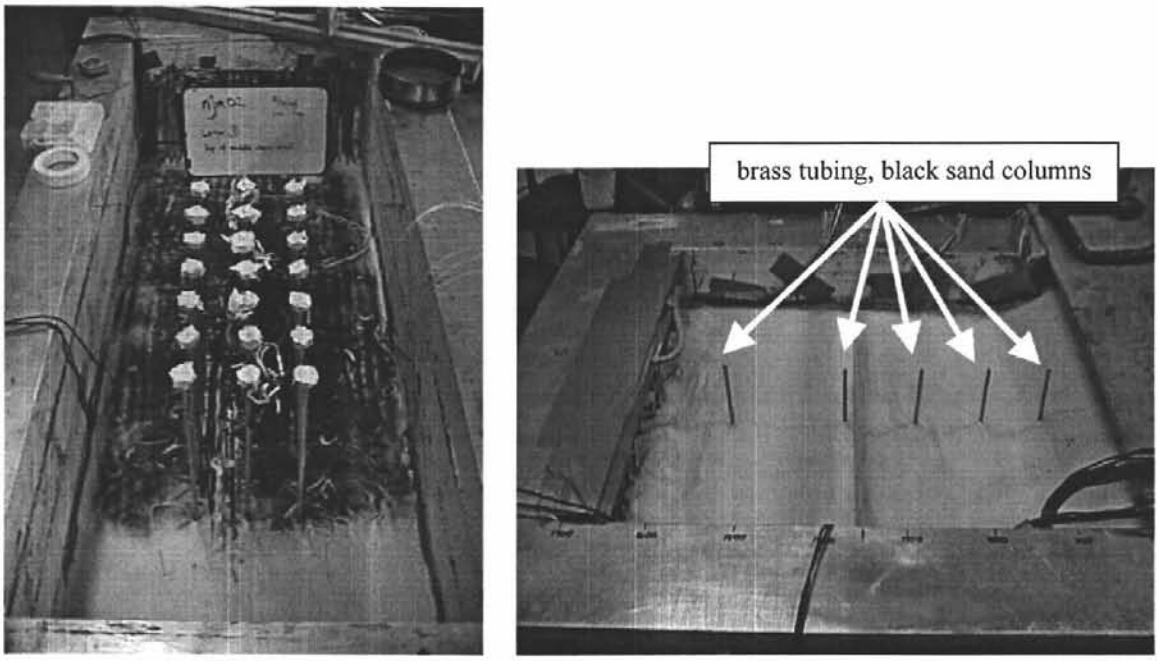

Figure 5-8: Black sand layer and black sand columns

Unfortunately, clay or moist sand from the lower layers plugged many of the brass tubes during insertion and the black sand was extracted along with the brass tubes instead of deposited as columns during NJM02. Spaghetti noodles were also placed vertically at similar intervals as the black sand columns. However, upon

dissection, it was noted that the spaghetti noodles were not visible as they had decomposed during the extended length of testing (Chapter 6).

5.7 SHEAR WAVE GENERATORS

To obtain in-flight shear wave velocity measurements, a series of "mini-" air hammers (MAH) were placed within the models. A mini-air hammer, as developed and tested by Arulnathan et al. (1999), consists of a 4.2-cm long, hollow aluminum cylinder with an outside diameter of 0.56-cm, with an internal, 1.9-cm long, Teflon piston (Figure 5-9). It is capped and fitted with air ports on both ends and is covered with epoxy and fine sand. These air hammers were positioned within the "ud" and "b" arrays. All MAHs were oriented along the x-axis of the container as shown in Figure 5-9. Details on their use in testing is provided in the section 6.2.3.

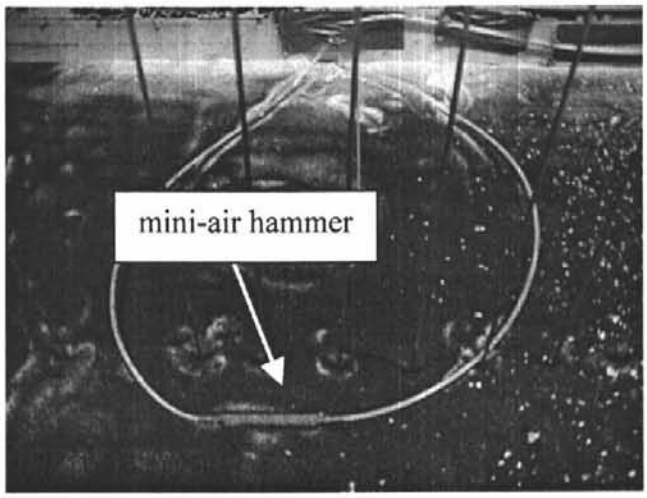

Figure 5-9: Mini-air hammer

5.8 SECONDARY SATURATION

After completion of the model construction, the box was moved down to the centrifuge (which is a self-contained underground facility) using a large forklift, and placed on the arm using an overhead electric crane (Figure 5-10). Secondary saturation of the upper model layers took place on the arm to limit disturbance to the model after saturation. The fluid for test NJM02 consisted of 2.25 percent HPMC by total weight, which when mixed with de-ionized water, produced a viscosity of approximately 4.7×10^{-5} m^2/s (47.6-cSt). Two percent (by weight of the HPMC) of benzoic acid was also added to the fluid as a preservative. The viscosity was measured with a size #2, No. C139, calibrated viscometer from the Cannon Instrument Co.

Figure 5-10: Moving the model box and placing it on the centrifuge arm

Saturation on the arm took place in a procedure similar to the initial saturation except that the model was not first flooded with carbon dioxide during secondary saturation. Saturation of the model on the arm took approximately three days and continued until the fluid level reached the target elevation. Since the lower layers (lower dense sand and the clay) of both models were saturated with water, it was

assumed that some mixing and dilution of the HPMC mixture would occur. Upon removal of the saturation lid, the viscosity was checked and found to have been reduced to 3.0 x 10^{-5} m^2/s (30-cSt). This reduction in viscosity is due to the mixing through the sand that was located at both ends of the clay layer (section 5.3). The viscosity remained constant throughout testing. The final saturated model on the arm is shown in Figure 5-11.

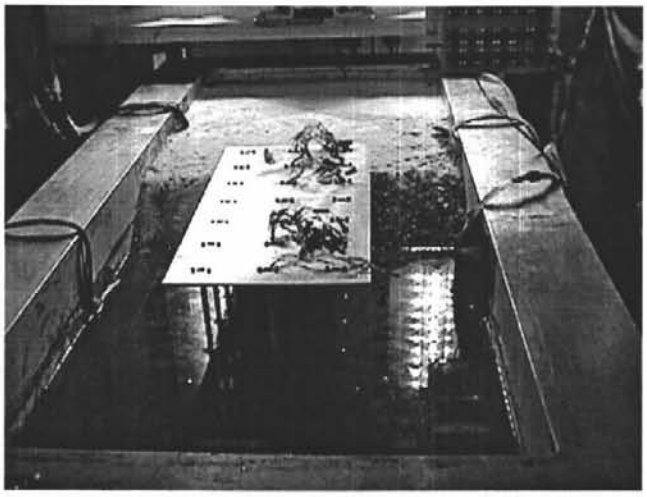

Figure 5-11: NJM02 model on the arm after final saturation

5.9 POST-TEST DISSECTION

After all of the dynamic tests were performed and surface profiles were measured, the model was drained of the majority of the fluid while still on the arm of the centrifuge. The model was unloaded from the arm and brought back to the model preparation room using the large forklift and overhead crane. At this point, the model was carefully *dissected* to obtain accurate deformation profiles and insights to model behavior. For example, locations of the black sand columns were carefully measured and recorded. Detailed photographs were taken of the entire procedure. Selected examples are provided in Figure 5-12. A careful profile is taken of the black sand

layers placed in the model for comparisons to pretest locations. These measurements are available in the corresponding data reports.

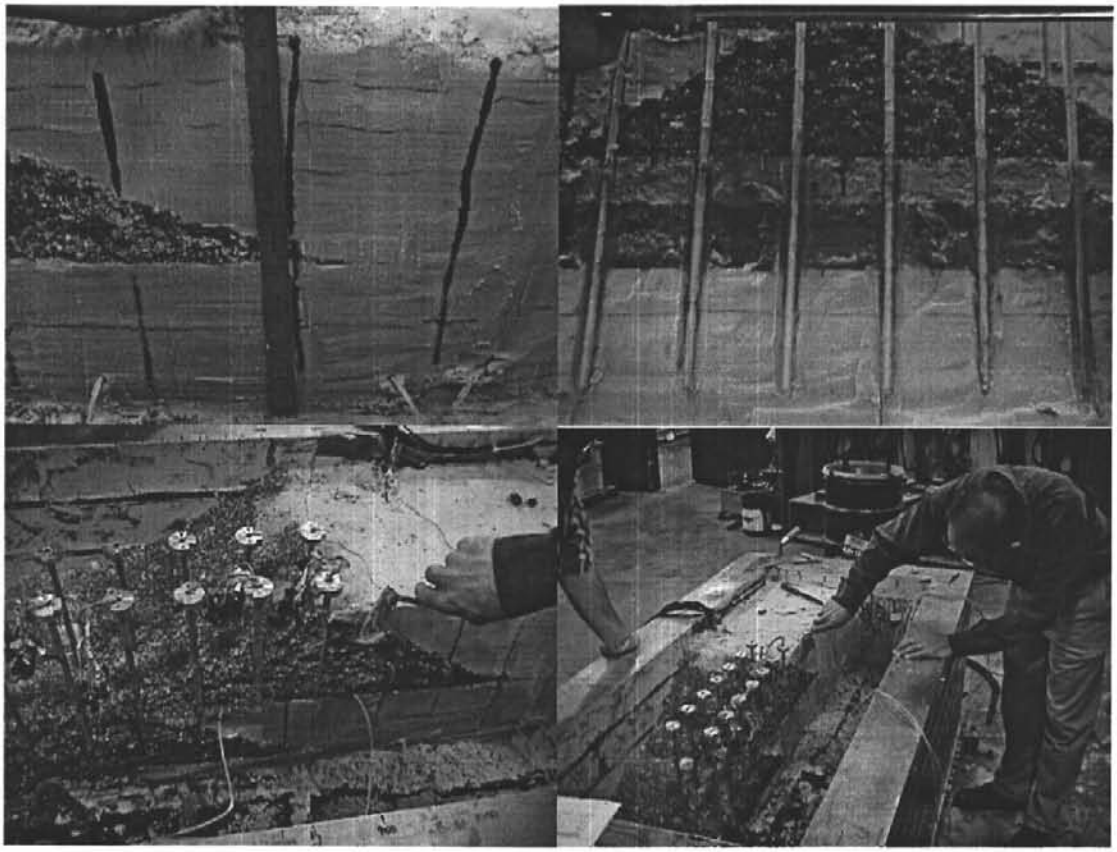

Figure 5-12: Examples of dissection cross sections

6 TESTING OF CENTRIFUGE MODEL NJM02

The complete description of the test sequence of model NJM02 will be described within this chapter. All earthquake motions and shear wave velocity tests run on the model are outlined along with their corresponding test numbers. The presentation of all data within the report and on the CD is described with explanations of the data reduction and organization.

6.1 NJM02 TEST SEQUENCE

6.1.1 July 29th and 30th Testing

On July 29, 1999, the centrifuge was spun up and the model was allowed to consolidate under the increased stresses due to centrifugal acceleration. The pore pressures in the soft clay were closely monitored to avoid a static failure and the acceleration levels were incrementally increased to 40-g. At the completion of clay consolidation, shear wave velocity tests were conducted using the miniature air-hammers and the accelerometers. After these tests, a small dynamic loading (peak input acceleration of approximately 0.04g) was applied and data was recorded. However, there were problems with the shaker sequencers that made it impossible to apply additional shaking events. After multiple attempts to solve the problem, the test was discontinued and the model spun-down for the evening.

On the morning of July 30th, the model was spun back up and reconsolidated. However, the shaker problems from the previous day were still occurring. In addition, a portion of the data acquisition system was malfunctioning. The signals from 16 channels of data were being corrupted due to a problem with one of the tech filters that is used to filter the data on the centrifuge. The spin was abandoned until the problems could be solved. Over the course of the next week, a variety of additional amplifier problems were identified and repaired. The source of the tech filter problem

was not yet known and a 16 channel, dual cascading, RC filter was built as a substitute (Section 6.5.3).

6.1.2 August 6th Testing

The model was then spun up again on August 6, 1999. A summary of the test sequence on August 6th is provided in Table 6-1. This table provides a time history of all recorded data. The file names and descriptions of all shaking events are included with their corresponding data files. The amplification factor columns refer to the number input into the computer for each shaker arm to obtain the desired acceleration within the model. A column is also included for comments on pertinent details during the testing sequence (e.g. changes in acceleration). Pore pressures in the clay were continuously monitored during spin-up and shaking.

Two *small* shakes and three *large* shakes (from a total of three different earthquake motions) were run in NJM02. Reference to *small* and *large* shakes refer to the relative magnitude of the input amplification factors and recorded accelerations for each event. The complete test sequence for all available NJM02 data is outlined in Table 6-2. The presentation of data is outlined in the following section. Test njm02_32 was shaken with the step motion (which was a basic step wave input motion). The two other earthquake motions were actual recorded earthquake motions. Loma2.txt was recorded at the Oakland Outer Harbor station during the 1989 Loma Prieta Earthquake and the north2.txt was recorded at the Rinaldi station during the 1991 Northridge Earthquake. Other than intensity scaling and slight adjustments in frequency content to match shaker capabilities, the motions are uncorrected. Because of problems with the base input shaker, test 34 used an earthquake motion that combined the loma2.txt and north2.txt input motions into one small shake, with the data being recorded and converted in a single file. For presentation purposes, this data file was split and presented herein as tests 34_A and 34_B. Test 42 was a large shake of the loma2.txt

earthquake motion and tests 49 and 55 were large shakes using the north2.txt input motion.

Table 6-1: NJM02 data from small and large shakes

Data File	Input Motion	Average Peak to Peak Acceleration (g)
njm02_32	Step Wave (step.txt)	0.054
njm02_34A	Northridge Rinaldi – First half of combined input motion file (N2_L2.txt)	0.058
njm02_34B	Loma Prieta – Second half of combined input motion file (N2_L2.txt)	0.075
njm02_42	Loma Prieta Outer Harbor (loma2.txt)	0.318
njm02_49	Northridge Rinaldi (north2.txt)	0.806
njm02_55	Northridge Rinaldi (north2.txt)	1.052

6.2 NJM02 Testing Details

6.2.1 Pre-Shake Activities

While the model was sitting on the arm, a rubber mallet was struck against the side of the container base-plate and the response of the accelerometers was monitored. This test was performed to determine if all of the accelerometers were responding prior to the centrifuge spinning. Voltage readings from the pore pressure transducers were adjusted based on instrument calibrations to reach an approximate zero while under 40-g.

Table 6-2: NJM02 testing day event summary

Date	Time	Centrifuge rpm	Centrifuge Acc at the 1/3 model depth	Input file name	Description	West ampl. factor	East ampl. factor	Channel gain list (cgl) used	Raw output file	Comments / Details
8/6	8:21 AM	0	0.0					slw03.cgl	njm02_22.slw	Start slow data
	8:40 AM	32.2	9.9					slw03.cgl	njm02_22.slw	Reached 10 g's
	9:35 AM	49.3	23.1					slw03.cgl	njm02_22.slw	Move up to 25g
	11:45 AM	49.9	23.7					slw03.cgl	njm02_22.slw	Start up to 40 at 11:47
	11:58 AM	64	39.0					slw03.cgl	njm02_22.slw	Just reached 40g's
	12:50 PM	65.8	41.2					shwv02cgl	njm02_23.out	Shear wave test
	12:53 PM	65.8	41.2					shwv01.cgl	njm02_24.out	Shear wave test (back array)
	12:55 PM	65.8	41.2					shwv02.cgl	njm02_25.out	Shear wave test (ud array)
	12:58 PM	65.8	41.2					shwv02.cgl	njm02_26.out	Shear wave test (ud array)
	1:16 PM	65.6	40.9					slw03.cgl	njm02_27.slw	Start taking slow data again (stopped at 1:27)
	1:35 PM	66.2	41.7					pwv01.cgl	njm02_28.out	Attempt to capture p-wave
	1:42 PM	65.9	41.3					pwv01.cgl	njm02_29.out	Try p-wave again
	1:51 PM	65.6	40.9					slw03.cgl	njm02_30.slw	Start taking slow data again
	2:55 PM	65.4	40.7					slw03.cgl	njm02_31.slw	Take more slow data (stopped to test a motion then restarted)
	3:06 PM	65.2	40.4					slw03.cgl	njm02_31.slw	Stop taking slow data
	3:11 PM	65.4	40.7	step.txt	step wave	3	3	fst05.cgl	njm02_32.out	
	3:42 PM	38	13.7							Run the shaker arm slowly through a full range of motion
	3:45 PM	54	27.7					slw03.cgl	njm02_33.slw	Take slow data as spinning up
	3:55 PM	65.6	40.9					slw03.cgl	njm02_33.slw	
	4:50 PM	65.9	41.3					slw03.cgl	njm02_33.slw	
	5:00 PM	65.9	41.3	N2_L2.txt	Combined Northridge and Loma Prieta motions	1	1	fst05.cgl	njm02_34.out	
	5:04 PM		0.0					slw03.cgl	njm02_35.slw	Take slow data as we are spinning down (stopped at 5.6g's)
	5:57 PM	0	0.0					slw03.cgl	njm02_36.slw	Note: The two PPT's in the clay were switched before this spin up. (Section **Error! Reference source not found.**)
	6:10 PM	34	11.0					slw03.cgl	njm02_36.slw	Wait for consolidation at 10 g's
	6:24 PM	50.5	24.3					slw03.cgl	njm02_36.slw	Wait for consolidation at 25 g's
	7:00 PM	51.9	25.6					slw03.cgl	njm02_36.slw	Start moving up to 40 g's
	7:10 PM	65.8	41.2					slw03.cgl	njm02_36.slw	Reached 40 g's
	7:40 PM	66.5	42.1					shwv01.cgl	njm02_37.out	Shear wave test (back array)
	7:40 PM	66.5	42.1					shwv01.cgl	njm02_38.out	Shear wave test (back array)
	7:42 PM	66.5	42.1					shwv02.cgl	njm02_39.out	Shear wave test (ud array)

Table 6-2 (Continued)

Date	Time	Centrifuge rpm	Centrifuge Acc at the 1/3 model depth	Input file name	Description	West ampl. factor	East ampl. factor	Channel gain list (cgl) used	Raw output file	Comments / Details
	7:59 PM	65.4	40.7					slw03.cgl	njm02_41.slw	Start taking slow data again
	9:12 PM	65.9	41.3	loma2.txt	Loma Prieta Outer Harbor	1	1	fst05.cgl	njm02_42.out	
	9:14 PM	65.8	41.2					slw03.cgl	njm02_43.slw	Start taking slow data at 40 g's and then spinning down to reset sequencer
	9:35 PM	26.7	6.8					slw03.cgl	njm02_43.slw	Begin back up (did not have too spin completely down)
	9:48 PM	65.6	40.9					slw03.cgl	njm02_43.slw	Just reached 40g's
	10:00 PM	66.9	42.6					shwv01.cgl	njm02_44.out	Shear wave test (back array)
	10:02 PM	66.4	41.9					shwv01.cgl	njm02_45.out	Shear wave test (back array)
	10:05 PM	66.4	41.9					shwv02.cgl	njm02_46.out	Shear wave test (ud array)
	10:07 PM	66.4	41.9					shwv02.cgl	njm02_47.out	Shear wave test (ud array)
	10:12 PM	66.3	41.8					slw03.cgl	njm02_48.slw	Restart slow data
	10:45 PM	65.9	41.3	north2.txt	Northridge Rinaldi motion	0.7	0.7	fst05.cgl	njm02_49.out	
	10:55 PM	66	41.4					slw03.cgl	njm02_50.slw	Back up to 40 g's (quit for shear wave velocity)
	11:05 PM	66.9	42.6					shwv01.cgl	njm02_51.out	Shear wave test (back array)
	11:06 PM	66.9	42.6					shwv01.cgl	njm02_52.out	Shear wave test (back array)
	11:06 PM	66.9	42.6					shwv02.cgl	njm02_53.out	Shear wave test (ud array)
	11:06 PM	66.9	42.6					shwv02.cgl	njm02_54.out	Shear wave test (ud array)
	11:15 PM	65.9	41.3	north2.txt	Northridge Rinaldi motion	0.95	0.95	fst05.cgl	njm02_55.out	
	11:30 PM	66	41.4					shwv01.cgl	njm02_56.out	Shear wave test (back array)
	11:35 PM	66	41.4					shwv01.cgl	njm02_57.out	Shear wave test (back array)
	11:37 PM	66	41.4					shwv02.cgl	njm02_58.out	Shear wave test (ud array)
	11:40 PM	66	41.4					shwv02.cgl	njm02_59.out	Shear wave test (ud array)
	11:39 PM		0.0					slw03.cgl	njm02_60.slw	Spinning down (stopped at 5 rpm)

6.2.2 *Changes in Data Acquisition Procedures Between Small and Large Shakes*

The accelerometer amplifiers were set with a gain of 10 for *small* shakes. These gains were switched to 1 for *large* shakes during the spin down period prior to test 35. All converted data accounts for these changes in amplifier gain settings. A change was also made between small and large shakes to obtain additional pore pressure data in the sand during large shakes. Two of the pore pressure transducers (PPT 7988 and PPT 7811) in the clay were recorded during the consolidation and small shakes, but were swapped with PPT 7984 and PPT 7370 in the sand during the large shakes.

6.2.3 *Shear Wave Velocity Tests*

In-flight shear wave velocity testing was performed in the model using the mini-air hammers installed in the model (section 0). They were triggered remotely during the test introducing high-frequency shear waves to the model. These shear waves were recorded by the accelerometers in the targeted arrays. Air hammer/shear wave velocity tests were conducted before and after most shaking events.

An example of the data obtained from the shear wave velocity tests is shown in Figure 6-1. The appearance of multiple waveforms is due to the fact that both shear hammers in the model fire simultaneously. Therefore, a corresponding number of propagating waves are recorded, with only the first waveform being relevant in estimating the shear wave velocities.

It should be noted that instrument locations change during the testing sequence due to behaviors such as post liquefaction volume change, clay consolidation, and permanent lateral displacements. A correct interpretation in calculating the shear wave velocities should include a careful examination of the "pre-" and post-test instrument locations for an estimation of their location during the shear wave velocity tests. During test NJM02, shear wave velocity tests were run before and after most large

shakes. An in depth study of the shear wave velocity data has not been completed, however, it is the author's opinion that the instrument locations from tests after the first large shake to before the final large shake must be examined carefully to obtain accurate shear wave velocities. For example, a 5-mm difference in instrument location can induce an uncertainty in shear wave velocities on the order of 8-percent and some instruments moved up to 25-mm. However, the shear wave velocity tests recorded after the final large shake are accurate as the instrument locations are recorded during dissection directly afterward.

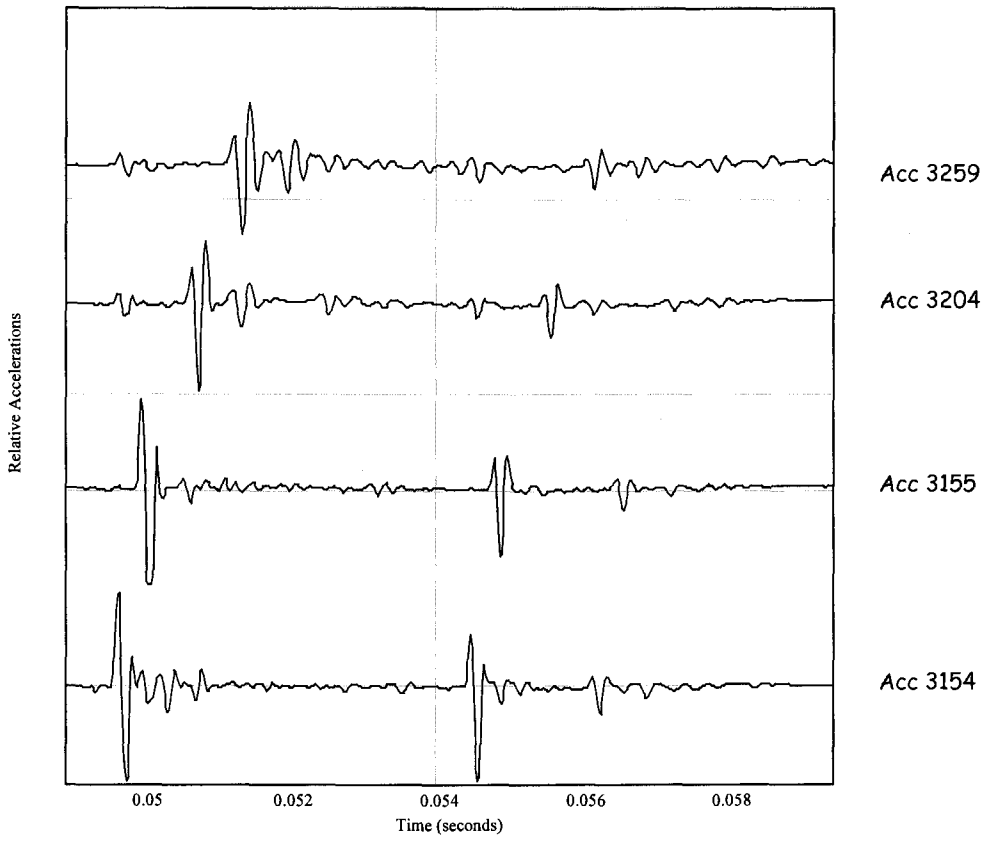

Figure 6-1: Shear wave velocity test results from NJM02

For the initial shear wave tests after spin-up and during small shakes, it is possible to make an estimate based on vertical settlements obtained during settlement

by assuming the settlements recorded up to this point are only due to clay consolidation. However, observations during centrifuge model SMS02, a model constructed later in this test series which was composed of only sand layers, showed approximately 5-mm of settlement without applying any dynamic events. This observation suggests some settlement in the previous models could have occurred between the instruments in the sand and a slight adjustment to the distances between instruments may be necessary when analyzing the initial shear wave velocity tests.

6.3 DATA ACQUISITION AND ORGANIZATION

The data acquisition system recorded a total of 89 channels for both tests. The term "channel" is used to refer to data being recorded from a single instrument. As described earlier (Section 6.1.1) the first 16 channels of strain gauges were recorded through an RC lowpass filter during NJM02. Channels 17-59 included filtering of instrument output using 5^{th} order programmable analog, low-pass filters prior to analog-to-digital (A/D) conversion. These filters are otherwise known as *tech filters* in this report and were set with a cut-off frequency generally equal to 40% of the sampling frequency to avoid signal aliasing. For example, if the sampling frequency was 2000Hz, the corresponding cutoff frequency would be 800 Hz. Thirty accelerometer channels were recorded but were not filtered before A/D conversion. All signals requiring amplification were amplified at the bucket except for the following PPT's: 7367, 7713, 7719, 8044, 7722, 7985, and 7714 during test NJM02. These channels were amplified at the center of the arm. Linear pots did not require signal amplification.

Small shakes and *large* shakes were sampled at different frequencies and durations to capture an appropriate amount of information. Sampling durations and frequencies are summarized in Table 9-3. For test NJM02, *small* shakes were typically recorded at 2000 Hz for 1 second. However, test 34 is an exception, as two input motions were combined and a longer duration was required to acquire all data. All *large* shakes were recorded at three frequencies and durations to capture the extended

duration of large excess pore pressures that accompany robust input motions. Shear wave velocity tests were recorded at 50 kHz.

Table 6-3: NJM02 sampling durations and frequencies (at model scale)

Data File	Frequency and Duration 1	Frequency and Duration 2	Frequency and Duration 3
njm02_32	2000 Hz, 1 sec	NA	NA
njm02_34	2000 Hz, 2 sec	NA	NA
njm02_42	2000 Hz, 1.5 sec	2000 Hz, 5 sec	10 Hz, 5 sec
njm02_49	2000 Hz, 1.5 sec	2000 Hz, 5 sec	10 Hz, 5 sec
njm02_55	2000 Hz, 1.5 sec	2000 Hz, 5 sec	10 Hz, 5 sec

The raw data was collected in two types of files. *Slow* data monitors instrument behavior during spin up, spin down, and between shaking events. This data was recorded directly as voltage readings and labeled as njm02_**.slw. Converted slow data is presented in *pseudo-prototype* units based on the geometric and centrifuge scaling factors used in each test. However, the data is not correct in absolute units unless the entire file was recorded at 40-g due to centrifuge scaling laws. For example, many of the slow data files include data from spin up and spin down (i.e., during a step-wise variation in the centrifugal acceleration). In these cases, the data only provides a relative picture of what happens during these periods between shaking events.

The second type of data is referred to as *fast* data. *Fast* data was recorded as binary offset data for the p-wave, shear wave, *small* shakes, and *large* shakes (njm02_**.out). The binary offset data is a relative value between 0 and 4096, which represents a range of 20 volts centered at 2048, so that:

$$Data_{volts} = \frac{Data_{binary\ offset} - 2048}{4096} \cdot 20\,volts$$

The *fast* data, has been converted from binary offset to volts. All slow and fast data was then converted from volts to representative prototype or model units based on instrument calibrations and amplifier gains. Appropriate centrifuge and geometric scaling factors are also included when converting to prototype units. None of the data has been zeroed during conversion. However, the following corrections were made:

- The signs of the accelerometers have been adjusted to be relative to each other and consistent with the direction of shaking (positive values are in the positive x and z directions).
- The signs of the linear pot calibrations were modified to have movement consistent with the positive axes as described previously (positive values are in the postive x and z directions).
- Small offsets in the data within a single test that occurred at changes in sampling frequency have been corrected.

After conversion, all data files have been converted to "njm02_**.dat" files. All slow and fast data recording was labeled sequentially starting at number one to maintain a time history. However, the NJM02 files start at test 22 because the data from the attempted July tests are not presented. The *slow* results are differentiated from the *fast* files upon conversion by appending "slw" to the beginning of the file name.

Caution must be used when analyzing instrument behavior between tests over the entire earthquake series due to changes in data that do not represent actual performance. For example, the author may have changed some instrument "zeros" between small and large shakes as the centrifuge was spun down. Amplifier zeros may also change after they have been shut down and repowered between separate days of shaking. These offsets in the data are most easily found by plotting the slow and fast data from a single instrument over the entire test sequence and comparing this record to the event summary table.

6.3.1 Plotted Data Presentation

The results of all recorded data has been plotted using a common format and template. Due to the large amount of the data, these plots will not be included within the hardcopy of the report, but are made available in Adobe Acrobat format on the accompanying CD. An example of this format is provided in Figure 6-2. All data plotted in this format has been converted to prototype units using appropriate centrifuge and geometric scaling factors. Each test requires 17 pages to plot all 83 channels of data. Titles of these data report pages and their corresponding instruments are given in Table 6-4. Data from the six bad strain gauge channels were recorded but are not included in the data reports. These channels correspond to the following strain gauges: SG 1-2,1-5,1-8,1-10, 2-6, and 3-2.

At the bottom right corner of each page, the output file name corresponding to an event and a description of the plotted instruments are given. It should be noted that the example provided is shown in a portrait view, however the descriptions provided within describe a landscape format. The bottom left corner of each page contains a label "Vertical Scale = ... units" which refers to the prototype-unit increment represented by the distance between tick marks on the ordinate axis, where the units correspond to the respective instruments of each page. The base accelerometer is plotted as the bottom instrument of every sheet. The final label at the bottom of the page "Base_ACC= "(not) to scale" refers to whether or not the base accelerometer is plotted to scale relative to the remainder of the instruments on the page. The top of each page contains the following three labels: "Instrument" which lists the type and labeling number of each instrument. "Units" lists the units of each instrument plotted (either "g", "N*m", "kPa", or "mm". "Peak to Peak" gives the peak to peak response in prototype units of each instrument. Labels read from left to right correspond to instruments plotted from the bottom to the top of the page. Each instrument's signal was zeroed for plotting purposes (the actual data is not zeroed). The time axis on the plots is in prototype units and has been truncated for a clearer representation of the data.

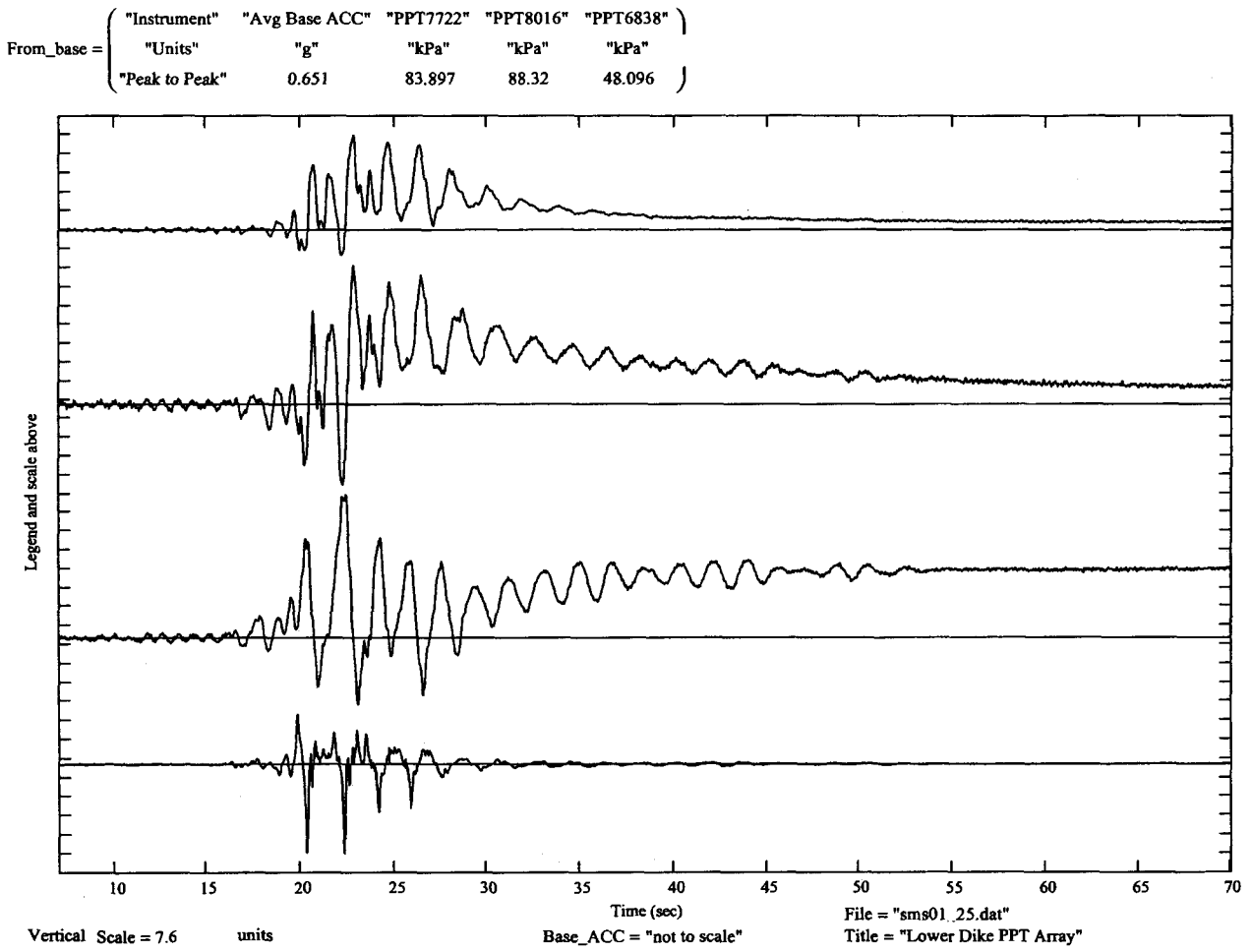

Figure 6-2: Example of data report page layout

Table 6-4: NJM02 data sheet instrument identifications

Description of data sheet instruments	Instrument Identifications (Small Shakes)	Instrument Identifications (Large Shakes)
Pile 1 Strain Gauges	SG1-11, SG1-12, SG1-13, SG1-16	SG1-11, SG1-12, SG1-13, SG1-16
Pile 2 Strain Gauges	SG2-4, SG2-10, SG2-11, SG2-12, SG2-13	SG2-4, SG2-10, SG2-11, SG2-12, SG2-13
Pile 3 Strain Gauges	SG3-5, SG3-10, SG3-11, SG3-13, SG3-13, SG3-15	SG3-5, SG3-10, SG3-11, SG3-13, SG3-13, SG3-15
Pile 6 Strain Gauges	SG6-1, SG6-2, SG6-3, SG6-4, SG6-6, SG6-7, SG6-9, SG 6-10	SG6-1, SG6-2, SG6-3, SG6-4, SG6-6, SG6-7, SG6-9, SG 6-10
Pile 7 Strain Gauges	SG7-2, SG7-5, SG7-8, SG7-10	SG7-2, SG7-5, SG7-8, SG7-10
Back PPT Array	PPT 7713, PPT 7817	PPT 7713, PPT 7817, PPT 7370
Upper Dike PPT Array	PPT 7719, PPT 7811, PPT 8013, PPT 8016, PPT 7986, PPT 7367	PPT 7719, PPT 8013, PPT 8016, PPT 7986, PPT 7367
Toe and Middle of the Upper Dike PPT's	PPT 7810, PPT 7984, PPT 7369	PPT 7810, PPT 6711, PPT 7984, PPT 7369
Lower Dike and Front PPT Arrays	PPT 7722, PPT 7985, PPT 7714, PPT 7988, PPT 8044	PPT 7722, PPT 7985, PPT 7714, PPT 8044
Back ACC Array	ACC 5269, ACC 3164, ACC 3154, ACC 3155, ACC 3204, ACC 3259	ACC 5269, ACC 3164, ACC 3154, ACC 3155, ACC 3204, ACC 3259
Upper Dike ACC Array	ACC 3157, ACC 5601, ACC 4436, ACC 3203, ACC 3951, ACC 4595, ACC 3963, ACC 3949	ACC 3157, ACC 5601, ACC 4436, ACC 3203, ACC 3951, ACC 4595, ACC 3963, ACC 3949
Toe and Middle of the Upper Dike ACC's	ACC 3166, ACC 3202, ACC 4523, ACC 3159	ACC 3166, ACC 3202, ACC 4523, ACC 3159
Lower Dike and Front ACC Arrays	ACC 3160, ACC 5271, ACC 3948, ACC 3962, ACC 3161	ACC 3160, ACC 5271, ACC 3948, ACC 3962, ACC 3161
Horizontal Linear Pots	LP 203, LP 204, LP 404, LP 402	LP 203, LP 204, LP 404, LP 402
Vertical Linear Pots	LP 405, LP 211, LP 214, LP 403, LP 401	LP 405, LP 211, LP 214, LP 403, LP 401
Wharf ACC's	V ACC 4437, V ACC 5270, ACC 5598, ACC 5603	V ACC 4437, V ACC 5270, ACC 5598, ACC 5603
Box ACC's	ACC 3955, ACC 5599, ACC 4596	ACC 3955, ACC 5599, ACC 4596

6.3.2 Raw and Converted Data Presentation

The data is also included on the CD-ROM in three (unplotted) formats: 1) the raw, unconverted, uncorrected data; 2) the converted data in model units; and 3) the converted data in prototype units. Files in model units may be differentiated from prototype files with the addition of "_m" before the file extension (e.g., njm02_42_m.dat). The raw data files have the "*.out" or "*.slw" extensions already described. The data files do not include a header that gives information on the instruments. Therefore, the appendices provide tables identifying each data column for all earthquake and shear wave velocity tests.

A table in Appendix A shows which column of data represents which instrument for each *small* or *large* shaking event. In the converted data (either model or prototype units), a time scale has been appended to the data file and is in the extreme right hand column. The data from the shear wave velocity tests has not been converted, but the heading includes the frequency at which the data was recorded, from which a time scale can be obtained.

6.4 NJM02 Malfunctioning Channels or Instruments

- Data Columns 1-4, 10, and 16, (SG 1-2,1-5,1-8,1-10, 2-6, and 3-2), were recorded with no signal due to amplifier problems.
- Data Column 13 (SG 2-12), is corrupted during shakes 49 and 55.
- Data Column 49 (PPT 7713) zeroed out during all large shakes. This data channel was unable to be zeroed relative to its elevation at the beginning of the test sequence.
- Data Column 60 (V ACC 4437) appears to have problems during test 55. There was a signal jump and residual offset noted.
- Data Column 86 (ACC 5598) appears to have problems during test 55. A similar problem to data column 60 is encountered with a signal jump and offset during the record with a residual offset.
- Data Column 87 (ACC 5603) did not work during any of the tests.
- Both pore pressure transducers at elevation 2 in the model (7713 and 7719) were placed in the direction of shaking rather than perpendicular, and thus may have some effect of *sloshing* of the soils, as noted in Section 4.2.2.

6.5 LIMITATIONS OF THE MODELING

6.5.1 Model Construction in a 1-g Field

Recent innovations have allowed the installation of piles in-flight while the centrifuge is spinning at the test g-level to properly reproduce the displacement and stress fields around the model pile. Craig (1985) reviewed a range of model pile installation procedures and concluded that, "it is imperative that installation be carried out at appropriate acceleration levels..." However he noted that for lateral, cyclic, and dynamic loadings, the effect may be less critical. The dynamic soil-structure interaction modeled in this investigation clearly falls under a less critical category. It should also be noted that hydraulically jetting of piles is commonly used at west coast ports. This instillation technique does not create a uniformly increasing stress field around the pile even under full-scale conditions. In addition, rockfill for some wharf structures is placed after the piles were driven (Diaz, Warwar, 1986). Therefore, the author feels that these concerns, though warranted, are minor due to these field construction techniques.

6.5.2 Saturation concerns

Upon removal of the saturation lid during NJM02, sand boils were discovered in the southeast corner of the box. This suggests that an air leak was present at one of the ring interfaces in FSB1. The quality of saturation in the back portion of the model could be questioned with this introduction of air. Because, the leak was located on the box edge and in the back of the free field soils, the author feels the effects of the leak on the overall model performance were minimal. Model NJM02 sat saturated for an additional week on the arm when laboratory temperatures ranged from approximately 60 to 100 degrees Fahrenheit. These temperatures contributed to an accelerated rate of reaction between the organic-rich Bay Mud and the HPMC. Oxidation and decomposition of the organic material was evinced by a strong odor emanating from

the model after roughly two days. Concerns were raised regarding the effects of these organic reactions on the model behavior. However, the author is not aware of any documented problems encountered with this situation. Pore pressure results in the model appeared reasonable throughout the test sequence.

6.5.3 RC Filter

As described previously, a 16 channel dual cascading low-pass RC filter was built to replace the malfunctioning tech filter for test NJM02. A schematic of this filter is shown in Figure 6-3. The first 16 channels of strain gauge data were therefore run through this RC filter. The resistors were 10,000-ohms and the capacitors were 0.018-μF. This filter introduced both a magnitude and phase shift in the digital output of the data. After examining fast Fourier transforms of all recorded data, very little signal was found above 80-Hz. Signal at this frequency would induce at most a 5 percent reduction in magnitude or a 15-degree phase shift. Since this offset (in both magnitude and phase) is even less at lower frequencies (from which most of the data consists), the author believes the effect of the RC filter is negligible, and as such, the data in this report has not been corrected for the effect of the filter. The filter was modeled using AIM-SPICE software to obtain theoretical output. In addition, a signal generator and digital oscilloscope were used to verify these numbers with the actual filter response. This data is provided in the NJM02 data report.

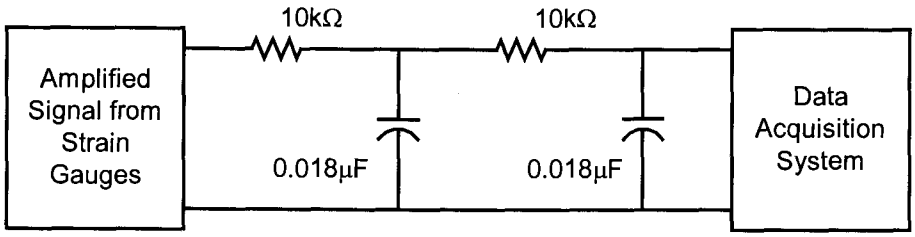

Figure 6-3: Schematic of dual cascading RC filter used in NJM02

6.5.4 Instrument Locations

As noted in the discussion of shear wave velocity data in section 6.2.3, the actual instrument locations during the test sequence change due to factors such as clay consolidation, post liquefaction volume change, permanent lateral deformations, and elastic (immediate) sand settlements. Therefore, the locations of the instruments are not exactly known, but can be interpolated from the pre-and post test instrument locations. This estimation and interpolation can be carried out by analyzing the vertical settlements recorded by the linear pots during spin-up and each shaking event. The amount of settlement at each layer could also be analyzed by noting the change in static pore pressures recorded by PPTs before and after each large shakes.

7 CONFIGURATION AND INSTRUMENTATION OF MODEL SMS01

This chapter describes the geometry and instrument layout of model SMS01. The model layout is described in a similar manner to NJM02 to provide an easy comparison with this test. In addition, comparisons will be also be made within the text of this chapter to provide a clearer picture of the similarities and differences between each model.

7.1 SMS01 MODEL LAYOUT

The design model layouts for test SMS01 (Figure 7-1) closely resembles the general configuration shown in Figure 3-4 and the design of NJM02. The layout of SMS01 differs only in the respect that it incorporates two regions that simulate soil improvement. The first improvement area replaces a portion of a relatively weak layer of clay with a grid of soil mixed with cement beneath the rock dikes. The second soil improvement modeled incorporates densification in the backfill adjacent to the rockfill. The densification was achieved by placing the sand at an increased density. This region of dense sand includes the foundation of the upper rock dike and the surrounding soil moving toward the back of the model. The area behind this *improved* section was built with a loose sand, thereby mimicking a loose hydraulically placed sandy fill. Although the dense sand was actually placed densely and not improved after construction (as it would be in the field), it will be referred to as an *improvement* area for the remainder of this thesis. Table 7-1 provides a description of all elevation layers used to describe model locations along with *design* model and prototype dimensions.

In addition to the changes in the design configurations due to soil improvement scenarios, a number of changes were made in regard to the clay and sand properties. The pretest clay consolidation is one of these modifications. The clay in NJM02 was initially consolidated in a large hydraulic press to obtain an OCR of 1.5 in the front of the model relative to the dredge line. This design resulted in variable settlements as the

thickness of soil increased along the length of the model due and more consolidation occurred under the centrifugal acceleration. To minimize the additional uncertainty in analysis due to clay consolidation, the entire clay layer in SMS01 was consolidated on the press to a pressure equivalent to the full overburden weight of the backfilled area. The measured strengths of the clays are presented along with the clay consolidation explanation in the construction sequence in section 8.3. As mentioned there, it is important to note the clay strengths provided within have *not* been adjusted to account for the geometric scaling factor.

Table 7-1: SMS01 design elevation descriptions and dimensions

Elevation	*Description*	*Model Elevation (mm)*	*Prototype Elevation (m)*
0	Base of Model Box – Datum	0	0.0
1	Instrument Layer – Lower Dense Sand	60	3.4
2	Instrument Layer – Lower Dense Sand	140	8.0
3	Interface – Lower Dense Sand and Bay Mud	180	10.3
4	Instrument Layer – Bay Mud	210	12.0
5	Interface – Bay Mud and Middle Dense Sand	240	13.7
6	Instrument Layer – Middle Dense Sand	270	15.4
7	Interface – Top of Middle Dense Sand	300	17.1
8	Instrument Layer – Loose Sand and Rock	380	21.7
9	Instrument Layer– Loose Sand and Rock	430	24.6
10	Interface Layer – Upper and Lower Rock Dikes	440	25.1
11	Instrument Layer – Loose Sand and Rock	490	28.0
12	Instrument Layer – Loose Sand and Rock	540	30.9
13	Interface – Ground Water Table	580	33.1
14	Instrument Layer – Upper Dense Sand	615	35.1
15	Top of Soil Profile	650	37.1

The other major difference between the models is the degree of densification for what has been referred to as "loose" or "dense" sands. The relative density of "dense" sands in NJM02 is approximately 85 percent while averaging 70 percent for test SMS01. "Loose" sands averaged 45 percent in NJM02 and 35 percent in SMS01.

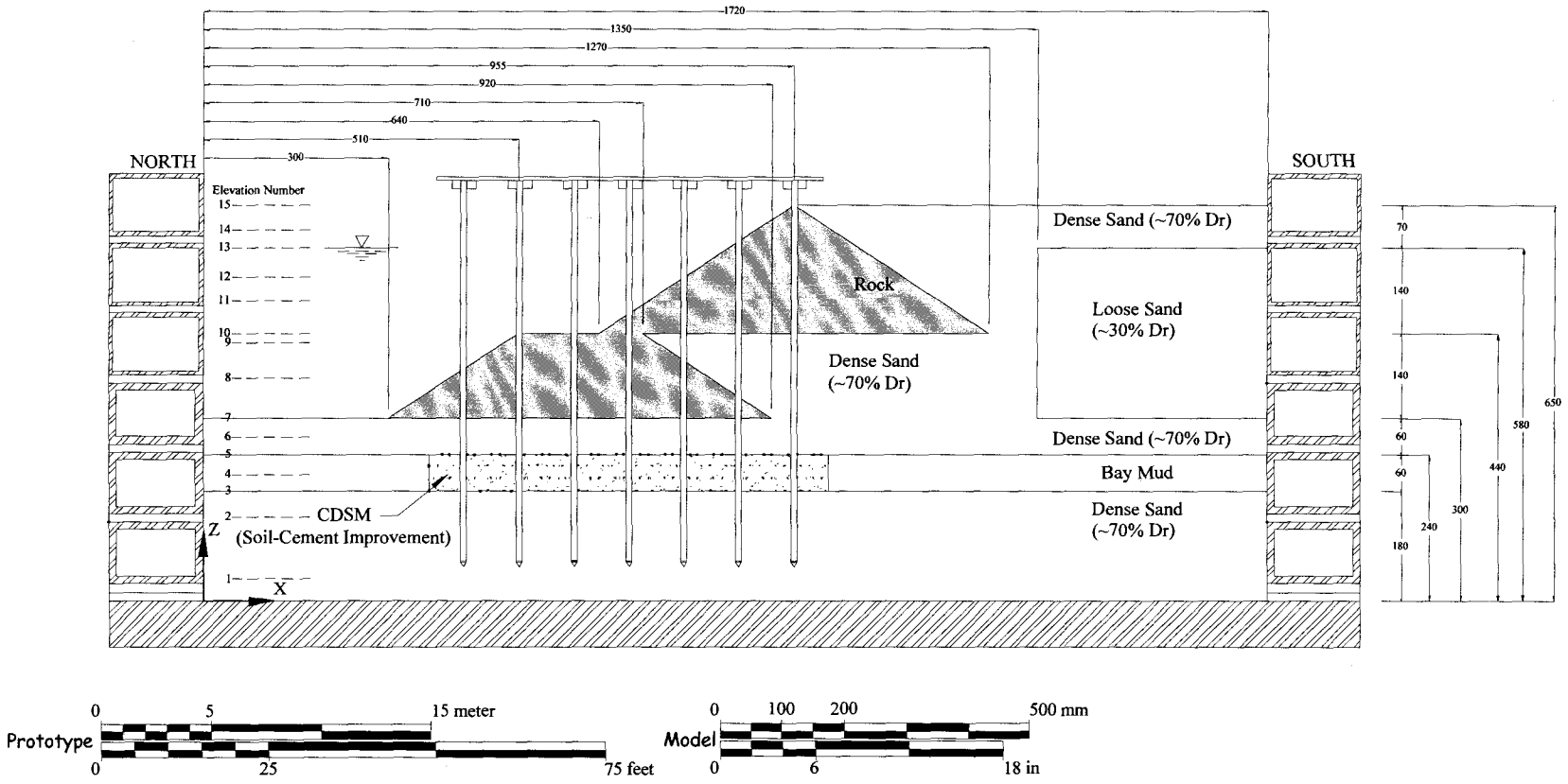

Figure 7-1: SMS01 soil profile and dimensions (mm)

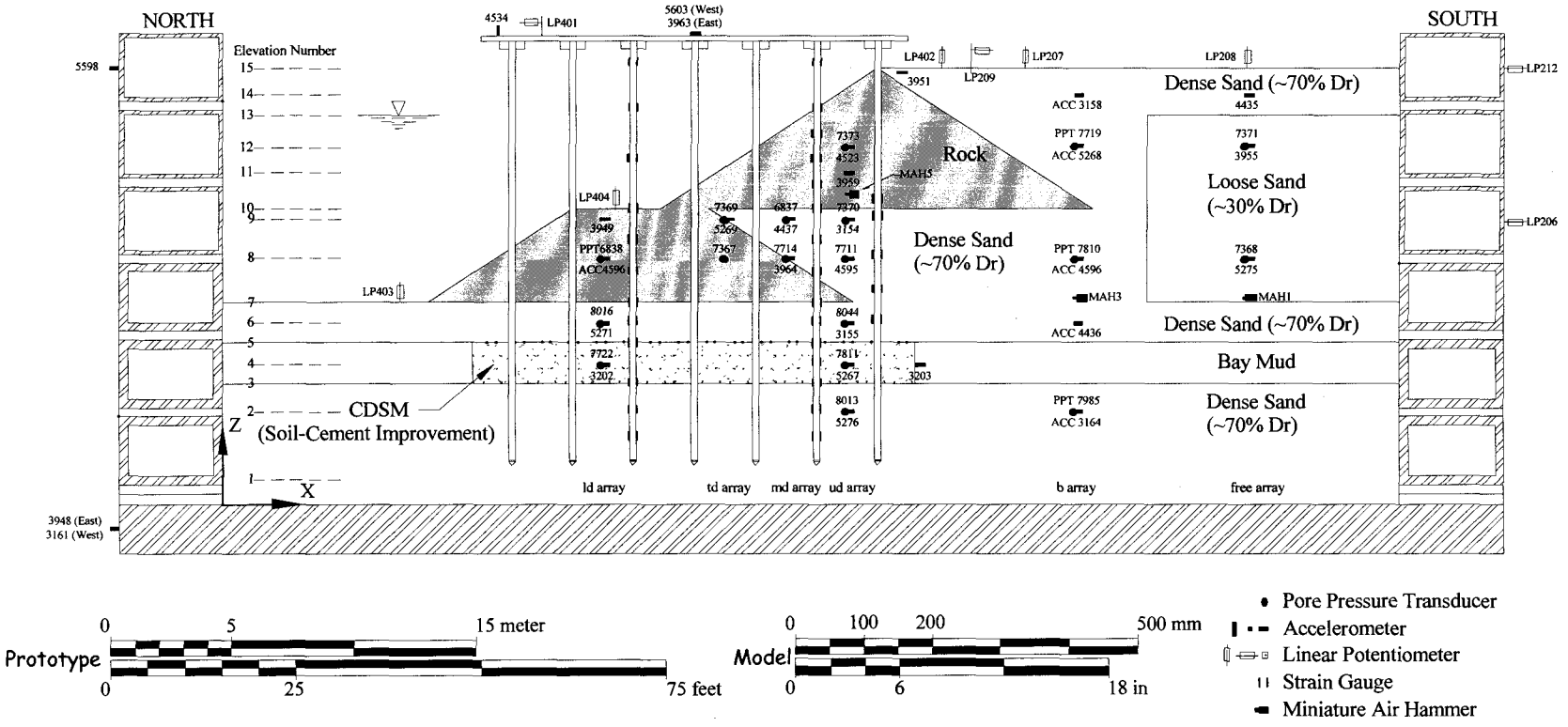

Figure 7-2: SMS01 design instrument locations and dimensions (mm)

7.2 INSTRUMENTATION

Instrumentation in the models was placed in a series of vertical arrays throughout the model to capture dynamic soil response with depth (Figure 7-2). The instrument array labels are described in Table 4-2. A complete tabulation of all pre- and post-test instrument locations is included in the corresponding data report (Schlechter et al., 2000b). The origin of coordinates and sign convention for SMS01 are consistent with those set for NJM02.

Table 7-2: Instrument array labels and descriptions

Array Label	*Location*
"free array"	Free Field Array (unimproved)
"b array"	Backland Array (improved)
"ud array"	Upper Dike Array
"md array"	Mid-slope of Upper Dike Array
"td array"	Toe of Upper Dike Array
"ld array"	Lower Dike Array

7.2.1 Accelerometers

A total of 32 accelerometers were placed in the model, with 30 of these channels recorded during testing (29 horizontal and 1 vertical). The location of all recorded instruments are shown in Figure 7-2. Accelerometers were placed on each of the centrifuge loading arms that applied the earthquake motion to the FSB container in order to measure the input motion. Additionally, accelerometers were placed on the top ring of the box to measure the box behavior. All accelerometers placed in the sand were centered between the middle and eastern set of piles. The accelerometers in the clay layer were located outside of the CDSM grid on the east side of the box. One accelerometer was also embedded in the south end of the CDSM grid to obtain the response of the grid and it was placed in line with the accelerometers in the sand

layers. The accelerometer (ACC) labels used within this thesis are consistent with their permanent UC Davis identification numbers.

7.2.2 Pore Pressure Transducers

Pore pressures within the model SMS01 were monitored using 18 pore pressure transducers PPTs throughout the testing sequence. All PPTs placed in the sand were centered between the middle and western set of piles. The PPTs in the clay layer were located outside of the CDSM grid on the west side of the box. The PPTs were placed oriented in the y direction (i.e. perpendicular to ground motion), so that any *sloshing* of the soil column into the head of the PPT would not be measured. The pore pressure transducers are of type Druck Miniature Series # PDCR 81. The PPT labels used within this thesis are consistent with their permanent UC Davis identification numbers.

7.2.3 Strain Gauges

As mentioned in Section 3.5, the same pile sizes were used for both tests. However, the strain gauge configuration, design, and layout were changed significantly. In order to enhance the definition of the pile moments, strain gauges were concentrated on a fewer number of piles. For test SMS01, two new piles were built and instrumented with 15 complete strain gauge bridges along the length of each pile. This allowed 32 strain gauge locations to be recorded on only 3 piles with 12 on pile 5, 15 on pile 2, and 5 on pile 1 (Figure 7-4). The strain gauge elevation identification numbers are shown in each of these figures with horizontal lines and are labeled differently for each test. The distances from the pile toe to each strain gauge is given in Figure 7-4. The notation *pile toe* refers to the bottom of the pile without the pile tip (i.e., the end of the aluminum tubing). The convention used for the strain

gauge identification labels is a direct combination of their respective pile number and elevation.

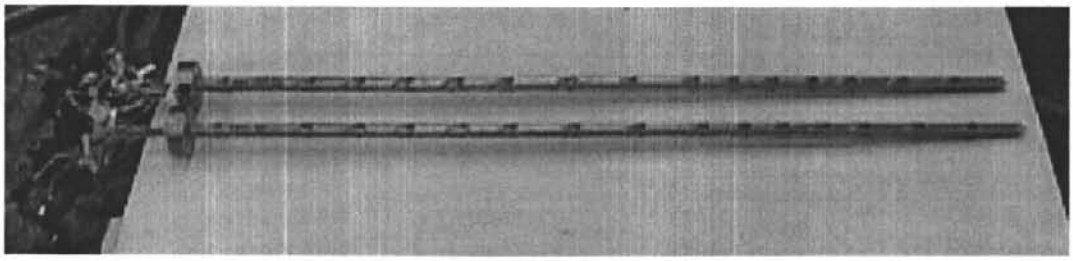

Figure 7-3: New piles with 15 strain gauge locations developed for test SMS01

The strain gauge installation and calibration for test SMS01 were identical to that done in NJM02. All strain gauges for test SMS01 on the two new piles (2 and 5) are Micromeasurements type CEA-13-062 WT-350. The remaining strain gauges on pile 1 and all other gauges that were used from NJM02 are CEA-13-125 WT-350. The smaller gauges for test SMS01 were chosen because of their relative size to more closely space gauges along the piles and to reduce the distance each gauge wraps around the pile.

After the piles have been driven, the distances from pile toe to strain gauge location can be adjusted to model elevations by adding an adjustment factor. This adjustment accounts for the distance from the pile toe to the base of the model box. SMS01 model elevations were obtained by adding 69.3-mm to the distances given in Table 7-3.

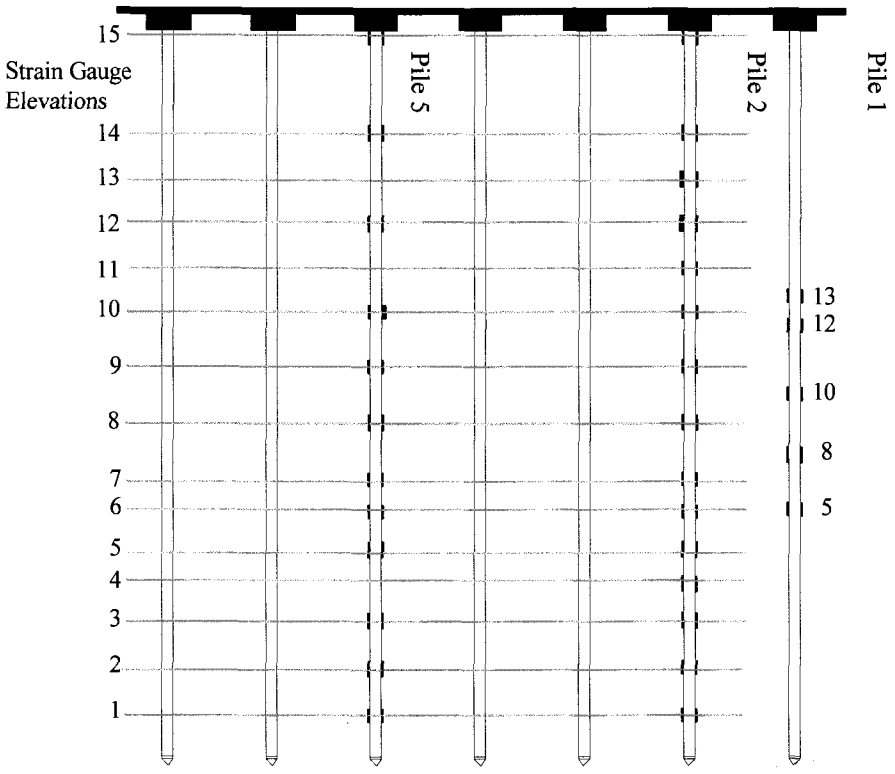

Figure 7-4: SMS01 strain gauge elevations

Table 7-3: Distances from the pile toe to each strain gauge (SMS01)

Instrument	Distance (mm)
SG1-5	149.75
SG1-8	208.75
SG1-10	256.5
SG1-12	364.25
SG1-13	389.75
SG 2-1	33.5
SG 2-2	74.0
SG2-3	113.8
SG2-4	143.5
SG2-5	173.8
SG2-6	203.3
SG2-7	233.3
SG2-8	280.3
SG2-9	326.5
SG2-10	374.0
SG2-11	411.0

Instrument	Distance (mm)
SG2-12	448.5
SG2-13	485.0
SG2-14	523.0
SG2-15	589.8
SG5-1	33.8
SG5-2	74.5
SG5-3	114.3
SG5-5	175.3
SG5-6	204.0
SG5-7	234.0
SG5-8	280.8
SG5-9	326.8
SG5-10	374.0
SG5-12	448.8
SG5-14	524.0
SG5-15	590.5

7.2.4 Linear Potentiometers

Linear potentiometers (linear pots) were used to measure both vertical and horizontal displacements within the models. Two linear pots measured the movement of the top and middle rings of the box, relative to the base of the box. The remaining linear pots were used to measure horizontal and vertical displacements within the model. These linear pots were attached from horizontal cross members mounted across the top ring of the box and therefore all movements are referenced to the top ring of the box. Their locations within the model can be seen in Figure 7-2. Horizontal displacements were measured with two linear pots. One of these horizontal linear pots was placed behind the wharf deck and measured displacements by using a thin aluminum plate that was inserted into the sand. The other linear pot measured the horizontal displacements of the wharf deck by attaching the instrument to a vertical member fastened to the wharf deck. Five linear pots were used to measure vertical displacements: three measured vertical displacements of the soil surface south of the wharf; one measured the vertical displacements of the top of the lower rock dike; and one measured the vertical displacements of the toe of the lower rock dike. Since all of the linear pots are referenced to the top ring of the box, absolute horizontal displacements are the sum of the linear pot within the model and the linear pot measuring the displacement of the top ring of the box. The linear pots used were Duncan Electronics 600 Series. The linear pot labels used within this thesis are consistent with their permanent UC Davis identification numbers.

8 CONSTRUCTION OF MODEL SMS01

The construction of centrifuge model SMS01 was carried out in a manner very similar to model NJM02. Therefore, the entire construction sequence will not be repeated within this chapter. However, the changes between the models will be highlighted where applicable. Where different techniques were employed to construct the model, comments will be included as to which method worked better

8.1 SAND PLUVIATION

During NJM02, difficulties were initially encountered using the small pluviator due to small debris (predominantly grass seeds) clogging the nozzle's mesh screen. To avoid the problem with plugging screens, a new nozzle drop system was developed for the small barrel pluviator for test SMS01 (Figure 8-1). This device used two rotating stainless steel plates with identically cut orifices. These plates were then rotated to different stages to vary the opening size and flow rate.

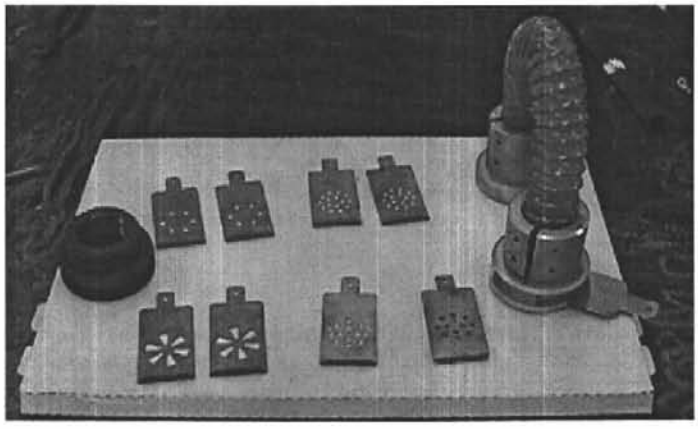

Figure 8-1: Small barrel pluviator attachment nozzle and interface drop plates used for test SMS01

The relative densities for the tests were similar but not an exact match. For NJM02, the calibration of the *large* pluviator provided dense sand relative densities of approximately 85 percent. Calibrations of the *small* pluviator during placement of the loose sand showed relative densities that varied between 41 and 53 percent, with an average relative density of approximately 45 percent. For SMS01, the *large* pluviator provided dense sand relative densities of approximately 70 percent and the *small* pluviator showed relative densities that averaged 35 percent.

8.2 INITIAL SATURATION

The initial saturation of the lower dense sand layer took place in a procedure similar to that used in NJM02. Small sand boils were discovered again in the in the southeast corner of the model box. This suggests an air leak occurred at one of the ring interfaces below this point. Therefore, an aluminum patch and silicone were applied to the exterior of the box as a temporary fix. As an added precaution, a strip of geocomposite was run along the interior wall to the surface of the model to allow any air that may enter during the secondary saturation to move directly to the surface. No subsequent problems were encountered with saturation.

8.3 CLAY CONSOLIDATION

In order to decrease the time to reach consolidation, the drainage path was shortened by dividing the clay layer into sub-layers, with each sub-layer separated by a horizontal drainage layer. In an attempt to reduce construction time, the amount of sub-layers were reduced to two for SMS01 compared to the three used in NJM02. The sub-layers were created using the same filter paper techniques described previously. The instruments in the clay layer were installed at the completion of the second sub-layer.

As described in section 7.1, the clay in SMS01 was consolidated to a different pressure than in NJM02. During NJM02, the clay was initially consolidated in the hydraulic press to obtain an OCR of 1.5 in the front of the model relative to the dredge line. However, in SMS01 the entire clay layer in SMS01 was consolidated on the press to a pressure equivalent to the full overburden weight of the backfilled area.

After the consolidation of each clay sub-layer, a Torvane was used to evaluate the undrained shear strength at the top of each sub-layer. The pre-test clay strengths for SMS01 would be expected to be similar to strengths during testing since the layer was consolidated on the press to the full expected backfill overburden pressure while spinning on the centrifuge. For SMS01, examples of these clay strengths obtained from the top and bottom sub-layers during construction are given in Table 8-1 and Table 8-2. A comparison can be made with the post-test dissection strengths shown in Table 8-3. The post-test readings were taken in the middle sub-layer. It must be emphasized that all clay strengths presented here are direct readings and conversions from Torvane calibrations. The strengths have therefore *not* been adjusted to account for the geometric scaling factor used to design the model.

Table 8-1: SMS01 pre-test clay strengths in bottom sub-layer

Location (approximate)		Torvane	
x (mm)	y (mm)	shear strength (kPa)	shear strength (psf)
300	228	27.8	580
300	456	28.7	600
700	228	30.6	640
700	456	32.6	680
1100	228	30.6	640
1100	456	30.6	640
1400	228	31.6	660
1400	456	31.6	660

Table 8-2: SMS01 pre-test clay strengths in top sub-layer

Location (approximate)		Torvane	
x (mm)	y (mm)	shear strength (kPa)	shear strength (psf)
300	228	28.7	600
300	456	24.9	520
600	228	28.7	600
600	456	25.9	540
900	228	26.8	560
900	456	24.9	520
1400	228	23.0	480
1400	456	23.0	480

Table 8-3: SMS01 post-test clay strengths

Location (approximate)	Torvane	
x (mm)	shear strength (kPa)	shear strength (psf)
300	25.9	540
500	30.6	640
850	30.6	640
1000	36.4	760
1100	31.6	660
1400	33.5	700

8.4 CDSM PLACEMENT (SMS01 ONLY)

After clay consolidation was complete in SMS01, the CDSM grid was constructed. The outline of the grid was carefully measured and etched into the clay surface. An aluminum ruler was used to excavate the 23-mm (0.9-in) wide trenches in the clay layer. The trenches were excavated through the clay to the top of the lower dense sand at elevation 3. The effective embedment of the CDSM into the lower dense sand varied between 0 and 5 mm. Figure 8-2 shows the outline of the CDSM grid during construction. The piles and wharf were actually driven after the middle dense sand was placed and are only in place for scale.

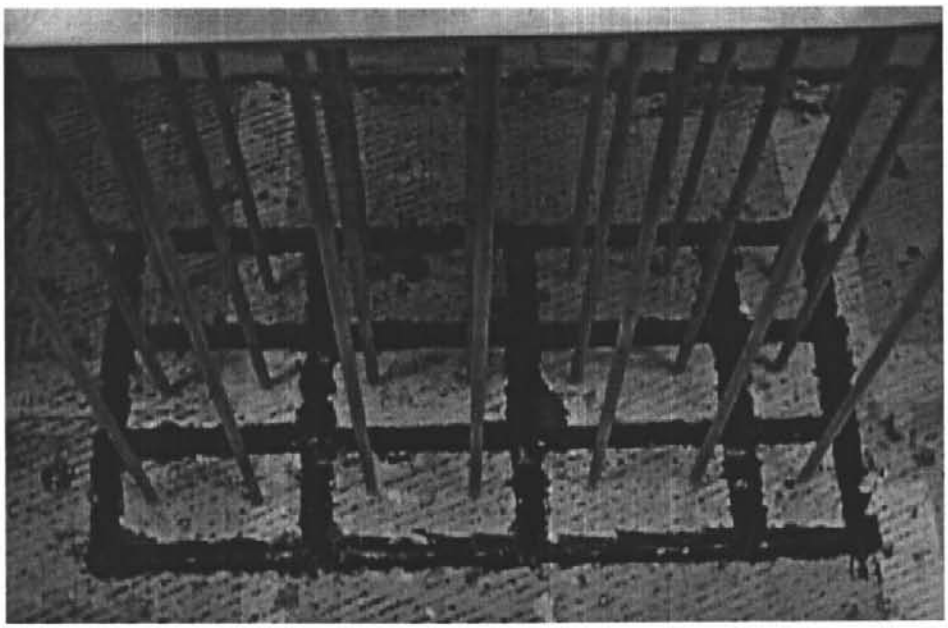

Figure 8-2: Outline of CDSM grid during construction (with piles and wharf for scale)

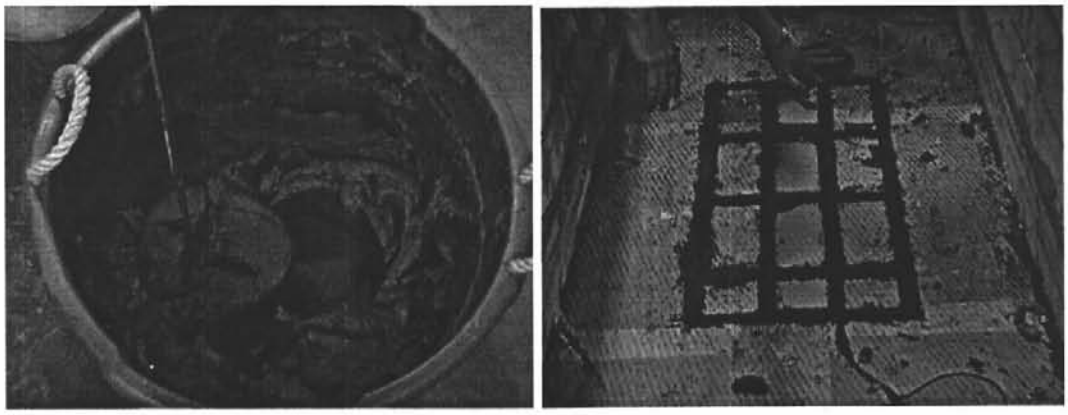

Figure 8-3: Mixing and placement of CDSM material

Figure 8-3 shows the mixing and placement of the CDSM material. A mixing attachment on a power drill was utilized to mix 3.63-kg (8-lbs) of Type I-II Portland Cement with 22.68-kg (50-lbs) of clay slurry at 133-percent water content. The CDSM material was then hand placed into the grid trenches. The material was

carefully compacted (by hand) to minimize any air voids. The CDSM grid was finished level with the surface of the top clay layer.

8.5 Pile Driving and Wharf Placement

After the clay, middle dense sand layers, and all corresponding instruments were placed, the pile-supported wharf was installed. Care was taken to align the wharf deck and piles parallel to their respective axes of the box to insure one-dimensional alignment with the primary direction of shaking. A four-piece template was attached at the approximate midpoint of the piles. This template helped insure that the piles were installed vertically so that any residual driving moment would be limited. Contrary to the technique used during NJM02, the pile driving was completed using only simultaneous blows from rubber mallets on opposite sides of the wharf deck until the target elevation was reached for SMS01 (Figure 8-4). Care was taken to orient individual piles (and their corresponding strain gauges) in the same direction so that the calibration sign could correctly be applied during data reduction.

Consistent with NJM02, the wharf deck was then removed to make it possible to place the remainder of the soil and rock layers. The tops of the piles were temporarily sealed with tape to prevent sand from filling the piles during subsequent construction. The wharf deck was then reattached prior to testing.

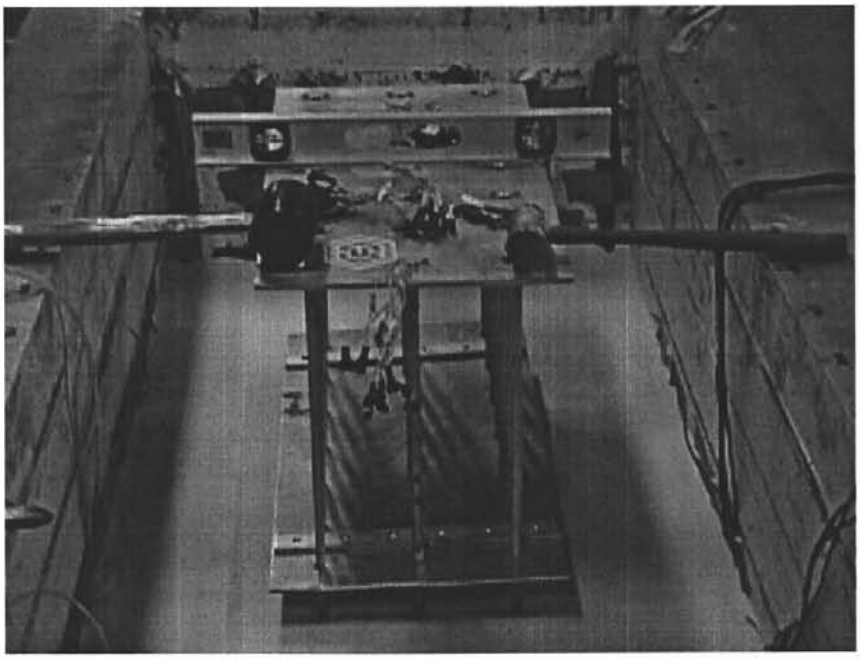

Figure 8-4: Template and hammers used to drive the wharf system with simultaneous blows on the deck (SMS01)

8.6 PLACEMENT OF THE ROCKFILL AND REMAINING SANDS

The rockfill and remainder of the sand was placed in a manner similar to NJM02. However, the vertical split in separation of densities required a different placement technique. For SMS01, the separation between improved and unimproved sands in the backland was achieved by using a thin sheet of aluminum (Figure 8-4). This sheet was firmly attached to the top ring of the box after the completion of the middle dense sand layer. The sheet was removed at the completion of elevation 13. The sand layers on either side were stepped up incrementally to allow minimal deflection of the aluminum sheet.

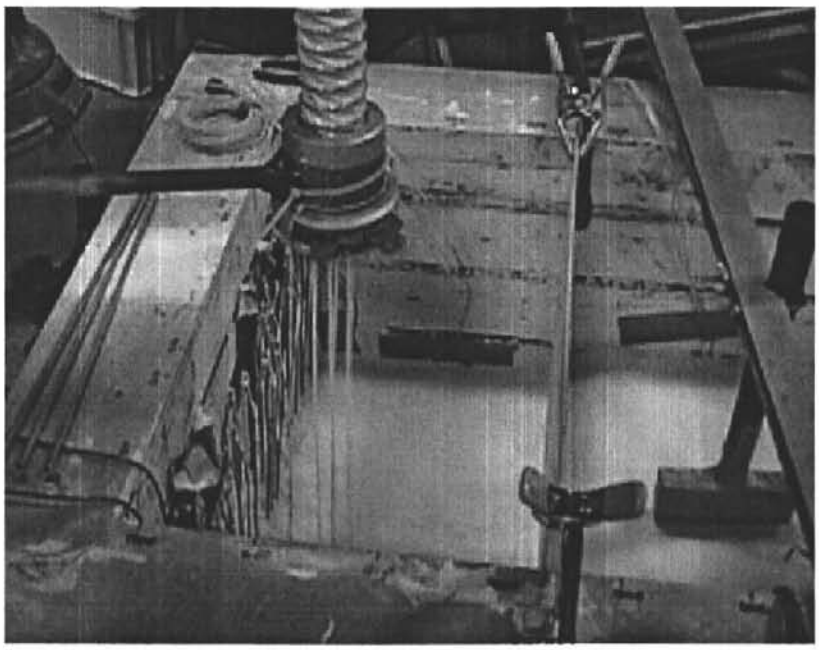

Figure 8-5: Separation sheet and placement of the loose sand

8.7 INDICATOR LAYERS

Black sand was placed in vertical columns and horizontal layers in a manner similar to that described for NJM02. However, the tubing size used to create black sand columns for SMS01 was increased to 3/16" to eliminate the plugging problems that occurred during NJM02. This increased tubing size worked significantly better.

8.8 SHEAR WAVE GENERATORS

To obtain in-flight shear wave velocity measurements, a series of "mini-" air hammers (MAH) were placed within the model. These air hammers were positioned within three arrays ("ud", "b", and "free") for test SMS01. All MAHs were oriented along the x-axis of the container as shown in Figure 5-9. A discussion describing the accuracy of these tests is included in the text provided with model NJM02.

8.9 SECONDARY SATURATION

Secondary saturation of SMS01 took place in a procedure similar to that described for NJM02 except that the initial HPMC mix design was modified because of the viscosity temperature dependency of HPMC. This variation of viscosity is further described by Stewart et al. Test SMS01 was run during January when the ambient temperature was significantly lower than NJM02, which was tested in early August. The fluid for test SMS01 was 1.9 percent HPMC by weight and yielded a viscosity of approximately 4.8×10^{-5} m^2/s (48-cSt). The fluid for test NJM02 consisted of 2.25 percent HPMC by total weight, which produced a viscosity of approximately 4.7×10^{-5} m^2/s (47.6-cSt).

After saturation was completed on the arm, the viscosity of the solution was reduced to 3.0×10^{-5} m^2/s (30-cSt), which was identical to the value achieved in NJM02. This reduction in viscosity is due to the mixing with the lower water saturated materials through the sand located at both ends of the clay layer (section 5.3). The viscosity remained constant at the post-mixing value throughout the remainder of the test sequence.

8.10 POST-TEST DISSECTION

Model dissection took place in a manner similar to that described for test NJM02.

9 TESTING OF CENTRIFUGE MODEL SMS01

9.1 SMS01 TEST SEQUENCE

The model was spun up on February 4, 2000. The model was brought up to 40-g incrementally as pore pressures were monitored closely and the clay was allowed to reconsolidate under the centrifugal acceleration. Table 9-1 outlines the three *small* shakes and three *large* shakes that were run in SMS01 and Table 9-2 provides a complete summary of the test sequence. The SMS01 test sequence used the same three earthquake motions as test NJM02. The three small shakes and the first large shake went smoothly. However, due to a software conflict with inputted sampling frequencies, the data from the next two large shakes (sms01_35 and sms01_40) was not recorded. These shakes were of similar magnitude to test sms01_44. A fast data file without an input shake (sms01_36) was recorded after test 35 and can be used to back out post-test values where applicable. Tests 37 and 38 were attempted shakes, however, the shaker did not respond. The only data available to back out what happened after test 40 is the slow data (test 42) during spin down and the datum values before the earthquake motion begins for test 43.

Table 9-1: SMS01 data from small and large shakes

Data File	Input Motion	Average Peak to Peak Acceleration (g)
sms01_11	Step Wave (step.txt)	0.041
sms01_12	Loma Prieta Outer Harbor (loma2.txt)	0.064
sms01_13	Northridge Rinaldi (north2.txt)	0.038
sms01_25	Loma Prieta Outer Harbor (loma2.txt)	0.651
sms01_43	Loma Prieta Outer Harbor (loma2.txt)	0.61
sms01_44	Northridge Rinaldi (north2.txt)	0.65

Table 9-2: SMS01 testing day event summary

Date	Time	Centrifuge rpm	Centrifuge Acc at the 1/3 model depth	Input file name	Description	West ampl. factor	East ampl. factor	Channel gain list (cgl) used	Raw output file	Comments / Details
2/4	12:10 PM	0		step.txt				slw01.cgl	slow01.slw	Pretest Sampling before spinup
	1:00 PM							slw01.cgl	slow01.slw	Begin Spinning Up
	1:11 PM	32.2	9.9					slw01.cgl	slow01.slw	
	1:40 PM							slw01.cgl	slow01.slw	Move up to 20 g's
	1:49 PM	46	20.1					slw01.cgl	slow01.slw	Just up to 20 g's
	2:57 PM							slw01.cgl	slow01.slw	Start spinning up to 30 g's
	3:00 PM	57.6	31.6					slw01.cgl	slow01.slw	
	3:42 PM							slw01.cgl	slow01.slw	Start spinning up to 40 g's
	3:47 PM	63.3	38.1					slw01.cgl	slow01.slw	Just reached 40 g's
	5:12 PM	64.9	40.1					shwv01.cgl	sms01_02.out	Fire upper dike array shear hammers (north)
	5:13 PM	64.9	40.1					shwv01.cgl	sms01_03.out	Fire upper dike array shear hammers (south)
	5:15 PM	64.7	39.8					shwv02cgl	sms01_04.out	Fire back array shear hammers (north)
	5:17 PM	64.8	39.9					shwv02cgl	sms01_05.out	Fire back array shear hammers (south)
	5:18 PM	64.7	39.8					shwv03.cgl	sms01_06.out	Fire free array shear hammers (north)
	5:19 PM	64.7	39.8					shwv03.cgl	sms01_07.out	Fire free array shear hammers (south)
	5:20 PM	64.8	39.9					pwv01.cgl	sms01_08.out	P-wave test (fired north)
	5:22 PM	64.8	39.9					pwv01.cgl	sms01_09.out	P-wave test (fired south)
	5:24 PM	64.9	40.1					slw01.cgl	slow10.slw	Start slow data again
	6:00 PM	65	40.2	step.txt	Step wave motion	4	4	fst01.cgl	sms01_11.out	
	6:22 PM	64.7	39.8	loma2.txt	Loma Prieta Outer Harbor	0.35	0.35	fst01.cgl	sms01_12.out	
	6:34 PM	64.9	40.1	north2.txt	Norhridge Rinaldi motion	0.08	0.08	fst01.cgl	sms01_13.out	
	6:43 PM							slw01.cgl	slow14.slw	Begin spinning down and take readings
	7:15 PM									Come to stop
	8:25 PM							slw01.cgl	slow15.slw	Begin spinning up
	8:41 PM	44.1	18.5					slw01.cgl	slow15.slw	Reached 20 g's
	9:05 PM							slw01.cgl	slow15.slw	Start to spin up to 40 g's
	9:12 PM	57.6	31.6					slw01.cgl	slow15.slw	
	9:18 PM							slw01.cgl	slow15.slw	Move up to 40 g's
	9:25 PM	64.9	40.1					slw01.cgl	slow15.slw	Reach 40 g's
	9:50 PM	64.9	40.1					shwv01.cgl	sms01_16.out	Fire upper dike array shear hammers (north)
	9:52 PM	64.9	40.1					shwv01.cgl	sms01_17.out	Fire upper dike array shear hammers (south)
	9:54 PM	64.9	40.1					shwv02.cgl	sms01_18.out	Fire back array shear hammers (north)
	9:54 PM	64.9	40.1					shwv02.cgl	sms01_19.out	Fire back array shear hammers (south)
	9:55 PM	64.9	40.1					shwv03.cgl	sms01_20.out	Fire free array shear hammers (north)
	9:56 PM	64.9	40.1					shwv03.cgl	sms01_21.out	Fire free array shear hammers (south)
	9:57 PM	64.9	40.1					pwv01.cgl	sms01_22.out	P-wave again (fired north)
	9:59 PM	64.9	40.1					pwv01.cgl	sms01_23.out	P-wave again (fired south)

Table 9-2 (Continued)

Date	Time	Centrifuge rpm	Centrifuge Acc at the 1/3 model depth	Input file name	Description	West ampl. factor	East ampl. factor	Channel gain list (cgl) used	Raw output file	Comments / Details
	10:00 PM	64.9	40.1					slw01.cgl	slow24.slw	Start taking slow data again
	10:25 PM	64.8	39.9	loma2.txt	Loma Prieta Outer Harbor	2	2	fst01.cgl	sms01_25.out	
	10:45 PM	64.9	40.1					slw01.cgl	slow26.slw	Take slow data and spin down
2/5	12:10 AM	0	0.0					slw01.cgl	slow27.slw	Start taking slow data
	12:48 AM	64.9	40.1					slw01.cgl	slow27.slw	Reach 40 g's
	1:00 AM	65	40.2					shwv01.cgl	sms01_28.out	Fire upper dike array shear hammers (north)
	1:02 AM	65	40.2					shwv01.cgl	sms01_29.out	Fire upper dike array shear hammers (south)
	1:03 AM	65	40.2					shwv02.cgl	sms01_30.out	Fire back array shear hammers (north)
	1:04 AM	65	40.2					shwv02.cgl	sms01_31.out	Fire back array shear hammers (south)
	1:04 AM	65	40.2					shwv03.cgl	sms01_32.out	Fire free array shear hammers (north)
	1:05 AM	65	40.2					shwv03.cgl	sms01_33.out	Fire free array shear hammers (south)
	1:05 AM	64.9	40.1					slw01.cgl	slow34.slw	Start slow data again
	1:30 AM	64.9	40.1					slw01.cgl	slow34.slw	Take readings and end slow data
	1:36 AM	64.9	40.1	north2.txt	Northridge Rinaldi motion	0.7	0.7	fst01.cgl	sms01_35.out	THIS SHOOK BUT THE DATA WAS LOST
	2:25 AM	64.7	39.8			null	null	fst01.cgl	sms01_36.out	This file is a snapshot of instrument values after the lost shake
	2:30 AM	64.7	39.8					fst01.cgl	sms01_37.out	Acquired data but this did NOT shake
	2:55 AM	64.9	40.1					fst01.cgl	sms01_38.out	Acquired data but this did NOT shake, spin down to fix problem
	4:07 AM	0						slw01.cgl	slow39.slw	Start spinning up
	4:23 AM	45.3	19.5					slw01.cgl	slow39.slw	
	4:40 AM	64.9	40.1					slw01.cgl	slow39.slw	
	5:00 AM	64.9	40.1	north2.txt	Northridge Rinaldi motion	0.7	0.7	fst01.cgl	sms01_40.out	THIS SHOOK BUT THE DATA WAS LOST
	5:11 AM	64.9	40.1					fst01.cgl	sms01_41.out	The camera came unplugged and this attempted shake did NOT occur
	6:13 AM	0	0.0					slw01.cgl	slow42.slw	
	6:38 AM	45.9	20.0					slw01.cgl	slow42.slw	
	6:50 AM	64.9	40.1					slw01.cgl	slow42.slw	
	7:11 AM	64.9	40.1	loma2.txt	Loma Prieta Outer Harbor	2	2	fst01.cgl	sms01_43.out	Good shake
	7:30 AM	64.9	40.1	north2.txt	Northridge Rinaldi motion	0.7	0.7	fst01.cgl	sms01_44.out	Good shake
	7:34 AM	64.9	40.1					shwv01.cgl	sms01_45.out	Fire upper dike array shear hammers (north)
		64.9	40.1					shwv01.cgl	sms01_46.out	Fire upper dike array shear hammers (south)
		64.9	40.1					shwv02.cgl	sms01_47.out	Fire back array shear hammers (north)
		64.9	40.1					shwv02.cgl	sms01_48.out	Fire back array shear hammers (south)
		64.9	40.1					shwv03.cgl	sms01_49.out	Fire free array shear hammers (north)
		64.9	40.1					shwv03.cgl	sms01_50.out	Fire free array shear hammers (south)
	7:41 AM	64.9	40.1					slw01.cgl	slow51.slw	Start slow data and spin down
	8:05 AM	1.3	0.0					slw01.cgl	slow51.slw	Stop taking data

9.2 TESTING DETAILS

9.2.1 Changes Between Small and Large Shakes

The accelerometer amplifiers were set with a gain of 10 for *small* shakes. These gains were switched to 1 for *large* shakes during the spin down period prior to test 15. All converted data accounts for these changes in amplifier gain settings.

9.2.2 Shear Wave Velocity Tests

Shear wave velocity data was recorded in a manner similar to the description given for NJM02.

9.3 DATA ACQUISITION AND ORGANIZATION

The data acquisition system recorded a total of 89 channels for both tests. Channels 1-18 and 26-59 included filtering of instrument output using 5^{th} order programmable analog, low-pass filters prior to analog-to-digital (A/D) conversion. These filters are otherwise known as *tech filters* in this thesis and were set with a cut-off frequency generally equal to 40% of the sampling frequency to avoid signal aliasing. For example, if the sampling frequency was 2000Hz, the corresponding cutoff frequency would be 800 Hz. Thirty accelerometer channels were recorded for but were not filtered before A/D conversion. All signals requiring amplification were amplified at the bucket. Linear pots did not require signal amplification.

Small shakes and *large* shakes were sampled at different frequencies and durations to capture an appropriate amount of information. Sampling durations and frequencies are summarized in Table 9-3. All *large* shakes were recorded at three frequencies and durations to capture the extended duration of large excess pore

pressures that accompany robust input motions. Shear wave velocity tests were recorded at 50 kHz.

Table 9-3: SMS01 sampling durations and frequencies

Data File	Frequency and Duration 1	Frequency and Duration 2	Frequency and Duration 3
sms01_11	2000 Hz, 1 sec	NA	NA
sms01_12	2000 Hz, 1.2 sec	NA	NA
sms01_13	2000 Hz, 1.2 sec	200 Hz, 1 sec	NA
sms01_25	2000 Hz, 1.5 sec	2000 Hz, 5 sec	10 Hz, 5 sec
sms01_43	2000 Hz, 1.5 sec	2000 Hz, 5 sec	10 Hz, 5 sec
sms01_44	2000 Hz, 1.5 sec	2000 Hz, 5 sec	10 Hz, 5 sec

The raw data was collected in two types of files. *Slow* data monitors instrument behavior during spin up, spin down, and between shaking events. This data was recorded directly as voltage readings and labeled "slow**.slw." Converted slow data is presented in *pseudo-prototype* units based on the geometric and centrifuge scaling factors used in each test. However, the data is not correct in absolute units unless the entire file was recorded at 40-g due to centrifuge scaling laws. For example, many of the slow data files include data from spin up and spin down while the centrifugal acceleration varies. In these cases, the data only provides a relative picture of what happens during these periods between shaking events.

The second type of data is referred to as *fast* data. *Fast* data was recorded as binary offset data for the p-wave, shear wave, *small* shakes, and *large* shakes (sms01_**.out). The binary offset data is a relative value between 0 and 4096, which represents a range of 20 volts centered at 2048, so that:

$$Data_{volts} = \frac{Data_{binary\ offset} - 2048}{4096} \cdot 20\,volts$$

The *fast* data, has been converted from binary offset to volts. All slow and fast data was then converted from volts to representative prototype or model units based on instrument calibrations and amplifier gains. Appropriate centrifuge and geometric scaling factors are also included appropriately when converting to prototype units. None of the data has been zeroed during conversion. However, the following corrections were made:

- The signs of the accelerometers have been adjusted to be relative to each other and consistent with the direction of shaking (positive values are in the positive x and z directions).
- The signs of the linear pot calibrations were modified to have movement consistent with the positive axes as described previously (positive values are in the postive x and z directions).
- Small offsets in the data within a single test that occurred at changes in sampling frequency have been corrected.

After conversion all data files have been converted to "sms01_**.dat" files. All slow and fast data recording was labeled sequentially starting at number one to maintain a time history. The *slow* results are differentiated from the *fast* files upon conversion by appending "slw" to the beginning of the file name.

Caution must be used when analyzing instrument behavior between tests over the entire earthquake series due to changes in data that do not represent actual performance. For example, the author may have changed some instrument "zeros" between small and large shakes as the centrifuge was spun down. Amplifier zeros may also change after they have been shut down and repowered between separate days of shaking. These offsets in the data are most easily found by plotting the slow and fast data from a single instrument over the entire test sequence.

9.3.1 Plotted Data Presentation

The results of all recorded data has been plotted using a common format and template. An example of this format is provided in the description of test NJM02. Due to the large amount of the data, these plots will not be included within the hardcopy of the report, but are made available in Adobe Acrobat format on the accompanying CD. All data plotted in this format has been converted to prototype units using appropriate centrifuge and geometric scaling factors. For SMS01, each test requires 20 pages to plot all 89 channels of data. Titles of these data report pages and their corresponding instruments are given in Table 9-4.

Table 9-4: SMS01 data sheet instrument identifications

Description of data sheet instruments	Instrument Identifications
Pile 1 Strain Gauges	SG1-5, SG1-8, SG1-10, SG1-12, SG1-13
Pile 2 Strain Gauges (bottom)	SG2-1, SG2-2, SG2-3, SG2-4, SG2-5, SG2-6, SG2-7, SG2-8
Pile 2 Strain Gauges (top)	SG2-9, SG2-10, SG2-11, SG2-12, SG2-13, SG2-14, SG2-15
Pile 5 Strain Gauges (bottom)	SG5-1, SG5-2, SG5-3, SG5-5, SG5-6, SG5-7, SG5-8
Pile 5 Strain Gauges (top)	SG5-9, SG5-10, SG5-12, SG5-14, SG5-15
PPT's in the Free Array	PPT 5275, PPT 3955
PPT's in the Back Array	PPT 7985, PPT 7810, PPT 7719
PPT's in the Upper Dike Array	PPT 8013, PPT 7811, PPT 8044, PPT 7711, PPT 7370, PPT 7373
PPT's in the Toe and Middle of the Upper Dike Arrays	PPT 7367, PPT 7369, PPT 7714, PPT 6837
PPT's in the Lower Dike Array	PPT 7722, PPT 8016, PPT 6838
All Horizontal Linear Pots	LP 209, LP 401, LP 206, LP 212
All Vertical Linear Pots	LP 402, LP 207, LP 208, LP 403, LP 404
ACC's in the Free Array	ACC 5275, ACC 3955, ACC 4435
ACC's in the Back Array	ACC 3164, ACC 4436, ACC 4596, ACC 5268, ACC 3158
ACC's in the Upper Dike Array	ACC 5276, ACC 5267, ACC 3155, ACC 4595, ACC 3154, ACC 3959, ACC 4523, ACC 3951
ACC's in the Toe and Middle of the Upper Dike Arrays	ACC 5269, ACC 3964, ACC 4437
ACC's in the Lower Dike	ACC 3202, ACC 5271, ACC 3157, ACC 3949
All Wharf ACC's	V ACC 4534, ACC 3963, ACC 5603
All Box ACC's	ACC 3948, ACC 3161, ACC 5598
CDSM array ACC comparison	ACC 5276, ACC 5267, ACC 3203, ACC 3155

9.3.2 Raw and Converted Data Presentation

The data is also included on the CD-ROM in three (unplotted) formats: 1) the raw, unconverted, uncorrected data; 2) the converted data in model units; and 3) the converted data in prototype units. Files in model units may be differentiated from prototype files with the addition of "_m" before the file extension (e.g., sms01_25_m.dat). The raw data files have the "*.out" or "*.slw" extensions already described. The data files do not include a header that gives information on the instruments. Therefore, the appendices provide tables identifying each data column for all earthquake and shear wave velocity tests.

A table in Appendix B shows which column of data represents which instrument for each *small* or *large* shaking event. In the converted data (either model or prototype units), a time scale has been appended to the data file and is in the extreme right hand column. The data from the shear wave velocity tests has not been converted, but the heading includes the frequency at which the data was recorded, from which a time scale can be obtained.

9.4 MALFUNCTIONING CHANNELS OR INSTRUMENTS

The following is a list of known instrumentation problems.

- SG 2-15 did not work after test 25.
- The connection for LP 401 to the wharf deck broke off during test 25.

9.5 LIMITATIONS OF THE MODELING

The following is an itemized list of known limitations of model SMS01. If the topic was discussed previously during NJM02, the reader is directed to the previous discussion. However, if new limitations arise or circumstances change in regard to previous discussions, they will be discussed herein.

9.5.1 Model Construction in a 1-g Field

The topics surrounding this issue were discussed under the same heading during the discussion of model NJM02.

9.5.2 Instrument Locations

The topics surrounding this issue were discussed under the same heading during the discussion of model NJM02.

9.5.3 Boundary Conditions

As illustrated in Figure 4-1, the elevation of the model surface varies across the length FSB box. This condition results in an unequal loading on the ends on the box due to earth pressures (static and dynamic) and the FSB box deforms accordingly. During the first large shake of SMS01, the top rings of the box retained a residual displacement after the first large shake because of the non-uniform soil profile. Deformations in the direction of the backfill (i.e., southward) of approximately 4.5 mm were recorded. This has the possibility of effecting soil depths, density, and model performance if significant movement occurs. The permanent vertical and lateral soil deformations due to cyclic loading that are measured after testing must account for the FSB deformations that occurred during shaking events.

9.5.4 3-Dimensional Effects

When dissecting test SMS01, it was found that surface displacement measurements in the backland (primarily the *unimproved* zone) were not uniform over the width of the box in the y-direction. Settlements in the backland region in the center of the box were generally higher than on the box edges particularly in the unimproved

region. The photo in Figure 9-1 shows this effect as the board spans the width of the box and the photo is taken at the center of model. The most significant differential settlement measured was approximately 15 mm. The author believes this is partly due to boundary effects of the box and radial effects of liquefaction in the g field (the sand therefore settled out after liquefaction in a radial pattern corresponding to the radius of the centrifuge). Theoretically, the radial effects could account for a 7-mm differential between the settlements measured at the center and edge of the box.

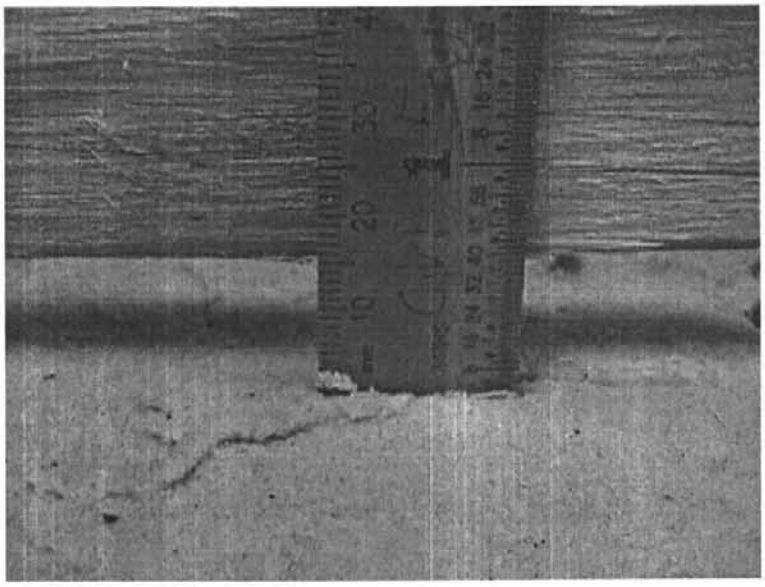

Figure 9-1: Photo of 3-dimensional settlement effects observed in the unimproved zone

10 NJM02 RESULTS

The focus of this research has been the presentation of the model construction procedures and the converted data in a format that is easily accessible for future researchers. A brief description of the recorded results of each type of instrumentation will also be included to help provide insights to the model behavior. A discussion will also focus on the general deformation characteristics of the model in relation to the given geometry. Most of the plots will provide qualitative results, however, some quantitative data will also be provided to compare results to expected performance or prototype strengths.

As previously described, the results of all the centrifuge data available on the CDROM in plotted and unplotted formats. The plotted time histories in Adobe Acrobat format will be referred to occasionally as a reference to the reader for further model analysis. Much of the data analysis and verification was carried out using plotted simulations of the instrument behavior. Animation capabilities within MathCAD software have allowed the author to analyze moment, pore pressure, linear pot, and acceleration data throughout the model simultaneously with a time history to provide a real time movie of model behavior. These animations are generated by compiling data from each of the instrument arrays described in the model layout chapters. Examples of these multimedia presentations can be accessed at http://www.ccee.orst.edu/geotech/wharfproject. Snapshots of these analyses will be included where appropriate to provide explanations of model behavior.

10.1 General Testing Comments

As explained in Chapter 6, a series of earthquake motions were run on the models. The *small* shakes are valuable for obtaining the low strain behavior of the model and the *large* shakes were run to record large strain soil behavior including liquefaction related movements. With the exception of the step wave motion during

small shakes, shakes were run with recorded earthquake motions scaled to specific intensities. The larger shakes were run to provide a representation of prototype behavior during earthquakes of similar ground motion intensity.

It is assumed that the small shakes do not influence the behavior of the model during later large shakes. However, the question arises as to the applicability of the centrifuge results after large strains have occurred during the first large shake. A number of issues may have influenced later tests such as:

- Large residual moments in the piles.
- Earthquake induced settlements due to post-liquefaction volume change of cohesionless soils.
- Increased soil density and associated change in stiffness/strength.
- Altered model geometry due to large deformations.

In light of these observations, an emphasis has been placed on the behavior of the model during the first large shake. Further comments on multiple shakes are included where appropriate.

10.2 General Deformation Patterns

An excellent picture of the overall deformation behavior of the model can be developed by plotting the movement of instruments from their pretest locations to post-test positions after all earthquakes have been run. Figure 10-1 shows these pre and post-test instrument locations of NJM02. Portions of the post-test dissection profiles have also been plotted in Figure 10-2 to provide an additional overall deformation picture. The surface profile readings were taken at the conclusion of all large shakes. The profile lines within the model represent readings taken at pertinent black sand layers placed during construction and measured during the dissection process. The backland profile of NJM02 shows vertical deformations increasing as the distance to the peak of the upper rock dike is reduced. Unfortunately, limited measurements down the face of the dike precluded an accurate profile for NJM02.

The deformations provided in both of these figures are generally accurate to within approximately 3-mm. However, it must be emphasized that the deformations shown within these figures are after all shakes. Because of the multiple large shakes that took place before these profiles were taken, this plot only represents the cumulative deformations. The actual deformations that occurred in each test can be estimated by beginning at the design configuration and incrementally moving to the desired profile by analyzing linear pot data.

10.3 NJM02 PILE BEHAVIOR

The strain gauge layout was designed to capture pile behavior at all key locations within the geometry for model NJM02 (e.g. soil interfaces, pile cap connection, variations with pile location). The pile behavior is presented herein includes recorded moment data. This moment data was converted from strains based on the calibrations described in section 4.2.3. The preliminary analysis of this data consisted of converting these moments into pile slope and pile deformations, however, the completion of these calculations and presentation of this data will be the subject of future work.

Snapshots of the model animations described previously are used to present the moment data. These figures are used primarily to show the following pile behavior: a) the time during shaking and location of the maximum moments, b) the timing and location of other significant moment concentrations, and c) the location of high residual moments after shaking. As outlined in Chapter 1, these moment concentrations are typically observed at the three following locations: 1) pile cap connection, 2) weak/stiff soil interfaces, and 3) about 1 to 3 diameters below grade in non-liquefying soils. Comments on these key locations will be provided throughout the analysis.

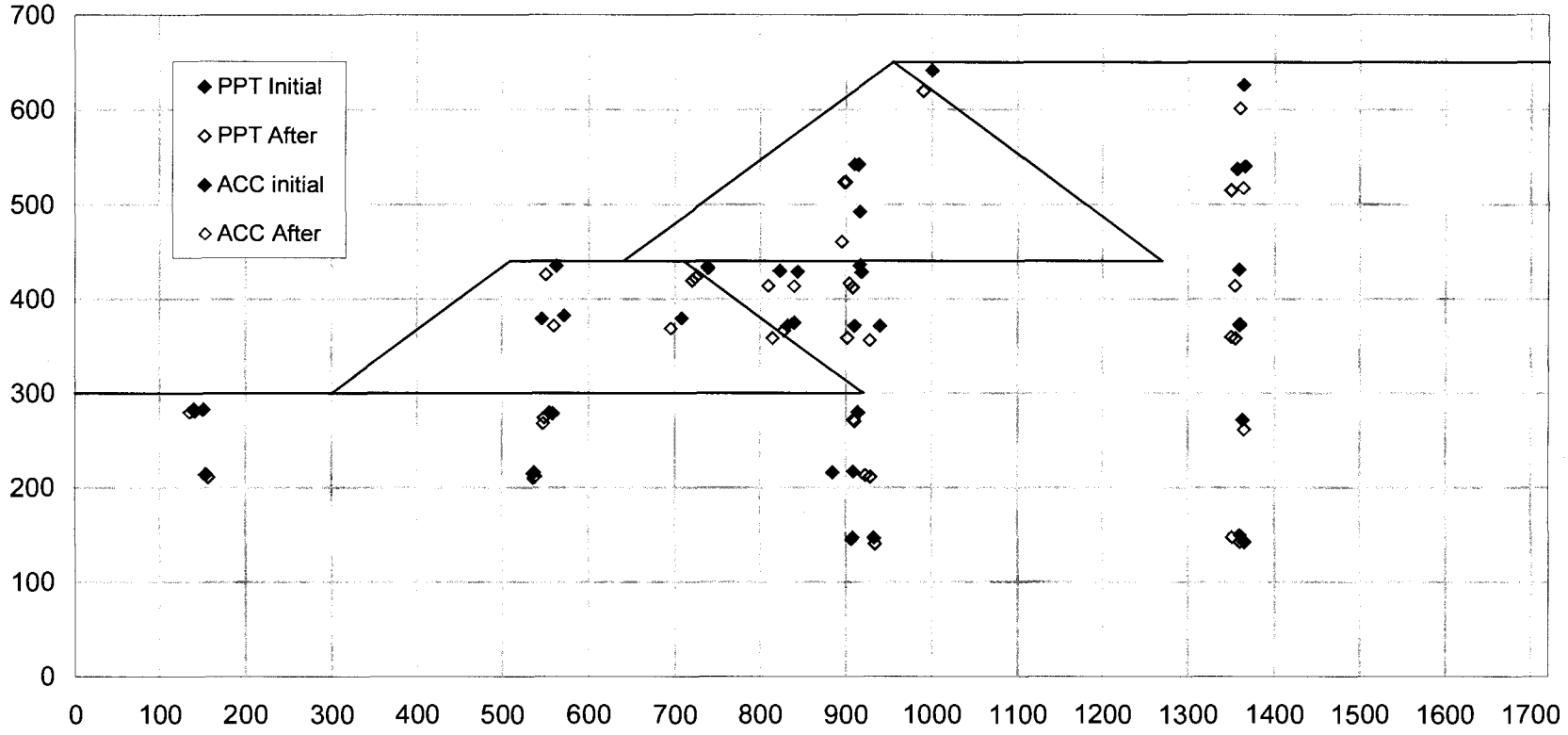

Figure 10-1: NJM02 instrument movement

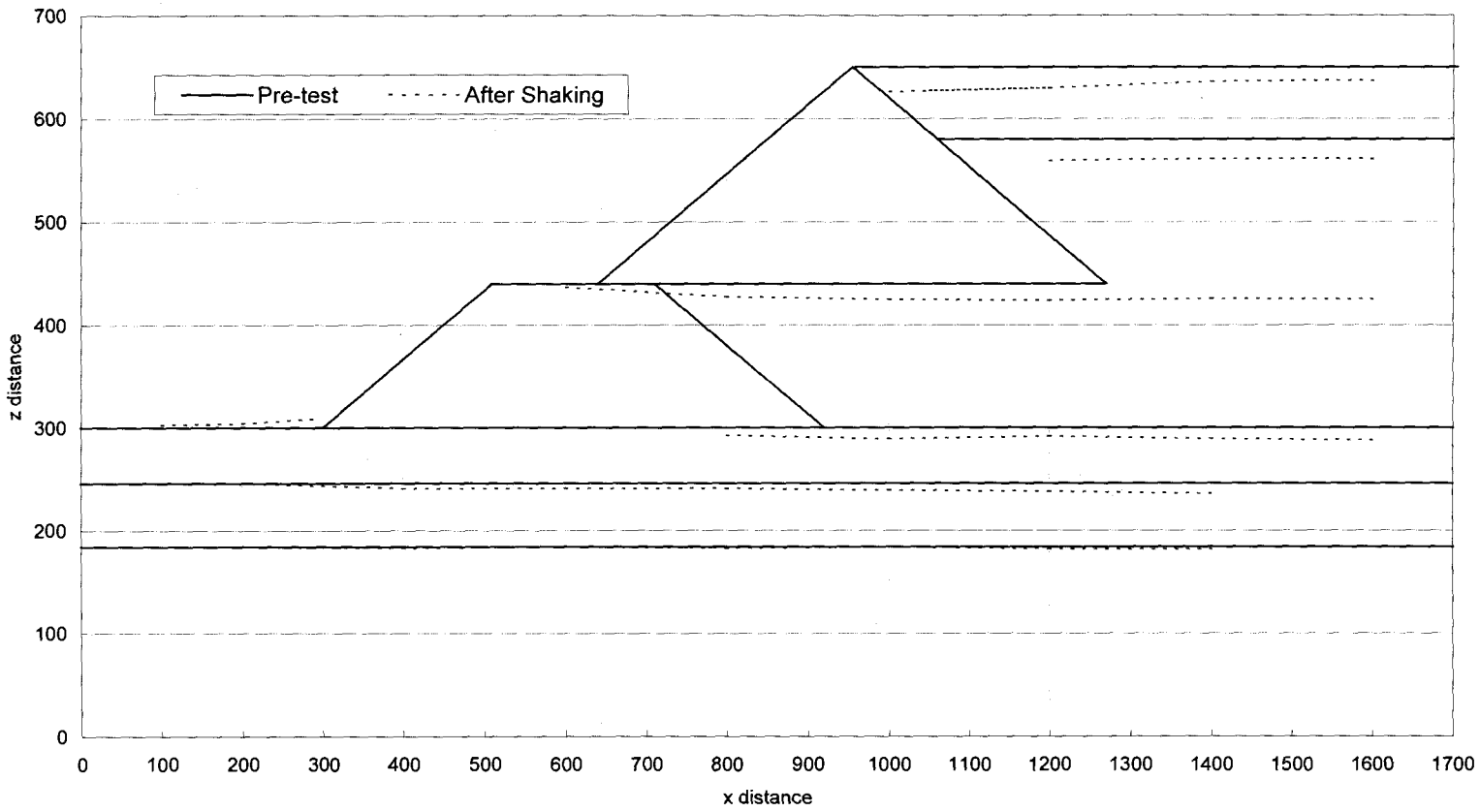

Figure 10-2: NJM02 dissection profiles (dimensions in mm)

Due to the problems with the data acquisition system described in section 6.1.1, data was not obtained at a number of design gauge locations. However, sufficient data was recorded to provide an overall picture of pile behavior. Figure 10-4 provides a snapshot of the pile behavior near the end of the first *large* earthquake loading of NJM02. This figure shows pile moments superimposed over the soil profile. Each circle represents a recorded strain gauge location and the dashed line was created using a cubic spline fit to the uncorrected data. This moment data has been plotted on top of a solid zero moment reference line. The interpolated line has been removed in areas where limited strain gauge data precludes representative interpretation of the pile behavior. Moment values are not shown on this figure, however, the moments are plotted to an equivalent scale. The approximate scale can be established based on the fact that the value of the moment at the base of the upper rock dike in pile 1 is –0.87 MN*m. The sign convention established for the piles is shown in Figure 10-3. Positive moments are shown in Figure 10-4 to the right of the solid reference line.

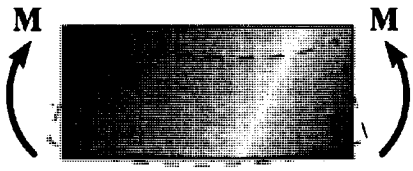

Figure 10-3: Sign convention for moments in relationship to deformed shape. Positive moments are plotted to the right hand side of zero lines in all figures.

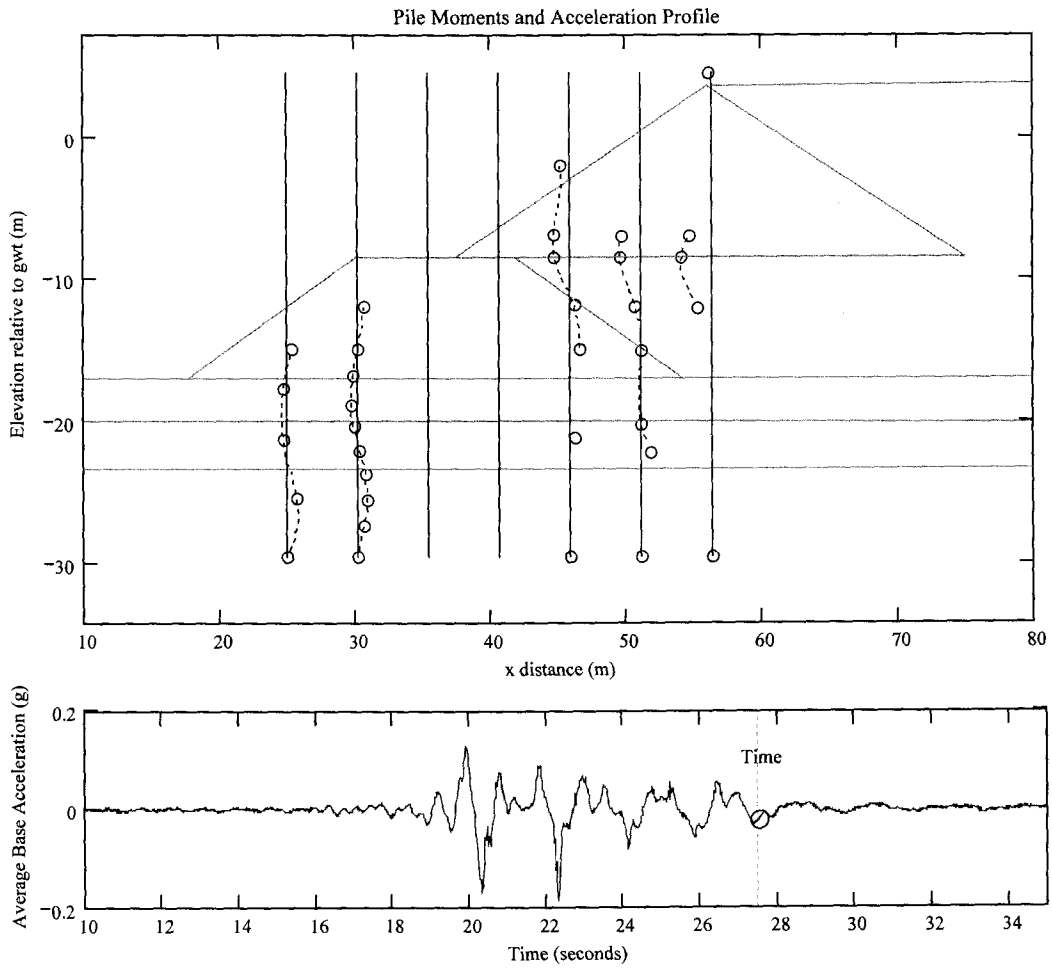

Figure 10-4: NJM02 pile behavior during test 42 plotted with time history

The actual input earthquake record with time marker is included below the plot to show what point in time the data represents. At the snapshot in Figure 10-4, the maximum recorded moments occur at the interface beneath the upper rock dike. The soil properties at this interface represent a significant contrast moving from the competent, stiff, rock material to the loose sand used as the dike foundation.

The interface of the piles and the rock slope face was identified as a potential area of large moment concentration. Unfortunately, problems with the amplification system caused a significant number of these design array gauges to go unrecorded and

insights on this behavior are unavailable. Although little data was recorded near the pile heads, the maximum moment during NJM02 was recorded at the top of pile 1 (SG 1-16) with a value of 1.0 MN*m. The moment profile during this peak moment is shown in Figure 10-5. As indicated by the timer marker, this peak moment occurs relatively early in the motion during movement back into the slope. Historically, a significant number of failures associated with piles in wharf structures have occurred in this pile head region. By examining the readings on pile 6 (second pile in from bay) in both figures, the moment readings are well below plastic moment capacity at the clay/sand interfaces.

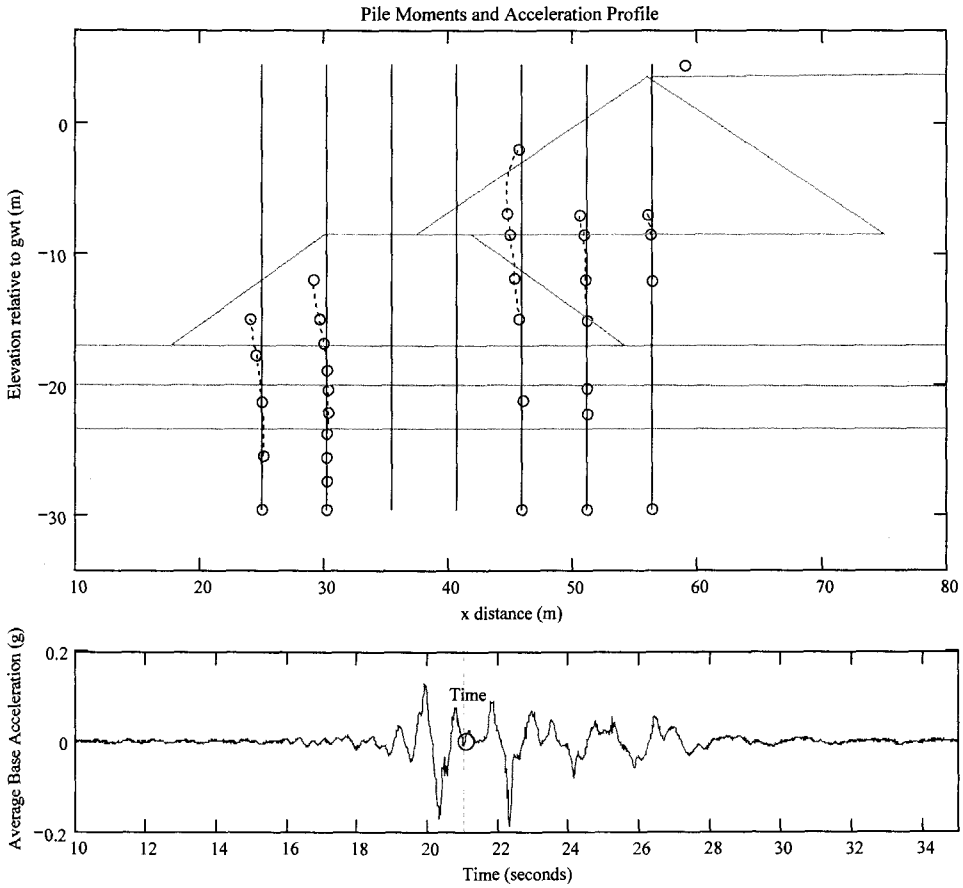

Figure 10-5: Moment profile at time of peak recorded moment

The residual moments recorded approximately 1.5 minutes after shaking are provided in Figure 10-6. The moments at the top of pile 1 where the maximum pile moments were recorded have now been greatly reduced. The residual stress concentration is now at the base of the upper rock dike. Therefore, the two key regions of concern that were identified during NJM02 were: 1) the rock/loose sand interface at the foundation of the upper dike and 2) the pile head connection.

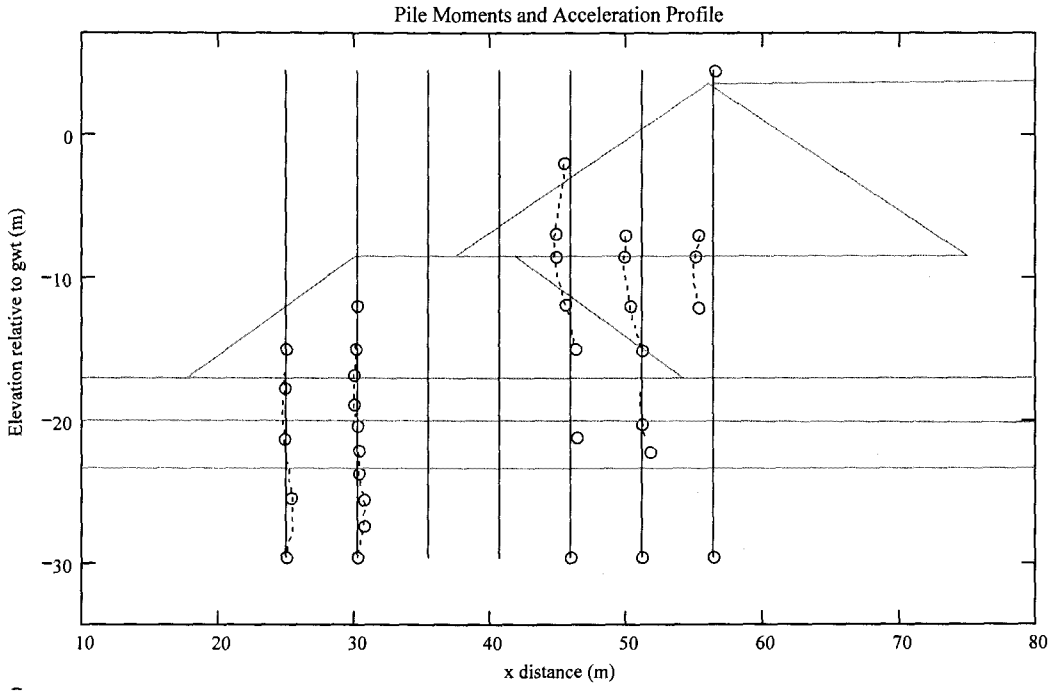

Figure 10-6: Residual moments in piles after test 42

As mentioned in section 3.5, the strength of the model piles are much greater than the scaled prototype plastic moments. Therefore, the pile behavior recorded was all in the elastic region of the model aluminum piles. The model should be analyzed with the understanding the pile (and wharf) performance could have been significantly different as the earthquake record proceeds if a series of plastic hinges developed through the earlier parts of the motion.

10.4 PORE PRESSURE BEHAVIOR

The deformation behavior of any saturated sand model during an earthquake is strongly dependent on the buildup of excess pore pressures within the soil structure. All the pore pressure data is plotted on the CDROM and is available for analysis. The presentation of pore pressures is commonly made using the excess pore pressure ratios. The excess pore pressure ratio is defined as the ratio of the excess pore pressures to the vertical effective stress. A state of liquefaction occurs when this relationship reaches a value of one. The brief discussion of pore pressures within this thesis will be limited to a single plot showing the development of excess pore pressures. Similar to other analysis within the thesis, these pore pressures will be presented as snapshots of an animated video of instrument behavior placed within each array in the model.

Figure 10-7 presents the pore pressure from each array within the model plotted as an excess pore pressure ratio. The array labels used on the plots are described in the model layout. Each pore pressure transducer is represented by a symbol shown in the legend corresponding to an array. Lines have been used to connect each array for clarity, but do not necessarily indicate interpolated pore pressures. The horizontal lines on the plot correspond to the soil or rock layers defined in the model layout section. Although the figure does not show variation over time, it shows the space variation of pore pressures through the model. A relevant point to note from analysis of the pore pressure data is shown by analyzing the data in the td and md arrays. These arrays record data from the loose sand material under the upper rock dike. As illustrated in Figure 10-7 and the converted data files, the largest excess pore pressure ratio recorded was approximately 0.5. Due to the loose state of the sand and the large pile moments recorded at the interfaces with the rock dike, it would be expected that these pore pressures would be higher. The author has two possible explanations for these relatively low pore pressures: 1) The sand has a short enough drainage path to the surrounding rock dike to quickly dissipate pore pressures, or 2) The sand was densified enough during placement of the upper rock dike that excess pore pressures

could not develop. The author believes that the latter option is not a primary concern as any densification during rock placement was minor. It should also be noted that the first large shake only had a PGA of approximately 0.2-g.

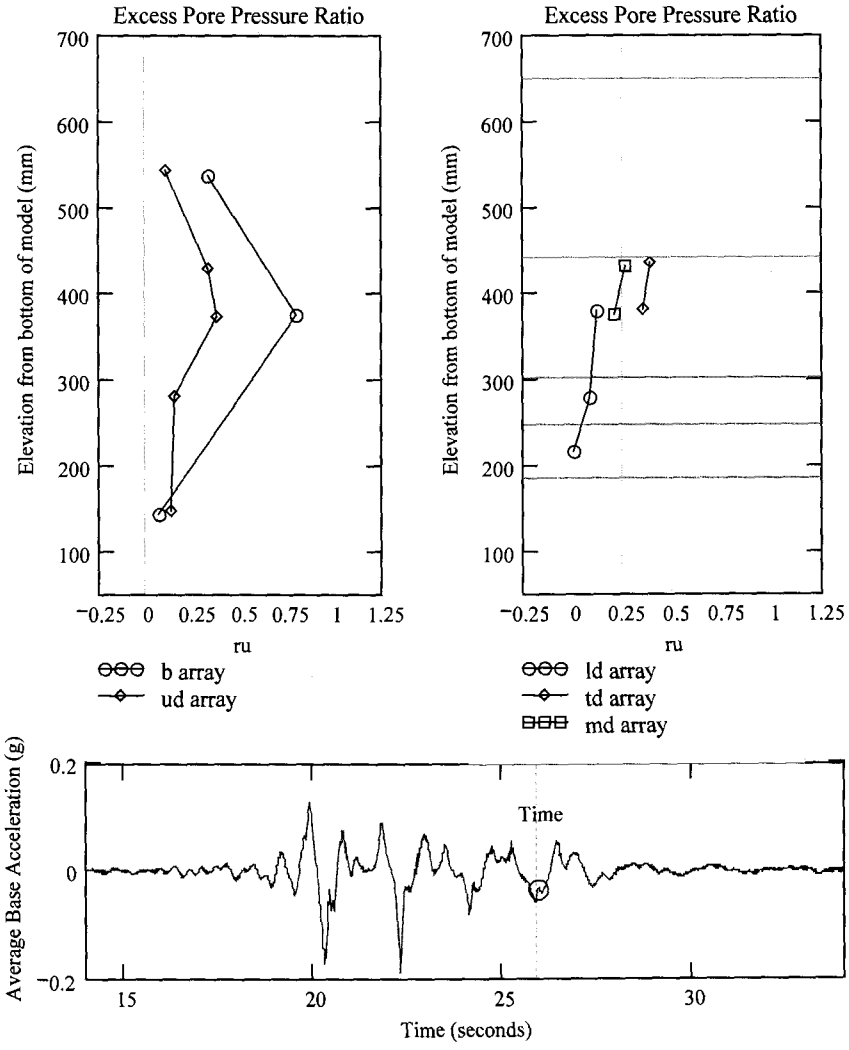

Figure 10-7: NJM02 pore pressure array data during test 42 (Loma Prieta earthquake)

10.5 NJM02 Wharf Behavior

The deformation behavior of the wharf deck during NJM02 will be discussed in a summary with model SMS01. However, all the linear pot movements are available on the accompanying CDROM.

10.6 Measured Site Response

An extensive evaluation of the overall model site response is beyond the scope of this thesis. However, comments will be provided on the preliminary data analysis and presentation methods used by the author. The time histories from all the instruments in each accelerometer array are provided on a page of the plotted data on the accompanying CDROM. Real time simulations of these time histories have been prepared in a similar manner to the previously described moment data. These simulations are available on the aforementioned project website.

The spectral model response is presented in two different manners. The first is shown in Figure 10-8 which plots the normalized spectral acceleration (defined as the spectral acceleration divided by the peak ground acceleration) of the base accelerometer and an accelerometer at the surface in the back array. This figure shows the normalized spectral accelerations of *small* and *large* shakes during NJM02 with the input and surface PGA values shown in the legend. The plot on the left shows the normalized spectral acceleration of the base input and the surface from the first *small* Loma Prieta and Northridge shakes. The plot on the right shows results from the same instruments for the large shakes of each test. The second method is more common for site response analysis and is shown in Figure 10-9. This figure shows the spectral amplifications (defined as the spectral acceleration at the surface divided by the spectral acceleration of the input) of the same instruments shown in Figure 10-8. The predominant period of the site is then defined by the period on the x-axis where the maximum amplification occurs.

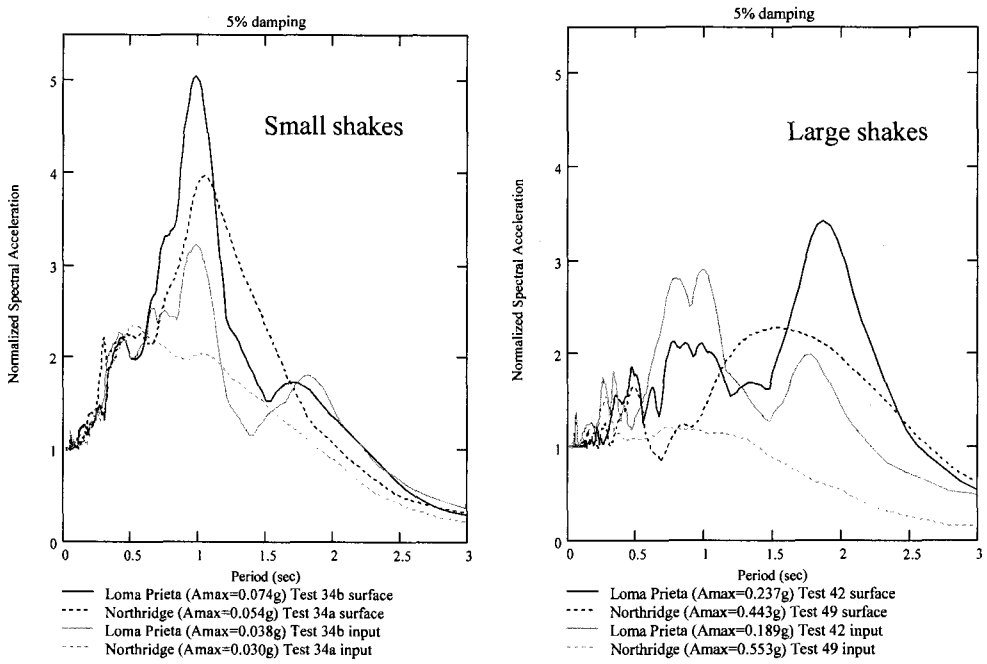

Figure 10-8: NJM02 normalized spectral acceleration during *small* and *large* shakes

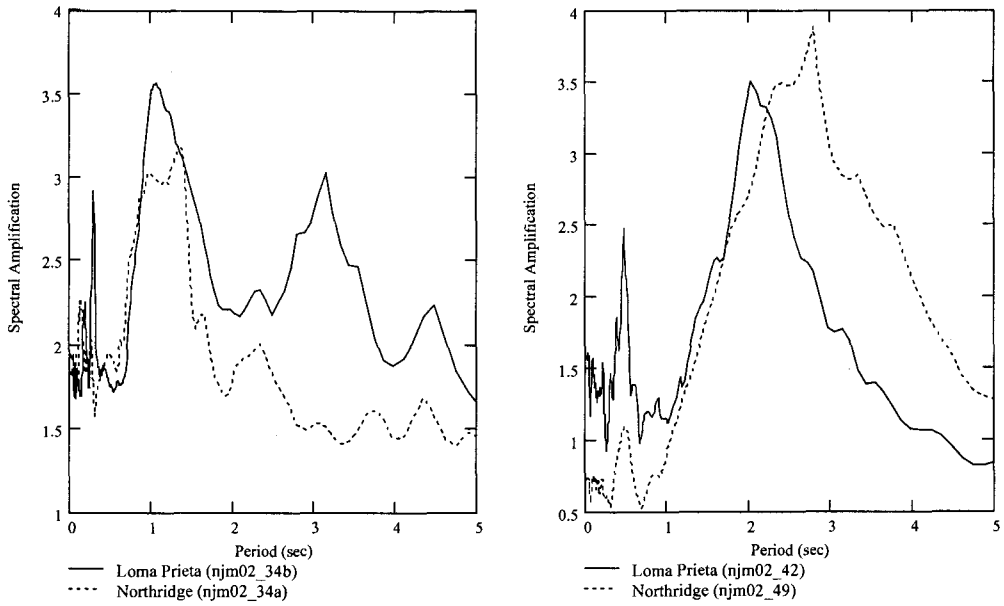

Figure 10-9: NJM02 spectral amplification during *small* and *large* shakes.

By analyzing the figures, it is seen that mid-frequency motions with a period of approximately 1 second are amplified during *small* shakes and lower frequency motions with a period of approximately 2 seconds are amplified during *large* shakes. More analysis of the site response is provided with the data from test SMS01.

10.7 Pile Effects and Soil Structure Interaction

A complete analysis of the soil structure interaction behavior of the models is outside the scope of this report. However, it is germane to comment on general observations in regard to the effect of the piles on the embankment stability seen during the test sequence. The effects of piles on the stability of the embankment are being addressed in a companion investigation. This concurrent investigation is addressing a variety of related issues including pile pinning effects and variable pile spacing.

The effects of the piles on the model will be described further during the discussion of SMS01. However, the pertinent observations from NJM02 will be provided here. The deformation patterns in Figure 10-10 provide an excellent introduction into this behavior. This photo was taken at the completion of all earthquakes in the NJM02 test series. The deformation cracks and pile gapping clearly show the wharf has moved farther than the surrounding soil at the surface. This can be attributed to either the combined behavior of two phenomena. The first is that soil deformations lower in the model induced permanent moments in the piles, resulting in permanent lateral wharf deformations. The second factor is that the dynamic inertial response of the wharf deck contributed to the response and created the additional displacement. The true behavior of the model is a combination of these two effects representing soil structure interaction.

Figure 10-10: Pile gapping and deformation cracks after all earthquakes in test NJM02.

11 SMS01 RESULTS AND COMPARISON WITH NJM02

The results of SMS01 will be described in a manner similar to NJM02. Additional sections have been added to discuss the performance of the soil improvement strategies within the model. Consistent with the previous format, comparison of SMS01 model behavior to that seen during NJM02 will be included where appropriate.

11.1 General Deformation Patterns

A plot of instrument movement from their pre-test locations can develop an additional set of deformation behavior within the model. Figure 11-1 shows these pre and post-test instrument locations of model SMS01. Portions of the post-test dissection profiles have also been plotted in Figure 11-2 to provide an additional overall deformation picture. The profile readings were taken at the conclusion of all large shakes. The profile lines within the model represent readings taken at black sand layers placed during construction and measured during the dissection process. The interpretation of these figures should be consistent with the discussion provided regarding the deformation patterns of NJM02. Because they were taken after all large shakes, the deformations shown are a cumulative deformation profile. The movements that occurred during each test can be deduced by analyzing the data from each shake.

Models NJM02 and SMS01 show significantly different overall deformation profiles. The backland profile of SMS01 distinctly shows the break between *improved* and *unimproved* sands with significantly more settlement in the unimproved zone. The backland profile of NJM02 shows surface settlements increasing toward the peak of the upper rock dike. The extent and location of deformations during SMS01 is also represented by the location of ground cracks shown in the post-test photo in Figure 11-3.

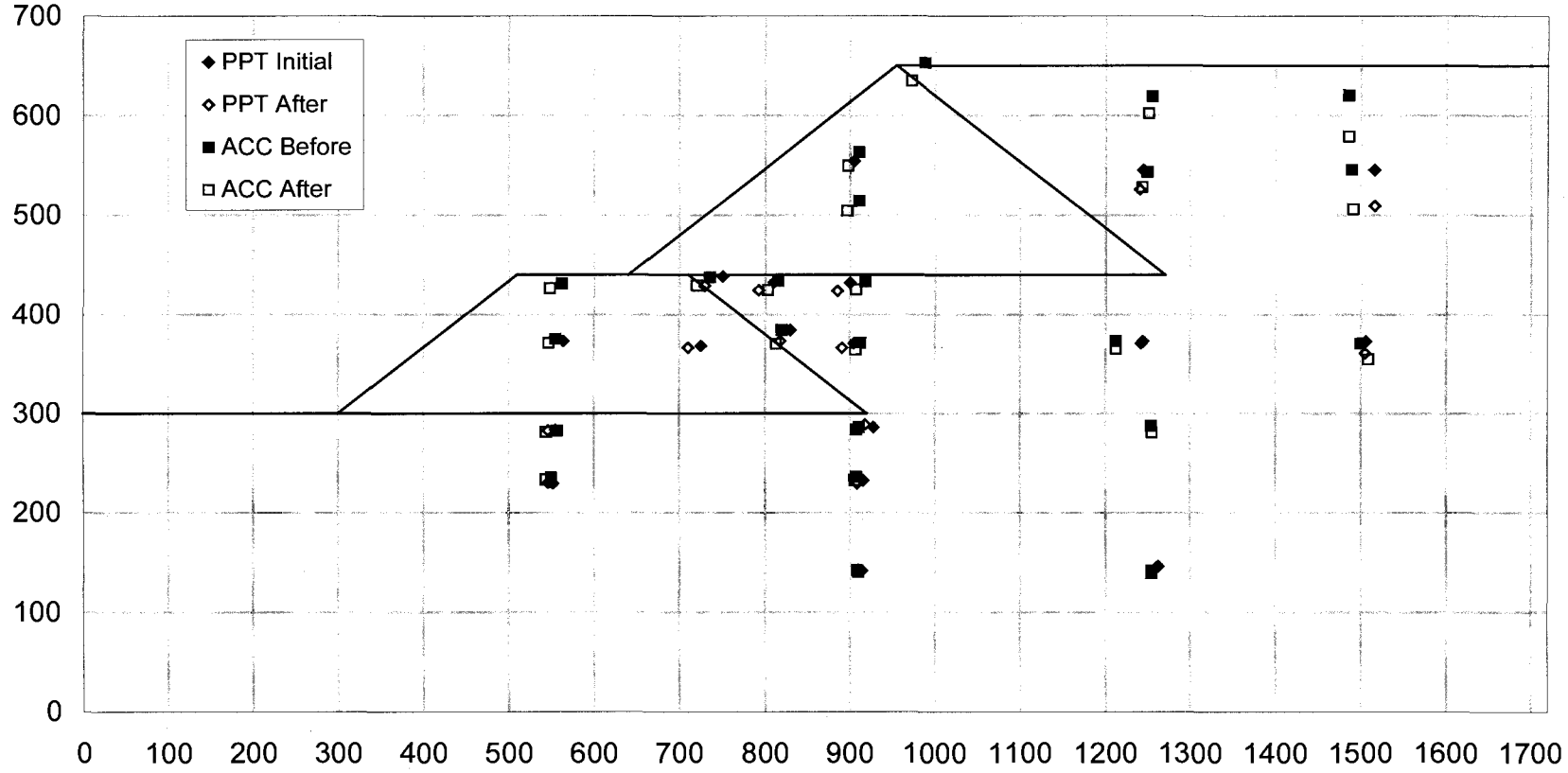

Figure 11-1: SMS01 instrument movement

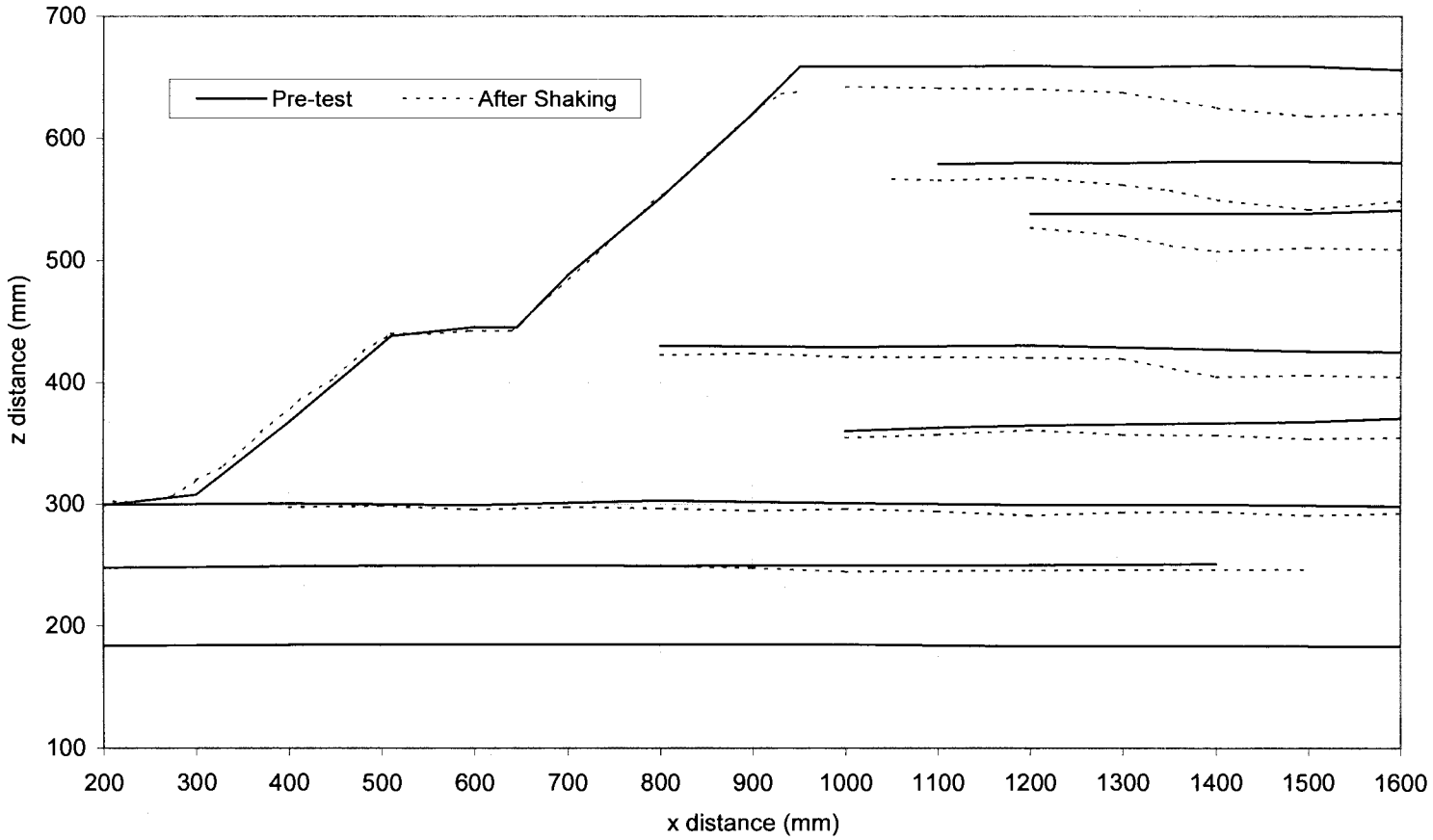

Figure 11-2: SMS01 dissection profile

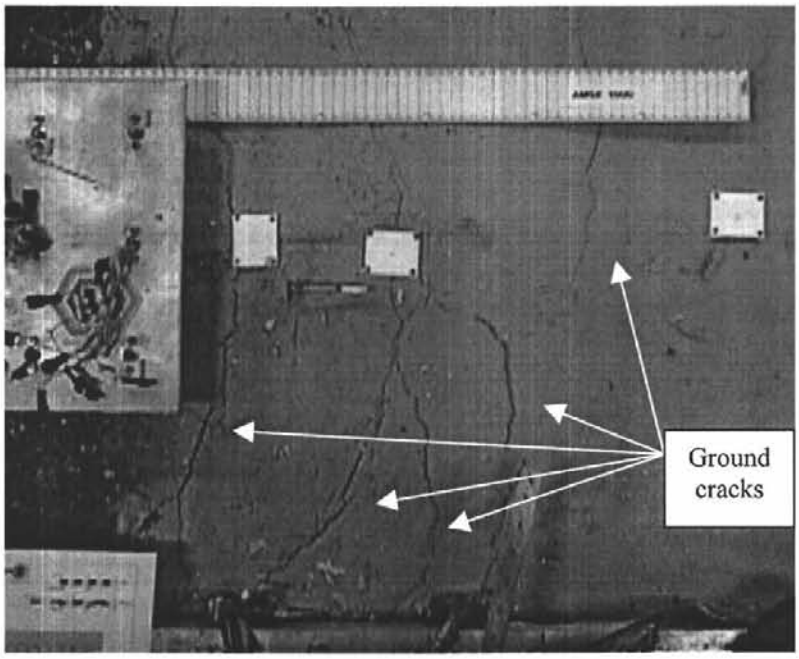

Figure 11-3: Ground cracks in the backfill after the completion of all shakes of SMS01.

11.2 PILE BEHAVIOR

The pile behavior of model SMS01 is qualitatively assessed in a manner similar to the procedure employed for model NJM02. Snapshots of animated data are plotted over the soil profile to provide a picture of the overall pile moment profiles. With the new strain gauge design implemented in test SMS01 and with the data acquisition system working appropriately, the available moment profile was significantly better than what was recorded during NJM02. Gauges were recorded on only three piles with the majority located over the full lengths of piles 2 and 5. Five gauges were recorded on pile 1 to see if the same concentration of moments at soil interfaces that were seen in NJM02 appeared in SMS01.

Consistent with the discussion provided in NJM02, these figures will be used primarily to show the following pile behavior: a) timing and location of the maximum moment occur, b) The timing and location of other significant moment concentrations,

and c) The location of high residual moments. As outlined in Chapter 1, these moment concentrations are typically at the three following locations: 1) pile cap connection, 2) weak/stiff soil interfaces, and 3) about 1 to 3 diameters below grade in non-liquefying soils. Comments on these key locations will be provided throughout the analysis.

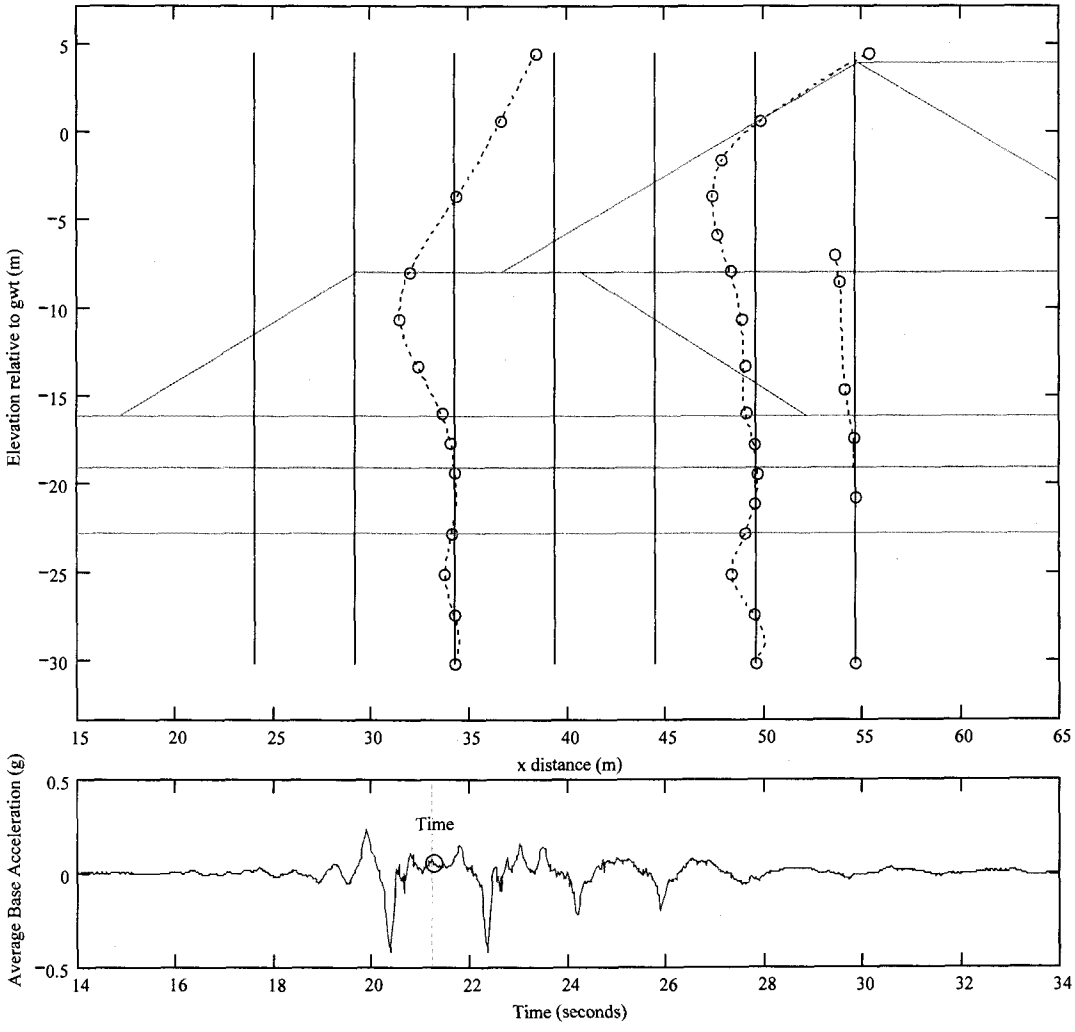

Figure 11-4: SMS01 moment profile at the time of peak recorded moment (in pile 2).

Figure 11-4 provides a snapshot at the time of the maximum recorded moment during the first large shake of SMS01 (test 25). This moment (1.36 MN*m) appears at

the top of pile 2 after the first large peak in the Loma Prieta motion during test 25. This moment occurs at a nearly identical time and location to the maximum recorded moment during the same test in NJM02.

Figure 11-5 provides a snapshot later during the same earthquake motion. Significant moments (1.0 MN*m) still exist at the top of pile 2, however, large moments (0.5 MN*m) have also developed at the interface of the base of the clay layer and CDSM grid. It should be noted that these moments did not occur at this interface in NJM02. However, with the addition of the *improved* sand foundation of the upper dike, the large interface moments present at the base of the dike in NJM02 did not appear in SMS01.

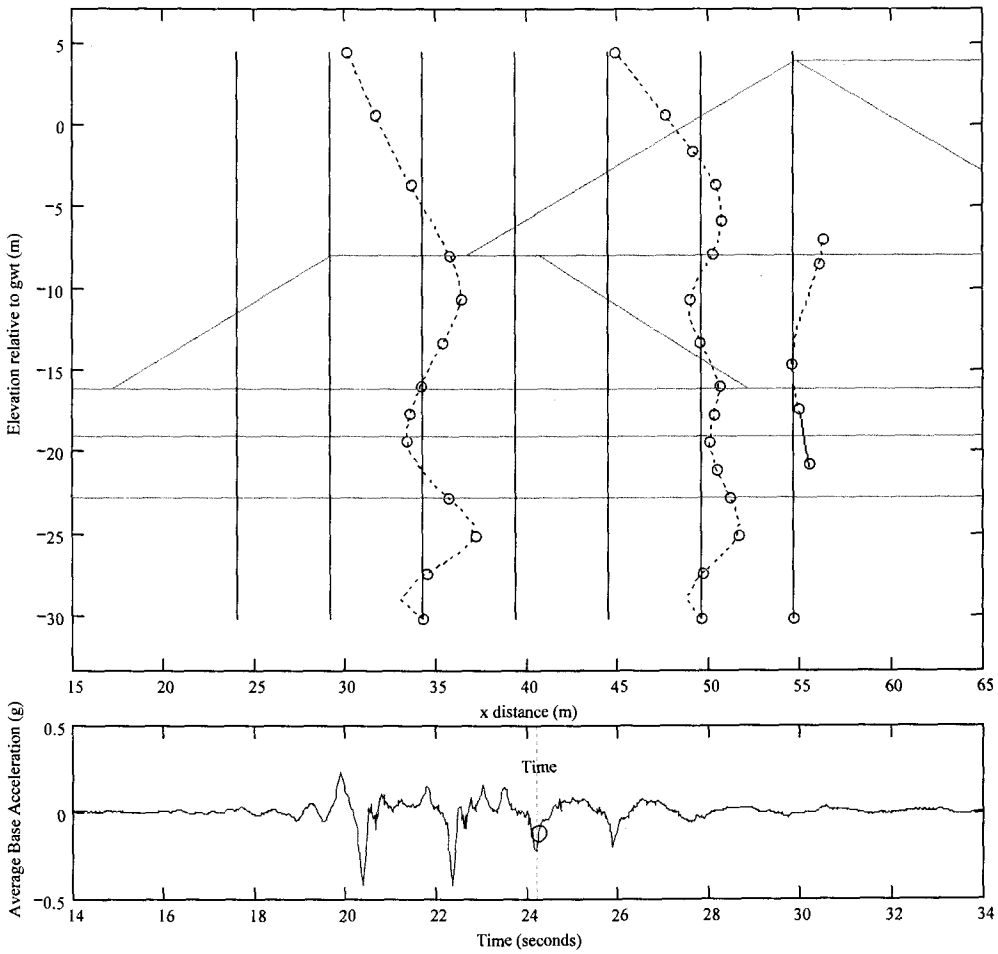

Figure 11-5: SMS01 moment profile during test 25

Figure 11-6 provides a snapshot of the residual moments recorded in the piles approximately 5 minutes after the end of shaking in test 25. This plot shows that large moments (0.69 MN*m) are left at the bottom of pile 5. In addition a moment of -0.45 MN*m is present at the top of pile 5.

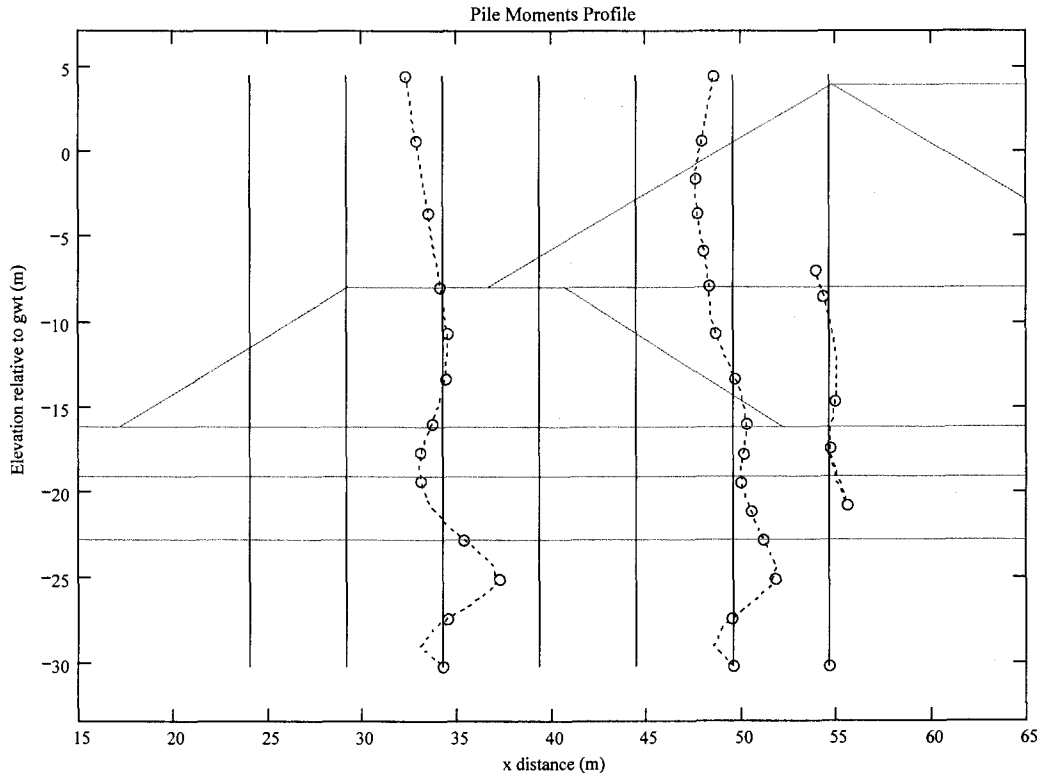

Figure 11-6: Residual moments in piles after test 25 (5 minutes after the end of shaking).

Typical plastic moments for 24-in octagonal reinforced concrete piles range between 0.6 and 1 MN-m. The moments presented in the three previous figures have shown pile moments developing in excess of the lower bound of this plastic moment range in at least three places: 1) connection to the pile deck, 2) below the pile 2 interface with the rock dike, and 3) at the base of the clay layer in both piles. It should be noted that the large moments measured at the base of the clay layer remain as residual moments well after the earthquake is over. These moment concentrations at

depth are due primarily to ground deformations and can be "locked in" as permanent residual moments after shaking. The highest moments recorded at the top of the piles dissipate a larger portion of their maximum value but are still near the lower bound of the plastic moment capacity of the piles. In contrast to the moments deeper within the soil profile, the moments at the pile head are due more largely to the inertial contributions of the wharf deck and soil-pile interaction and hence the moments can decrease to a higher degree after shaking.

11.3 Pore Pressure Behavior

The brief analysis of pore pressure data for SMS01 will be presented in a similar manner to NJM02. Figure 11-7 presents the pore pressure from each array within the model plotted as an excess pore pressure ratio. The array labels used on the plots are described in the model layout. Each pore pressure transducer is represented by a symbol corresponding to a respective array within the model. Lines have been used to connect each array for clarity but do not necessarily indicate interpolated pore pressures. The horizontal lines on the plot correspond to the soil or rock layers defined in the model layout section. Although the figure does not show variation over time, it shows the space variation of pore pressures through the model.

The top left plot of Figure 11-7, yields some interesting insights to the behavior of model by showing the buildup of excess pore pressures during SMS01. The pore pressure transducers show liquefaction occurring first in the *unimproved* soils in the free-field array. However, significant pore pressures (r_u=0.8 – PPT 7810) and liquefaction (r_u=1.0 -- PPT 5268) were also recorded later in the motion by the transducers in the back array despite their location in sand that was placed at a higher relative density to represent *improved* soils. In the author's opinion, this behavior could be due to excess pore pressure migration from the unimproved zone to the densified zone. The transducers in the *improved* sand at the base of the upper dike

showed highly varying values of excess pore pressure ratio and still need further interpretation.

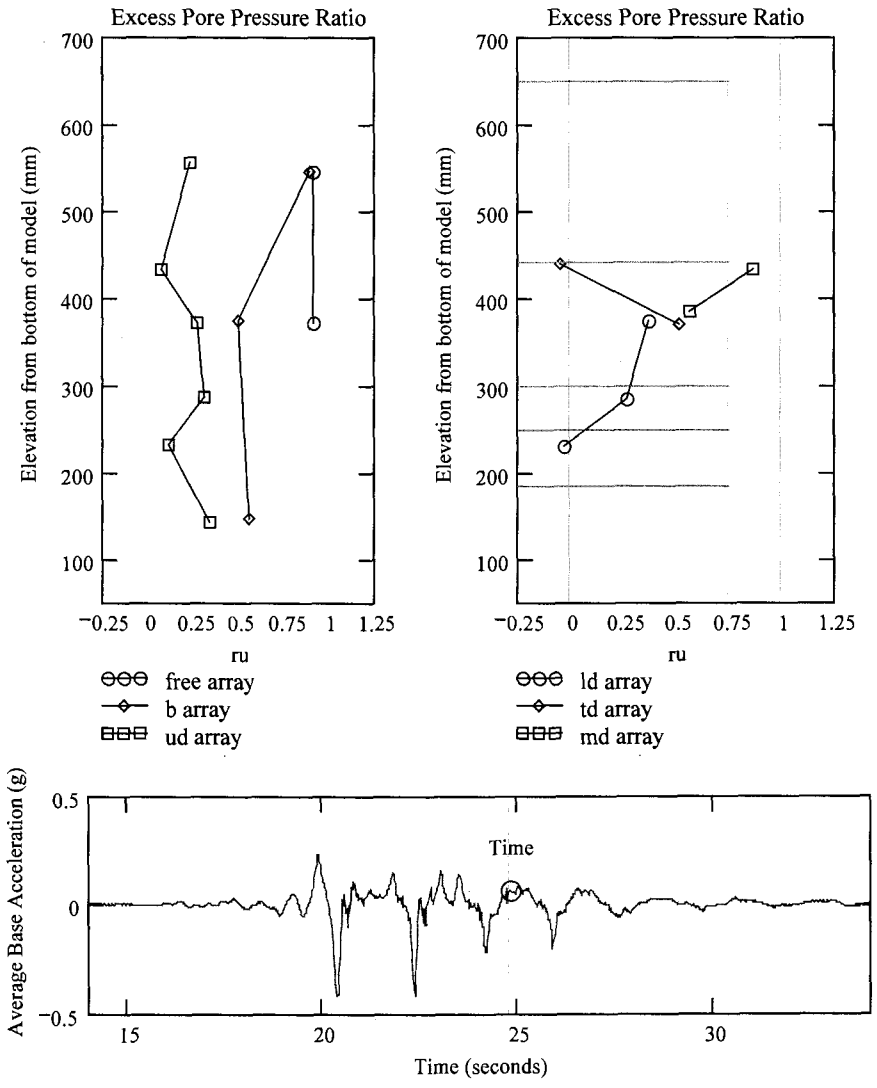

Figure 11-7: SMS01 pore pressure data during test 25 (Loma Prieta earthquake)

The performance of improved ground can be further analyzed through the pore pressure data plotted in Figure 11-8. This figure plots a time history of pore pressures in terms of excess pore pressure ratio for three transducers at elevation 8 in the model.

PPT 7368 is located in the free array in unimproved soils. The other two transducers are located in *improved* soils in the ud and b arrays. PPT 7368 clearly reaches a state of liquefaction while pore pressures dissipate in the other arrays before reaching full liquefaction. More analysis is needed to interpret the pore pressures throughout the model. Specific issues include the behavior of the transducers at interface layers and in the foundation soils of the upper rock dike.

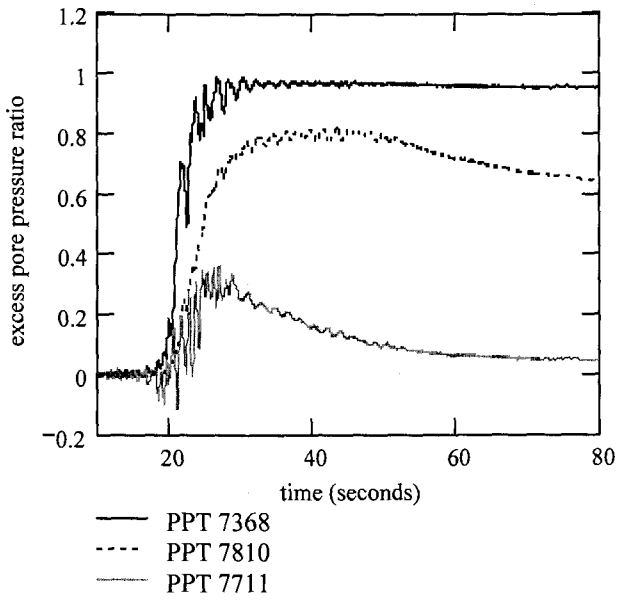

Figure 11-8: Pore pressure behavior of three transducers at elevation 8 within the model. PPT 7810 and 7711 are in improved soils while PPT 7368 is located in loose sands

11.4 WHARF BEHAVIOR

The permanent lateral deformation of the wharf deck is a significant seismic design issue. Figure 11-9 shows the performance of the modeled pile-supported wharves, characterized by the permanent lateral deformations and peak ground surface accelerations. The data in this figure is from the two models discussed with this report

(NJM02 and SMS01), with the addition of the first centrifuge model in this series of tests (NJM01). The geometries between NJM01 and the two models discussed within were generally the same, except NJM01 did not include the layer of clay. In comparing the behavior shown in the figure, it should also be noted that the initial relative density of the backfill for each of the three models also varied as indicated in the figure legend. The backfill in SMS01 was composed of approximately half 30 percent relative density sand and the remainder was improved to 70 percent.

The lines connecting the points in Figure 11-9 indicate the time sequence of the tests. The points hovering around zero are the initial small shakes, while the larger displacement values correspond to the larger shakes. The decreased lateral deformation, for the same or greater peak ground accelerations, after the first several large shakes demonstrates the effects of incremental densification of the loose sands within the model and the greater liquefaction resistance, as well as slightly increased stability due to embankment deformations and redistribution of stresses within the model. This reduction is also due to the fact displacements are recorded from the point of residual displacement of the deck after the previous shake.

The single point from the Port of Oakland from the 1989 Loma Prieta Earthquake indicates the performance of the 7th Street Marine Terminal (Egan et al., 1992). The 7th Street Marine Terminal consisted of a single-lift rock dike (in comparison to the multi-lift rock dike of these studies) and included a row of battered piles (in comparison to the all vertical pile systems that were modeled). However, the data point seems to indicate the same relative deformation-acceleration trend as that of the centrifuge models. It should also be noted that the majority of the battered piles failed at the pile-wharf deck connection during the earthquake.

Lateral deformations are a function of static factor of safety against slope failure (and therefore K_{yield}), the liquefaction resistance of the backfill and foundation soils, the post-liquefaction stability of the embankment, and the strength and duration of the ground motions. Although the wharf geometries are not identical between our models and the 7th Street terminal, many of these parameters are roughly equivalent.

Therefore, the agreement between model and prototype deformations seems reasonable.

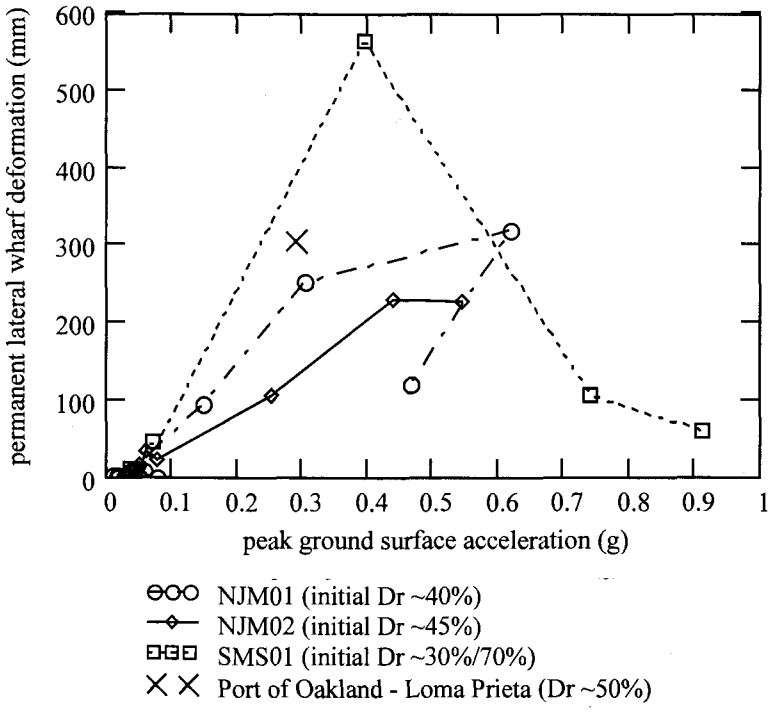

Figure 11-9: Relationship between the peak ground surface acceleration and the seaward permanent lateral deformations of the wharf deck.

11.5 Measured Site Response

The spectral model response for test SMS01 is presented in a similar manner to the discussion provided with test NJM02 and is presented using two methods. The first is shown in Figure 11-10 which plots the normalized spectral acceleration (defined as the spectral acceleration divided by the peak ground acceleration) of the

base accelerometer and an accelerometer at the surface in the back array. This figure shows the normalized spectral accelerations of *small* and *large* shakes during NJM02 with the input and surface PGA values shown in the legend. The plot on the left shows the normalized spectral acceleration of the base input and the surface from the first *small* Loma Prieta and Northridge shakes. The plot on the right shows results from the same instruments for the large shakes of each test. The second method is more common for site response analysis and is shown in Figure 11-11. This figure shows the spectral amplifications (defined as the spectral acceleration at the surface divided by the spectral acceleration of the input) of the same instruments shown in Figure 11-10. The predominant period of the site is then defined by the period on the x-axis where the maximum amplification occurs.

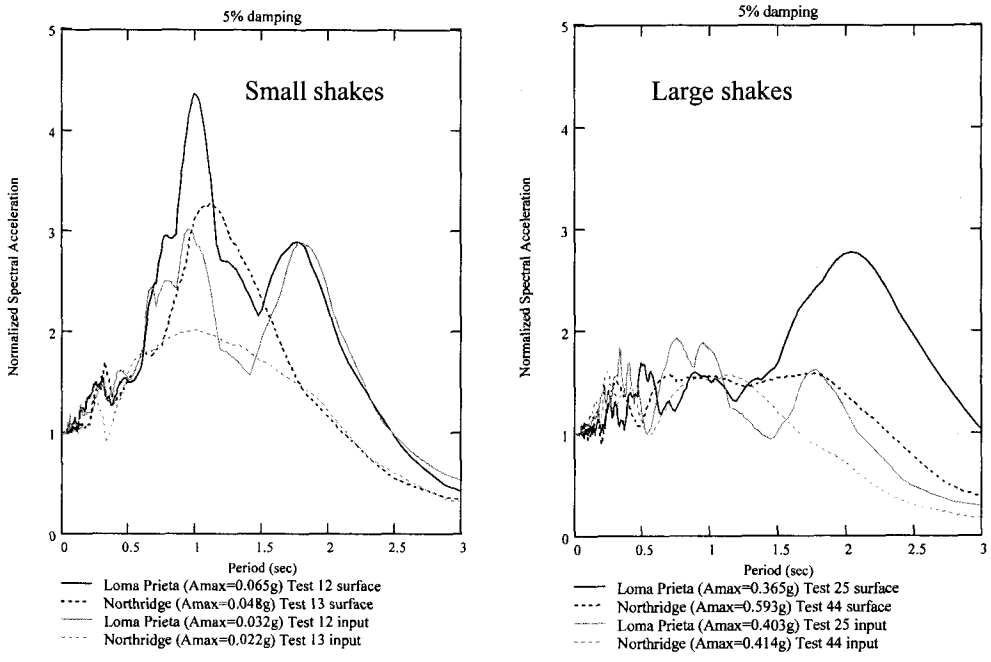

Figure 11-10: SMS01 normalized spectral acceleration during *small* and *large* shakes.

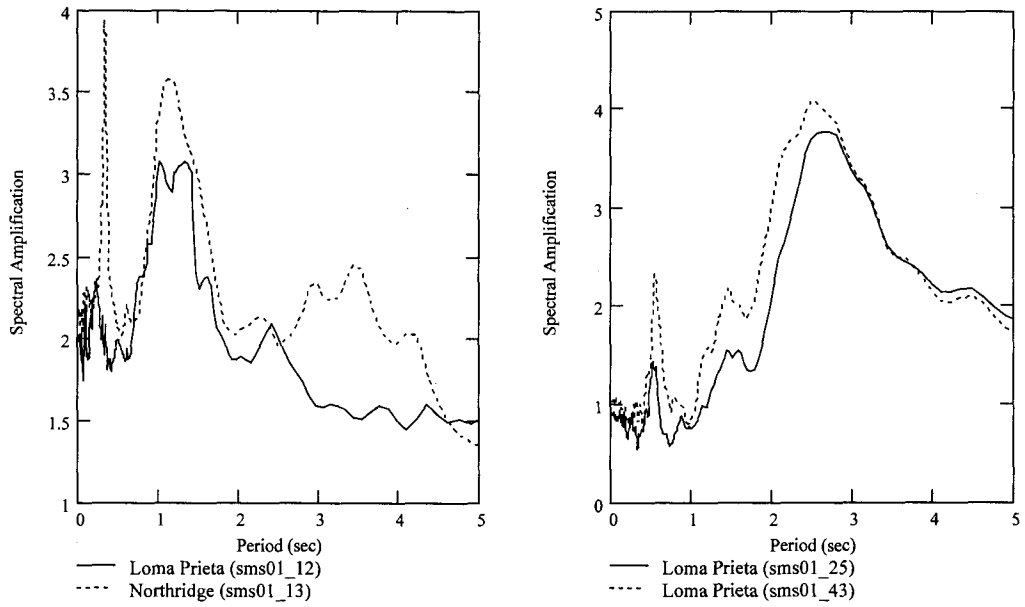

Figure 11-11: SMS01 spectral amplification during *small* and *large* shakes.

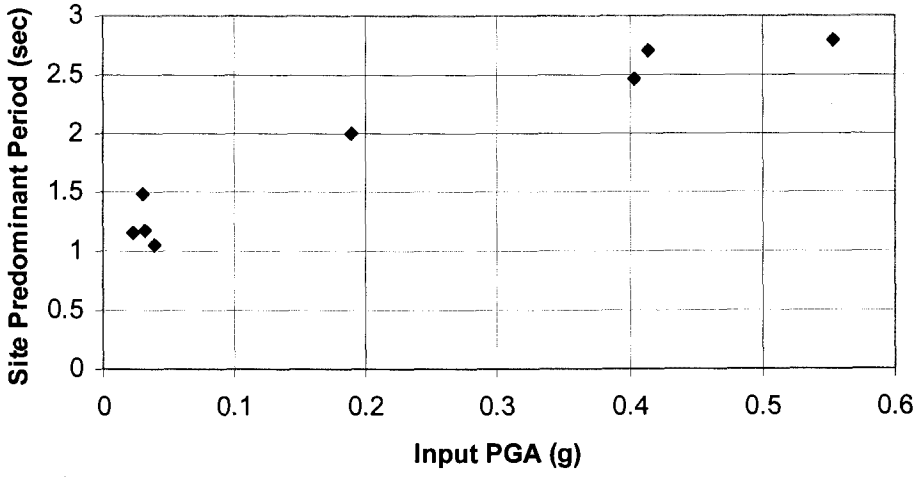

Figure 11-12: Plot of site predominant period vs. input motion PGA values from models NJM02 and SMS01

During the analysis of NJM02, it was seen that mid-frequency motions with a period of approximately 1 second are amplified during *small* shakes and lower frequency motions with a period of approximately 2 seconds are amplified during *large* shakes. To quantify the input amplitude dependency of the model amplification behavior, the predominant period of each test was extracted from spectral amplification plots of both tests (Figure 10-9 for NJM02 and Figure 11-11 for SMS01). These values were plotted versus input PGA values in Figure 11-12. The values plotted in this figure show the predominant period increasing as the input PGA value increases.

11.6 Behavior of Improved Ground

11.6.1 Behavior of CDSM

As mentioned in section 3.6.3, the CDSM modeled in SMS01 model was designed to reflect the recent work at Berths 55 and 56 at the Port of Oakland (Subsurface Consultants et al., 1999). One aspect of the POOAK specifications was not matched accurately in the centrifuge study due to the technique used to fabricate the CDSM material. Construction specifications called for at least 18-in of CDSM embedment into surrounding dense sand layers, however little to no embedment was utilized within the model. It is the author's opinion that the large moments in excess of plastic moment capacity shown in Figure 11-4 and Figure 11-5 might have been avoided if the embedment depth could have been accurately modeled.

11.6.2 Improved Sand Density

The most obvious effect of the *improved* sand density is provided by looking at the post-test dissection profile provided in Figure 11-2. The boundary between the improved and unimproved zones (i.e., x = 1350 mm) is marked with significantly less

settlement in the *improved* zone compared to the extreme backland soils. This improvement is quantified in Figure 11-13 with settlement in the *improved* zone less than half that recorded in the looser, *unimproved* soils. However, the improved soil also settled roughly 19-cm prototype. The break in performance was seen at the surface by the appearance of a ground crack. This surface crack is shown in Figure 11-14a with a ruler indicating the location at 135 cm from the front of the box where the improvement scheme began. By examining the black sand columns in the model (Figure 11-14b), it appears the improved soils settled back into the unimproved area possibly increasing the displacements that would have occurred otherwise. Other comments pertaining to the pore pressure behavior in improved soils were discussed in section 11.3.

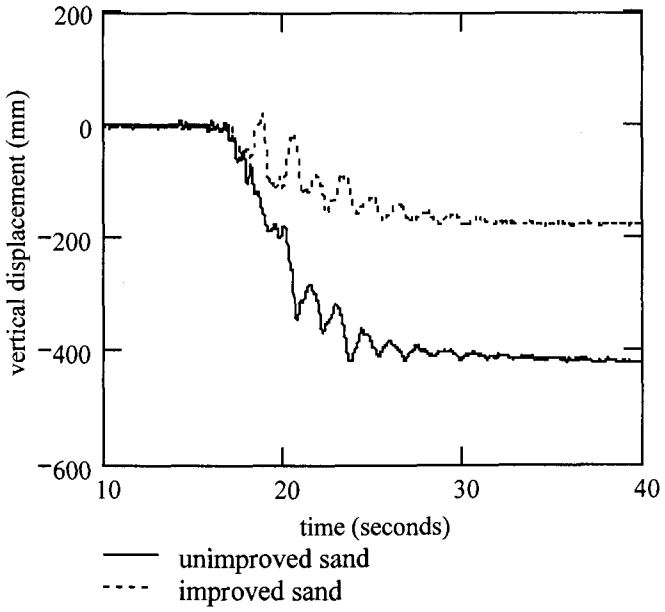

Figure 11-13: Vertical displacements at the ground surface comparison between the improved and unimproved soils in test SMS01_25.

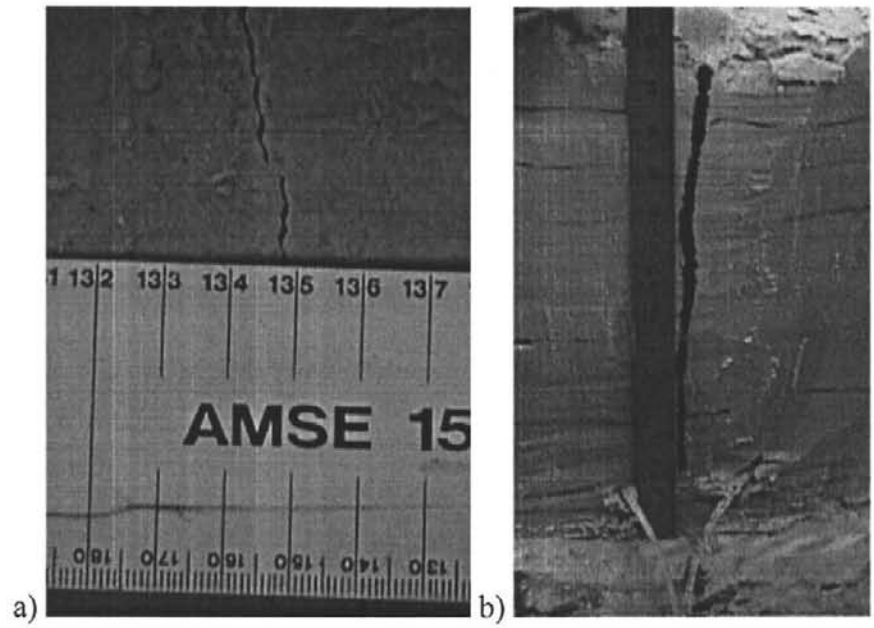

a) b)

Figure 11-14: a) Surface ground crack development at x=1350 b) black sand column at x= 1360 showing movement toward the unimproved region

11.6.3 Summary of Soil Improvement Effects on Overall Model Behavior

In comparing the pile and soil behavior between NJM02 and SMS01, it appears that the improved ground had a number of significant effects on the overall system behavior. During NJM02, the relatively large interface moments at the base of the upper dike demonstrated that a significant amount of movement occurs at this interface. In SMS01, the moments are much more uniform through the rock dike/improved sand transition. Also, despite lower clay strengths in the first model, much larger moments appear in the SMS01 test series. These two changes in behavior suggest that the primary failure plane (i.e., deep seated, or global stability) has shifted to the base of the clay layer. The improved soil and rockfill zones behave more as a competent rigid body, possibly transferring larger loads to the lower relatively weaker interface under the CDSM. This is in contrast to the behavior in NJM02, wherein it is surmised that the dikes moved more independently of the surrounding soil. With this

increased mass, a wedge type failure could have occurred following the base of the CDSM grid creating the large moments in Figure 11-5.

11.7 Pile Effects and Soil Structure Interaction

The effects of piles on the model behavior and deformations were introduced in the discussion of model NJM02. Cracks in the rock dike and the pile-soil gapping phenomena clearly show the piles are affecting deformations, however the extent of this behavior is not known. Figure 11-15 from test SMS01, shows a similar picture in regards to the pile gapping seen during NJM02. A soil structure interaction analysis of this pile behavior has not been completed. However, a portion of the performance of the next model in this test series (SMS02) is provide in regard to this subject because it provides additional insight to this behavior. The configuration of SMS02 was changed to a single lift rock dike and a wharf deck that includes batter piles. During testing of this model, earthquake motions were run on this model with the batter piles connected and disconnected to the wharf deck during different tests. The initial tests were run with the batter piles attached to the wharf deck. The batter pile cap connections were then removed for subsequent tests. Cracks in the dike similar to those seen in Figure 10-10 only appeared after the batter pile connections were removed. Therefore, the wharf behavior had a much more significant effect on the embankment movement without the added stiffness of the batter piles. It is hoped that further analysis of upcoming and past tests will add to the understanding of the soil-structure interaction behavior of wharf structures.

This chapter has provided an introduction to the behavior of model SMS01 by analyzing deformations during the test sequence. The recorded data was also plotted in a primarily qualitative method to provide general deformation characteristics or model performance. However, qualitative results were also provided to compare performance to representative prototype strengths or expected behaviors.

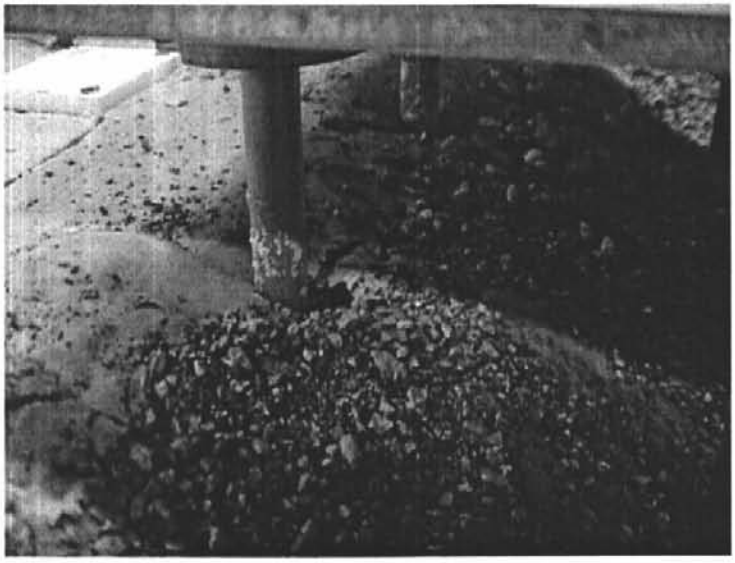

Figure 11-15: Pile gapping and deformation cracks after all earthquakes in test SMS01.

12 SUMMARY AND CONCLUSIONS

The results of two large-scale centrifuge model tests of the dynamic behavior of embankment-pile-wharf structures have been presented. This work is a component of an on-going research program aimed at evaluating the seismic performance of these structures, the effectiveness of soil improvement for mitigating seismic hazards, as well as the development of performance-based seismic design guidelines for port structures. As a portion of this coordinated research program, this thesis has focused on the design, fabrication and testing of two models. The geometry of these centrifuge models was based on typical pile-supported wharves employed at major ports located along the Pacific coast of the United States. The generalized configuration, which formed the basis for the first model addressed in this thesis, consists of a multi-lift rock dike backfilled with sands and a pile-supported wharf structure installed through the rock dike. The second model described in this thesis involved two regions of soil improvement that proved to significantly affect the overall deformation pattern of the model when subjected to cyclic loading.

In light of the tremendous volume of data that has been collected during the suite of tests on these two models, this thesis has focused primarily on the modeling limitations, data reduction, preparation of model animations, and preliminary interpretation of the model performance. A complete description of the model test sequence and recorded data is provided. All data from the models was converted and made available on an accompanying CDROM.

12.1 CENTRIFUGE MODELING ISSUES

Given the complexity of the models, many lessons pertaining to centrifuge modeling have been learned. Pertinent lessons with respect to the fabrication of the models include:

- Full saturation of a soil profile around an intermediate layer of clay is possible with good results.
- The technique developed to model Cement Deep Soil Mixing within the model was effective and with minor modifications could be used to incorporate design embedment depths.
- The creation of adjacent zones of sand with dramatically different soil densities simulating soil improvement was accurately modeled.
- The effect of a soil profile of significantly different thickness along the length of a flexible model container needs to be analyzed.
- Placing model instrumentation in arrays for subsequent analysis and presentation on the form of real time animations, or simulations is a very beneficial way of analyzing the overall performance of complex soil and structural applications.

12.2 Interpretation of Model Response

An analysis of the data from both tests showed pile moments exceeding prototype plastic moment capacities during larger earthquake motions. Based on these results and other observations of the model behavior within this study, the following pertinent aspects of the seismic design and performance of pile supported wharves in regard to seismic pile design are highlighted:

- The maximum pile moments were recorded at the pile head-wharf deck connection.
- Additionally, large moments (in excess of the plastic moment capacity) were recorded at depth within the soil profile. Therefore, methods of analysis for lateral pile behavior and pile-wharf deck response that are based on a depth of fixity for piles may not accurately represent the location of other moments in excess of plastic moment capacity deeper in the soil profile due to inertial effects of the soil.

- Peak moments at the pile head occur early in the earthquake shaking, and not necessarily at the time when the maximum PGA is observed. The higher moments are distributed throughout the piles within the soil profile later in the record and these are associated with soil deformations.
- The practice of reducing the amount of pile reinforcement with depth should be used cautiously, especially within stratified soils with weak/stiff soil interfaces.
- High residual moments can remain "locked" into the piles after shaking. This behavior is more significant as the soil depth increases.
- The effect of piles on embankment deformations warrants further analysis.

Based on the model behavior in this study, the following pertinent aspects regarding the use of soil improvement were observed:

- The use of CDSM in foundation layers provides little benefit without appropriate embedment depths into the surrounding stiff soil layers
- The densification of the backfill sands, which provide the foundation material for the upper rock dike, may have shifted the failure plane of the model deeper into the soil profile. This may be caused by the improved soil and rockfill zones behaving more as a competent rigid body, possibly transferring larger loads to the lower relatively weaker interface under the CDSM.
- The sand improvement scenario for model SMS01 did not reduce deformations to an acceptable level during high intensity shaking (i.e., PGA > 0.35 g).
- The sand improvement scenario beneath the upper dike did significantly reduce the pile moments at this interface.

12.3 SUGGESTIONS FOR FUTURE RESEARCH

Suggestions for future research and seismic modeling of pile supported wharves include the following:

- A clearer picture of the effect of piles on the overall stability of the embankment is necessary. A control test without any piles run would be an excellent addition to this research. The same configuration could then be run with varying numbers of piles across the dike section. These tests should be run with a simpler cross-section (not a two-lift rock dike) to more accurately obtain and analyze the soil-pile interaction.
- The wharf configuration used for these two tests involved a wharf deck protruding above the backfill soils. The wharf deck should be lowered to the soil level so that it more accurately represents the soil/structure interaction that is present in prototype configurations. This change has already been made in the next two models in this test series.
- Models that incorporate batter piles into the configuration should be run. The next two tests in this series have been run with this configuration.
- Models that incorporate different rock dike configurations to determine the most cost effective design. The next two tests in this series incorporate different dike configurations.
- More centrifuge modeling of soil improvement scenarios is suggested. A suite of test incorporating varying degrees of soil improvement which focus on the particular issues surrounding the amount of improvement necessary and in the case of CDSM techniques, the appropriate embedment depths.
- It is deemed worthwhile to run fewer large earthquakes (possibly only one) during the testing of a model to better separate and identify earthquake induced movements.

BIBLIOGRAPHY

Arulmoli, K. (1994). "VELACS: Selection, distribution, and laboratory testing of soils, "Proceedings of the International Conference on the Verification of Numerical Procedures for the Analysis of Soil Liquefaction Problems, Volume 2. Edited by Kandiah Arulanandan, Ronald F. Scott. 1994.

Baez, J.I. and Martin, G.R. (1992). "Quantitative Evaluation of Stone Column Techniques for Earthquake Liquefaction Mitigation." Proceedings of the Tenth World Conference on Earthquake Engineering. A.A. Balkema, Rotterdam. pp 1477-1483.

Chari, T.R. and Meyerhoff, G.G. (1983). "Ultimate Capacity of rigid single piles under inclined loads in sand," Canadian Geotechnical Journal., Vol. 20, pp. 849-854.

Chen, L.T. and Poulos, H.G. (1997). "Piles Subjected to Lateral Soil Movements" Journal of Geotechnical Engineering, ASCE, Vol. 123, No. 9, September, pp. 802-811.

Chen, L.T., Poulos, H.G, and Hull, T.S. (1997). "Model Tests on Pile Groups Subjected to Lateral Soil Movement." Soils and Foundations. Japanese Geotechnical Society. Vol. 37, No. 1, March 1997.

Dewoolkar, M.M., H.Y., Ko, and R.Y.S. Pak. (1999, a). "Centrifuge Modeling of models of seismic effects on saturated earth structures." Geotechnique. Vol. 49, No. 2. April 1999 pp 247-266.

Dewoolkar (1999, b). M.M., H.Y., Ko, A.T.,Stadler, and S.M.F., Astaneh. "A substitute Pore Fluid for Seismic Centrifuge Modeling," Geotechnical Testing Journal, GTJODJ, Vol.. 22, No. 3, September 1999, pp. 196-210.

Dickenson, S.D., Ferritto, J., Kaldveer, P., and Soydemir, C. (1998). "Chapter 4, Seismic and Geologic Hazards." Seismic Guidelines for Ports. ASCE-TCLEE Monograph No. 12. S.D. Werner (ed.). 376 p.

Dickenson, S.E. and Yang D.S. (1998). "Seismically Induced Deformations of Caisson Retaining Walls in Improved Soils." Proceedings of a Specialty Conference. Geotechnical Earthquake Engineering and Soil Dynamics III. Geotechnical Special Publication No. 75. Vol. II. pp1071-1081.

Diaz, G.M., Patton, B.W., Armstrong, G.L., and Joolazadeh., M. (1984). "Lateral Load Tests of Piles in Sloping Rockfill." Analysis and Design of Pile Foundations. Proceedings from ASCE Geotechnical Engineering Division, ASCE National Convention. October 1-5, 1984.

Diaz, G.M. and Warwar, J.F. (1986). "Container Wharves Supported on all Vertical Piles Embedded in Rock-fill Dikes." Ports '86. American Society of Civil Engineers. pp 571-582.

Divis, C.J., Kutter, B.L., Idriss, I.M., Goto, Y., and Matsuda, T. (1996). "Uniformity of specimen and response of liquefiable sand model in a large centrifuge shaker." Proceedings, Sixth Japan-US Workshop on Earthquake Resistant Design of Lifeline Facilities and Countermeasures against Liquefaction, Hamada and O'Rourke, Eds., NCEER-96-0012, SUNY, Buffalo, pp. 259-273.

Egan, J.A., Hayden, R.F., Scheibel, L.L., Otus, M., and Serventi, G.M. (1992). "Seismic Repair at Seventh Street Marine Terminal." Proceedings from GT Division/ASCE Grouting, Soil Improvement and Geosynthetics. ASCE. New Orleans, LA. February 25-28. pp. 867-878.

Finn, W.D.L., Wu, G., and Ledbetter, R.H. (1994). "Recent Developments in the Static and Dynamic Analysis of Pile Groups" Deep Foundations, Vancouver Geotechnical Society, May, pp. 1-24.

Gibson, A. (1996). "Physical Scale Modeling of Geotechnical Structures at one-G," Ph.D. Dissertation, California Institute of Technology. Pasadena.

Iai, S. ed. (in press). Seismic Design Guidelines for Port Structures. PIANC/PCT/Working Group 34.

Iai, S. (1998). "Seismic Analysis and Performance of Retaining Structures," Geotechnical Earthquake Engineering and Soil Dynamics III. Geotechnical Special Publication No. 75. Volume 2., 1020-1044, August 1998.

Iai, S. (1989). "Similitude for Shaking Table Tests on Soil-Structure-Fluid Model in 1g Gravitational Field," Soils and Foundations, 29, (1), 105-118, March 1989.

Johnson, R.K., Riffenburgh, R. Hodali, R., Moriwaki, Y., and Tan, P. (1998). "Analysis and design of a container terminal wharf at the Port of Long Beach." Ports '98. American Society of Civil Engineers. pp. 436-444.

Koelling, M.A. and Dickenson, S.E. (1998). "Ground improvement case histories for liquefaction mitigation of port and near harbor facilities." Proceedings from the 1998 ASCE Geotechnical Earthquake Engineering and Soil Dynamics Conference. ASCE. Seattle, WA. August 3-6.

Kutter, B.L., Idriss, I.M., Kohnke, T., Lakeland, J., Li, X.S., Sluis, W., Zeng., Tauscher, R., Goto, Y., and Kubodera, I. (1994). "Design of a large earthquake simulator at UC Davis." Proceedings, Centrifuge 94, Lueng, Lee, and Tan, Eds., Balkema, Rotterdam, pp.169-175.

Kutter, B.L., Li, X.S., Sluis, W., and Cheney, J.A. (1991). "Performance and instrumentation of the large centrifuge at Davis," Proceedings, Centrifuge 91, Ko and Mclean, Eds., Balkema, Rotterdam, pp. 19-26.

Lee, C.Y., Poulos, H.G. and Hull, T.S. (1991). "Effect of seafloors instability on offshore pile foundations." Canadian Geotechnical Journal., Vol. 28, No. 5, pp 729-737.

Liu, L. and Dobry, R. (1995). "Effect of Liquefaction on Lateral Response of Piles by Centrifuge Model Tests." NCEER Bulletin, SUNY-Buffalo, NY., pp 7-11.

Martin, G., (ed), (1999). Draft Proceedings Joint PEER/Industry Workshop on the Seismic Vulnerability of Port Facilities, July 13-15, 1998, San Pedro, CA.

Martin, G.R., and Lam, I.P. (1995). "State of the Art Paper Seismic Design of Pile Foundations: Structural and Geotechnical Issues" Proceedings of Third International Conference on Recent Advances in Geotechnical Earthquake Engineering and Soil Dynamics, St. Louis, Missouri, April.

Meyersohn, W.D., O'Rourke, T.D., and Miura, F. (1992). "Lateral Spread Effects on Reinforced Concrete Pile Foundations" Proceedings of the Fifth U.S.-Japan Workshop on Earthquake Disaster Prevention for Lifeline Systems, Tsukuba, Japan, Oct. 26-30.

Meyersohn, W. (1994). "Pile Response to Liquefaction-Induced Lateral Spread," Ph.D. Dissertation, Cornell University, Ithaca.

Meymand, P.J. (1998). "Shaking Table Tests of Non-Linear Soil-Pile Superstructure Interaction in Soft Clay" PhD. Dissertation. University of California, Berkeley.

McCullough, N.J., Schlechter, S.M., Dickenson, S.E., Kutter, B.L., and Wilson, D.W., (2000). Data Report: Pile-Supported Wharf Centrifuge Model (NJM01), Geotechnical Engineering Group, Department of Civil, Construction and Environmental Engr., Oregon State University.

McCullough, N.J., and Dickenson, S.E. (1998). "Estimation of Seismically-Induced Lateral Deformations for Anchored Sheetpile Bulkheads." Proceedings of a Specialty Conference. Geotechnical Earthquake Engineering and Soil Dynamics III. Geotechnical Special Publication No. 75. Vol. II. pp. 1095-1105.

Mukhopadhyay, G. (1998). "Preparing for Pier A," Civil Engineering. August 1998. pp 36-39.

Muraleetharan, K.K., Arulmoli, K., Wittkop, R.C., and Foxworthy, J.E. (1997). "Use of Centrifuge and Numerical Modeling in Design of Pier 400 at the Port of Los Angeles," Transportation Research Record 1582, Transportation Research Board, National Research Council.

Muraleetharan, K.K., K.D. Mish, C. Yogochandran, and K. Arulandran. (1998). DYSAC 2: Dynamic Soil Analysis Code for 2-Dimensional Problems. Computer Code. Department of Civil Engineering, University of California, Davis.

Ohtomo, K. and Hamada, M. (1996). "Soil Force Acting on Pile in Lateral Flowing Ground by Soil Liquefaction." Proc. 5th U.S. National Conference on Earthquake Engineering., Chicago, Vol. 4, pp 241-250.

PHRI (Port and Harbour Research Institute). 1997. Handbook on Liquefaction Remediation of Reclaimed Land. A.A. Balkema. Rotterdam, Netherlands. 312 p.

Roth, W.H., Fong, H., de Rubertis, C. (1992). "Batter Piles and the Seismic Performance of Pile-Supported Wharves." Proceedings from the Ports'92 Conference. ASCE.

Schlechter, S.M., McCullough, N.J., Dickenson, S.E., Kutter, B.L., and Wilson, D.W., (2000,a). Data Report: Pile-Supported Wharf Centrifuge Model (NJM02), Geotechnical Engineering Group, Department of Civil, Construction and Environmental Engr., Oregon State University.

Schlechter, S.M., McCullough, N.J., Dickenson, S.E., Kutter, B.L., and Wilson, D.W., (2000,b). Data Report: Pile-Supported Wharf Centrifuge Model (SMS01), Geotechnical Engineering Group, Department of Civil, Construction and Environmental Engr., Oregon State University.

Schofield, A.N. (1980). "Cambridge geotechnical centrifuge operations." Geotechnique. London. Vol. 30, No. 3. pp 227-268.

Scott, R.F., (1983). "Centrifuge Model Testing at Caltech," Journal Soil Dynamics and Earthquake Engineering, Vol. 2. No. 4. pp 188-198.

Scott, Ronald F. (1991). "Modeling of Earth Structures," Port of Los Angeles Seismic Workshop Proceedings.

Stewart, D.P. Chen, Y.R., and Kutter, B.L. (1998). "Experience with the use of methylcellulose as a viscous pore fluid in centrifuge models," Geotechnical Testing Journal, GTJODJ, 21 (4), December. pp.365-369.

Stewart, H.E., Miura, F., and O'Rourke T.D. (1988). "Pile Damage due to Large Ground Displacement," *Proceedings* of 1st Japan-U.S. Workshop on Liquefaction, Large ground Deformation and their Effects on Lifeline Facilities, November 16-19, Tokyo, Japan, pp. 173-182.

Subsurface Consultants, CH2MHill, and Warren (1999). "Summary Report, Cement Deep Soil Mixing Test Section, Berths 55/56, Inner Harbor Channel, Port of Oakland." July 1999.

Taboada, V. (1995). "Centrifuge Modeling of Earthquake Induced Lateral Spreading in Sand Using a Laminar Box." Ph.D. Thesis, Rensselar Polytechnic Institute, Troy, NY.

Tarin, R. (1997). "Bay Mud Binder." Center for Geotechnical Modeling. University of California, Davis.

Tokimatsu, K. Mizuno, H. and Kakurai, M. (1996). "Building Damage Associated with Geotechnical Problems." Soils and Foundations, Special Issue of Geotechnical Aspects of the 1995 Hyogoken Nanbu Earthquake, January, pp. 219-234.

Werner, S.D., and Hung, S.J. (1982). Seismic Response of Port and Harbor Facilities. National Science Foundation. R-8122-5395. Agbabian Associates. El Segundo, California. 348 p.

Werner, S.D. (1990). "Seismic Risks to Port and Harbor Facilities." Proceedings of the POLA Seismic Workshop on Seismic Engineering. R.D. Wittkop and G.R. Martin (eds.). Port of Los Angeles. San Pedro, CA. March 21-23.

Werner, S.D. (ed.) (1998). Seismic Guidelines for Ports. ASCLE-TCLEE Monograph No 12. ASCLE-TCLEE Ports and Harbors Committee. 376 p.

Wilson, D.W. (1998). "Soil-Pile-Superstructure Interaction in Liquefying Sand and Soft Clay." Ph.D. Dissertation. University of California, Davis.

Woodward-Clyde (1997). "Experimental Results of Maximum and Minimum Dry Densities of Nevada Sand." Memorandum (Feb. 13, 1997) from Woodward-Clyde to the Center for Geotechnical Modeling, University of California, Davis, CA.

Yasuda, S, Ishihara, K., Harada, K., and Shinkawa, N. (1996). "Effect of Soil Improvement on Ground Subsidence due to Liquefaction." Special Issue of Soils and Foundations on Geotechnical Aspects of the January 17, 1995 Hyogoken-Nanbu Earthquake. Japanese Geotechnical Society. January. pp 99-107.

Yenumula, V.S., Prasad, S.N., and Chari, T.R. (1999). "Lateral Capacity of Rigid Piles in Cohesionless Soils." Soils and Foundations. Japanese Geotechnical Society. Vol. 39, No. 2, 21-29, April 1999.

APPENDICES

APPENDIX A
(NJM02 DATA COLUMN IDENTIFICATION)

Table A-1: NJM02 data column instrument identification for small shakes

Instr.	Data Column	Instr.	Data Column	Instr.	Data Column
SG1-2	1	SG7-2	31	V ACC5270	61
SG1-5	2	SG7-5	32	ACC3161	62
SG1-8	3	SG7-8	33	ACC3160	63
SG1-10	4	SG7-10	34	ACC5271	64
SG1-11	5	PPT7988	35	ACC3948	65
SG1-12	6	PPT8044	36	ACC3962	66
SG1-13	7	PPT7722	37	ACC3166	67
SG1-16	8	PPT7985	38	ACC3202	68
SG2-4	9	PPT7714	39	ACC4523	69
SG2-6	10	PPT7810	40	ACC3159	70
SG2-10	11	PPT7984	41	ACC3157	71
SG2-11	12	PPT7369	42	ACC5601	72
SG2-12	13	PPT7719	43	ACC4436	73
SG2-13	14	PPT7811	44	ACC3203	74
SG3-2	15	PPT8013	45	ACC3951	75
SG3-5	16	PPT8016	46	ACC4595	76
SG3-10	17	PPT7986	47	ACC3963	77
SG3-11	18	PPT7367	48	ACC3949	78
SG3-12	19	PPT7713	49	ACC5269	79
SG3-13	20	PPT7817	50	ACC3164	80
SG3-15	21	LP203	51	ACC3154	81
SG6-1	22	LP204	52	ACC3155	82
SG6-2	23	LP404	53	ACC3204	83
SG6-3	24	LP402	54	ACC3259	84
SG6-4	25	LP405	55	ACC4596	85
SG6-6	26	LP211	56	ACC5598	86
SG6-7	27	LP213	57	ACC5603	87
SG6-9	28	LP403	58	ACC5599	88
SG6-10	29	LP401	59	ACC3955	89
SG6-11	30	V ACC4437	60	Time	90

Table A-2: NJM02 data column instrument identification for large shakes

Instr.	Data Column
SG1-2	1
SG1-5	2
SG1-8	3
SG1-10	4
SG1-11	5
SG1-12	6
SG1-13	7
SG1-16	8
SG2-4	9
SG2-6	10
SG2-10	11
SG2-11	12
SG2-12	13
SG2-13	14
SG3-2	15
SG3-5	16
SG3-10	17
SG3-11	18
SG3-12	19
SG3-13	20
SG3-15	21
SG6-1	22
SG6-2	23
SG6-3	24
SG6-4	25
SG6-6	26
SG6-7	27
SG6-9	28
SG6-10	29
SG6-11	30

Instr.	Data Column
SG7-2	31
SG7-5	32
SG7-8	33
SG7-10	34
PPT6711	35
PPT8044	36
PPT7722	37
PPT7985	38
PPT7714	39
PPT7810	40
PPT7984	41
PPT7369	42
PPT7719	43
PPT7370	44
PPT8013	45
PPT8016	46
PPT7986	47
PPT7367	48
PPT7713	49
PPT7817	50
LP203	51
LP204	52
LP404	53
LP402	54
LP405	55
LP211	56
LP213	57
LP403	58
LP401	59
V ACC4437	60

Instr.	Data Column
V ACC5270	61
ACC3161	62
ACC3160	63
ACC5271	64
ACC3948	65
ACC3962	66
ACC3166	67
ACC3202	68
ACC4523	69
ACC3159	70
ACC3157	71
ACC5601	72
ACC4436	73
ACC3203	74
ACC3951	75
ACC4595	76
ACC3963	77
ACC3949	78
ACC5269	79
ACC3164	80
ACC3154	81
ACC3155	82
ACC3204	83
ACC3259	84
ACC4596	85
ACC5598	86
ACC5603	87
ACC5599	88
ACC3955	89
Time	90

Table A-3: NJM02 instrument lists for shear wave velocity tests

Back Array Tests	
Column	**Instrument**
1	ACC 3259
2	ACC 3204
3	ACC 3155
4	ACC 3154

Upper Dike Array Tests	
Column	**Instrument**
1	ACC 3963
2	ACC 4595
3	ACC 3951
4	ACC 3203
5	ACC 4436

APPENDIX B
(SMS01 DATA COLUMN IDENTIFICATION)

Table B-1: SMS01 data column instrument identification

Instrument	*Data Column*
PPT7719	1
PPT7985	2
PPT7810	3
PPT7371	4
PPT7368	5
PPT7722	6
PPT8016	7
PPT6838	8
PPT7714	9
PPT6837	10
PPT7367	11
PPT7373	12
PPT8013	13
PPT7811	14
PPT8044	15
PPT7711	16
PPT7369	17
PPT7370	18
LP402	19
LP207	20
LP208	21
LP209	22
LP401	23
LP403	24
LP404	25
LP212	26
LP206	27
SG1-10	28
SG1-12	29
SG1-13	30

Instrument	*Data Column*
SG1-5	31
SG1-8	32
SG2-1	33
SG2-2	34
SG2-3	35
SG2-4	36
SG2-5	37
SG2-6	38
SG2-7	39
SG2-8	40
SG2-9	41
SG2-10	42
SG2-11	43
SG2-12	44
SG2-13	45
SG2-14	46
SG2-15	47
SG5-1	48
SG5-2	49
SG5-3	50
SG5-14	51
SG5-5	52
SG5-6	53
SG5-7	54
SG5-8	55
SG5-9	56
SG5-10	57
SG5-12	58
SG5-15	59
ACC3164	60

Instrument	*Data Column*
ACC4436	61
ACC4596	62
ACC5268	63
ACC3158	64
ACC5275	65
ACC3955	66
ACC4435	67
ACC3202	68
ACC5271	69
ACC3157	70
ACC3949	71
ACC3964	72
ACC4437	73
ACC5269	74
ACC5276	75
ACC5267	76
ACC3155	77
ACC4595	78
ACC3154	79
ACC3959	80
ACC4523	81
ACC3951	82
ACC3203	83
ACC3948	84
ACC3963	85
ACC5598	86
ACC3161	87
ACC5603	88
VACC4534	89
Time	90

Table B-2: SMS01 instrument lists for shear wave velocity tests

Upper Dike Array Tests		*Back Array Tests*		*Free Array Tests*	
Column	**Instrument**	**Column**	**Instrument**	**Column**	**Instrument**
1	ACC 4523	1	ACC 3158	1	ACC 4435
2	ACC 3959	2	ACC 5268	2	ACC 3955
3	ACC 3154	3	ACC 4596	3	ACC 5275
4	ACC 4595	4	ACC 4436		
5	ACC 3155				